INVESTIGATION OF TERNARY BLENDED BINDER PVA FIBRE REINFORCED CEMENTITIOUS COMPOSITES AS REPAIR MATERIAL

LOH ZHI PIN

FACULTY OF ENGINEERING
UNIVERSITY OF MALAYA
KUALA LUMPUR

2019

INVESTIGATION OF TERNARY BLENDED BINDER PVA FIBRE REINFORCED CEMENTITIOUS COMPOSITES AS REPAIR MATERIAL

LOH ZHI PIN

DISSERTATION SUBMITTED IN FULFILMENT OF THE REQUIREMENTS FOR THE DEGREE OF MASTER OF ENGINEERING SCIENCE

FACULTY OF ENGINEERING
UNIVERSITY OF MALAYA
KUALA LUMPUR

2019

UNIVERSITY OF MALAYA

ORIGINAL LITERARY WORK DECLARATION

Name of Candidate:

Matric No:

Name of Degree:

Title of Project Paper/Research Report/Dissertation/Thesis (“this Work”):

Field of Study:

I do solemnly and sincerely declare that:

(1) I am the sole author/writer of this Work;
(2) This Work is original;
(3) Any use of any work in which copyright exists was done by way of fair dealing and for permitted purposes and any excerpt or extract from, or reference to or reproduction of any copyright work has been disclosed expressly and sufficiently and the title of the Work and its authorship have been acknowledged in this Work;
(4) I do not have any actual knowledge nor do I ought reasonably to know that the making of this work constitutes an infringement of any copyright work;
(5) I hereby assign all and every rights in the copyright to this Work to the University of Malaya (“UM”), who henceforth shall be owner of the copyright in this Work and that any reproduction or use in any form or by any means whatsoever is prohibited without the written consent of UM having been first had and obtained;
(6) I am fully aware that if in the course of making this Work I have infringed any copyright whether intentionally or otherwise, I may be subject to legal action or any other action as may be determined by UM.

Candidate’s Signature Date:

Subscribed and solemnly declared before,

Witness’s Signature Date:

Name:

Designation:

UNIVERSITI MALAYA

PERAKUAN KEASLIAN PENULISAN

Nama: (No. K.P/Pasport:)

No. Matrik:

Nama Ijazah:

Tajuk Kertas Projek/Laporan Penyelidikan/Disertasi/Tesis ("Hasil Kerja ini"):

Bidang Penyelidikan:

Saya dengan sesungguhnya dan sebenarnya mengaku bahawa:

(1) Saya adalah satu-satunya pengarang/penulis Hasil Kerja ini;
(2) Hasil Kerja ini adalah asli;
(3) Apa-apa penggunaan mana-mana hasil kerja yang mengandungi hakcipta telah dilakukan secara urusan yang wajar dan bagi maksud yang dibenarkan dan apa-apa petikan, ekstrak, rujukan atau pengeluaran semula daripada atau kepada mana-mana hasil kerja yang mengandungi hakcipta telah dinyatakan dengan sejelasnya dan secukupnya dan satu pengiktirafan tajuk hasil kerja tersebut dan pengarang/penulisnya telah dilakukan di dalam Hasil Kerja ini;
(4) Saya tidak mempunyai apa-apa pengetahuan sebenar atau patut semunasabahnya tahu bahawa penghasilan Hasil Kerja ini melanggar suatu hakcipta hasil kerja yang lain;
(5) Saya dengan ini menyerahkan kesemua dan tiap-tiap hak yang terkandung di dalam hakcipta Hasil Kerja ini kepada Universiti Malaya ("UM") yang seterusnya mula dari sekarang adalah tuan punya kepada hakcipta di dalam Hasil Kerja ini dan apa-apa pengeluaran semula atau penggunaan dalam apa jua bentuk atau dengan apa juga cara sekalipun adalah dilarang tanpa terlebih dahulu mendapat kebenaran bertulis dari UM;
(6) Saya sedar sepenuhnya sekiranya dalam masa penghasilan Hasil Kerja ini saya telah melanggar suatu hakcipta hasil kerja yang lain sama ada dengan niat atau sebaliknya, saya boleh dikenakan tindakan undang-undang atau apa-apa tindakan lain sebagaimana yang diputuskan oleh UM.

Tandatangan Calon Tarikh:

Diperbuat dan sesungguhnya diakui di hadapan,

Tandatangan Saksi Tarikh:

Nama:

Jawatan:

INVESTIGATION OF TERNARY BLENDED BINDER PVA FIBRE REINFOCED CEMENTITIOUS COMPOSITES AS REPAIR MATERIAL

ABSTRACT

Fibre reinforced cementitious composites (FRCC) is a type of high-performance concrete with unique features suitable for repair application. To develop a well-performed FRCC, good fibre dispersion is crucial and it is achievable via high binder content without compromising the mechanical properties. Therefore, supplementary cementitious material is used to reduce the heat of hydration as well as improving the workability of FRCC. In this research, the focus was on using fixed water-to-binder ratio to study the effect of different binder (900 kg/m^3, 1100 kg/m^3 and 1300kg/m^3) and ground granulated blast furnace slag (GGBS) (0, 30 % and 60 % as fly ash replacement) content on the performance of FRCC as repairing material. Overall, the research was planned into two phases. The initial phase served as a preliminary stage in selecting the FRCC by fulfilling the minimum requirement in terms of workability and compressive strength; whereas the final phase was the testing of mechanical properties, namely, splitting tensile, flexural, slant shear and impact strength tests. The results showed that workability and rheology of FRCC can be improved with higher binder content or using 30 % GGBS replacement. Conversely, FRCC with lower binder content and higher GGBS content induced higher compressive strength. Ultimately, six mixtures of FRCC were selected in the final phase by fulfilling the minimum requirement in terms of workability and compressive strength. Based on the experimental results, the effect of GGBS was observed to be varied at different binder contents on the mentioned mechanical properties and ductility of FRCC; as this is primarily attributed to the interfacial bond of matrix-fibre and matrix strength. Based on the performance and the economic considerations, binder content at 1100kg/m^3 and 30% GGBS replacement in FRCC was the most optimum. In overall, the usage of GGBS as partial replacement for fly ash showed positive effect in developing FRCC for

repair work as the minimum requirement for mechanical properties of repair material could be fulfilled.

Keywords: Ternary blended binders, PVA fibre, FRCC, GGBS, repair materials

PENYELIDIKAN KOMPOSIT BERSIMEN BERTETULANG GENTIAN (FRCC) PVA DENGAN TIGA CAMPURAN BAHAN PENGIKAT SEBAGAI BAHAN PEMBAIKAN

ABSTRAK

Komposit bersimen bertetulang gentian (FRCC) merupakan sejenis konkrit berprestasi tinggi berciri unik yang sesuai untuk aplikasi pembaikan. Demi menghasilkan satu FRCC yang berprestasi, penyebaran gentian yang baik adalah amat penting dan ia boleh dicapai melalui kandungan bahan pengikat yang tinggi. Namun begitu, kandungan simen yang tinggi akan menghasilkan haba hidrasi yang tinggi. Jadi, pengganti simen digunakan untuk merendahkan haba hidrasi dan juga menambahbaikkan kebolehgunaan FRCC. Penyelidikan ini menggunakan nisbah air dengan bahan pengikat yang tetap untuk mengkaji kesan kandungan bahan pengikat (900 kg/m^3, 1100 kg/m^3 dan 1300kg/m^3) dan kandungan kisaran sanga relau bagas yang digiling (GGBS) (0, 30 % dan 60 % sebagai pengganti abu terbang) yang berlainan dalam prestasi FRCC sebagai bahan pembaikan. Secara keseluruhannya, penyelidikan ini dibahagikan kepada dua fasa. Fasa awal merupakan peringkat pemilihan FRCC yang memenuhi syarat-syarat minima dalam bentuk kebolehgunaan dan kekuatan mampatan; manakala fasa akhir merupakan pengajian sifat-sifat mekanikal, iaitu kekuatan tegangan, lenturan, ricih condong dan hentakan. Keputusan menunjukkan bahawa kebolehgunaan dan reologi FRCC boleh ditambah baik dengan kandungan bahan pengikat yang lebih tinggi atau menggunakan penggantian 30% GGBS. Sebaliknya, FRCC yang mengandungi bahan pengikat yang lebih rendah dan GGBS yang lebih tinggi mendorong kekuatan mampatan yang lebih tinggi. Akhirnya, enam campuran FRCC dipilih dalam fasa akhir selepas memenuhi syarat-syarat minimum atas kebolehgunaan dan kekuatan mampatan. Berdasarkan keputusan eksperimen, dalam kandungan bahan pengikat yang berbeza, kesan GGBS adalah berlainan terhadap sifat-sifat mekanikal tersebut. Ini boleh dikaitkan dengan ikatan antara gegentian dengan matriks bersimen dan kekuatan matriks. Kandungan bahan pengikat pada 1100kg/m^3 dan gantian 30% GGBS memberikan keputusan yang paling optima dari segi pertimbangan prestasi dan nilai ekonomik. Secara keseluruhannya, penggunaan GGBS sebagai gantian abu terbang dalam FRCC menunjukkan kesan positif dalam penghasilan FRCC untuk kerja pembaikan.

Kata kunci: Tiga campuran bahan pengikat, gentian PVA, FRCC, GGBS, bahan pembaikan

ACKNOWLEDGEMENTS

I would like to express my gratitude towards my supervisors, Dr. Mo Kim Hung, Dr. Tan Chee Ghuan and Dr. Yap Soon Poh for their continuous support, guidance and knowledgeable advices throughout the research.

Special thanks to my friends and colleagues Mr. Yeo Shih Horng and Miss Leong Geok Wen for providing their technical knowledge, opinion and resources. Without them, this research could not have been successfully conducted.

Lastly, I would like to take this opportunity to express my gratefulness to my family and friends. For their unconditional support and continuous encouragement throughout my years of study and the process of researching and thesis writing.

TABLE OF CONTENTS

LIST OF FIGURES

LIST OF TABLES

LIST OF SYMBOLS AND ABBREVIATIONS

0% GGBS replacement	:	0% of FA replaced with GGBS
30% GGBS replacement	:	30% of FA replaced with GGBS
60% GGBS replacement	:	60% of FA replaced with GGBS
A-(0,0)	:	Mortar with 900 kg/m^3 binder content without GGBS
A-(0,1.5)	:	FRCC with 900 kg/m^3 binder content without GGBS and 1.5% PVA fibre dosage
A-(0,2.5)	:	FRCC with 900 kg/m^3 binder content without GGBS and 2.5% PVA fibre dosage
A-(30,0)	:	Mortar with 900 kg/m^3 binder content with 30% GGBS replacement
A-(30,1.5)	:	FRCC with 900 kg/m^3 binder content, with 30% GGBS replacement and 1.5% PVA fibre dosage
A-(30,2.5)	:	FRCC with 900 kg/m^3 binder content, with 30% GGBS replacement and 2.5% PVA fibre dosage
A-(60,0)	:	Mortar with 900 kg/m^3 binder content with 60% GGBS replacement
A-(60,1.5)	:	FRCC with 900 kg/m^3 binder content, with 60% GGBS replacement and 1.5% PVA fibre dosage
A-(60,2.5)	:	FRCC with 900 kg/m^3 binder content, with 60% GGBS replacement and 2.5% PVA fibre dosage
AAR	:	Alkali-aggregate reactivity
A_c	:	Cross sectional area
ASTM	:	American Society for Testing and Materials
B-(0,0)	:	Mortar with 1100 kg/m^3 binder content without GGBS

B-(0,1.5)	:	FRCC with 1100 kg/m^3 binder content without GGBS and 1.5% PVA fibre dosage
B-(0,2.5)	:	FRCC with 1100 kg/m^3 binder content without GGBS and 2.5% PVA fibre dosage
B-(30,0)	:	Mortar with 1100 kg/m^3 binder content with 30% GGBS replacement
B-(30,1.5)	:	FRCC with 1100 kg/m^3 binder content, with 30% GGBS replacement and 1.5% PVA fibre dosage
B-(30,2.5)	:	FRCC with 1100 kg/m^3 binder content, with 30% GGBS replacement and 2.5% PVA fibre dosage
B-(60,0)	:	Mortar with 1100 kg/m^3 binder content with 60% GGBS replacement
B-(60,1.5)	:	FRCC with 1100 kg/m^3 binder content, with 60% GGBS replacement and 1.5% PVA fibre dosage
B-(60,2.5)	:	FRCC with 1100 kg/m^3 binder content, with 60% GGBS replacement and 2.5% PVA fibre dosage
BSI	:	British Standard Institution
C-(0,0)	:	Mortar with 1300 kg/m^3 binder content without GGBS
C-(0,1.5)	:	FRCC with 1300 kg/m^3 binder content without GGBS and 1.5% PVA fibre dosage
C-(0,2.5)	:	FRCC with 1300 kg/m^3 binder content without GGBS and 2.5% PVA fibre dosage
C-(30,0)	:	Mortar with 1300 kg/m^3 binder content with 30% GGBS replacement
C-(30,1.5)	:	FRCC with 1300 kg/m^3 binder content, with 30% GGBS replacement and 1.5% PVA fibre dosage

C-(30,2.5)	:	FRCC with 1300 kg/m^3 binder content, with 30% GGBS replacement and 2.5% PVA fibre dosage
C-(60,0)	:	Mortar with 1300 kg/m^3 binder content with 60% GGBS replacement
C-(60,1.5)	:	FRCC with 1300 kg/m^3 binder content, with 60% GGBS replacement and 1.5% PVA fibre dosage
C-(60,2.5)	:	FRCC with 1300 kg/m^3 binder content, with 60% GGBS replacement and 2.5% PVA fibre dosage
C_2S	:	Dicalcium silicate
C_3A	:	Tricalcium aluminate
C_3S	:	Tricalcium silicate
C_4AF	:	Tetracalcium aluminoferrite
CH	:	Calcium hydroxide
CIMA	:	Cement Industries of Malaysia Berhad
COV	:	Coefficient of variation
CSH	:	Calcium silicate hydrate
ECC	:	Engineered cementitious composite
F	:	Force
FA	:	Fly ash
f_c	:	Compressive strength
f_{ct}	:	Splitting tensile strength
FDOT	:	Florida Department of Transportation
F_f	:	Load applied to the middle of the prism at fracture
FRCC	:	Fibre reinforced cementitious composites
FRP	:	Fibre reinforced polymer
GGBS	:	Ground granulated blast furnace slag

HES	:	High early strength
HRWR	:	High range water reducer
I	:	Second moment of area
LS	:	Lignosulphonates
MSC	:	Microsilica concrete
OPC	:	Ordinary Portland cement
PCE	:	Polycarboxylate ether
PE	:	Polyethylene
PP	:	Polypropylene
PVA	:	Polyvinyl alcohol
REM	:	Marketing available repair material
R_f	:	Flexural strength
SCM	:	Supplementary cementitious material
SEM	:	Scanning electron microscope
Series A	:	900 kg/m^3 binder content
Series B	:	1100 kg/m^3 binder content
Series C	:	1300 kg/m^3 binder content
SMF	:	Sulphonated melamine formaldehyde
SNF	:	Sulphonated naphthalene formaldehyde
SP	:	Superplasticizer
SSD	:	Saturated surface dry
w/b ratio	:	Water-to-binder ratio
w/c ratio	:	Water-to-cement ratio
η	:	Viscosity
σ_1	:	First crack stress
σ_2	:	Post peak stress

σ_1/σ_2 ratio	:	First crack to post peak stress ratio
σ_f	:	Flexural strength
τ	:	Shear stress

LIST OF APPENDICES

CHAPTER 1: INTRODUCTION

1.1 Background

Infrastructure development such as bridges, road and skyscrapers has become the catalyst in boosting economic growth, especially in developing countries. Therefore, concrete material is literally becoming the building block of economic development and as a result, large quantities of Portland cement as well as aggregates are in demand for concrete material production. This brings negative impact to the public health as well as the environment. It is reported that 6.3 mg of less than 10 microns particle is released with the production of every ton of Portland cement (Marlowe, 2003). Besides, one ton of Portland cement uses approximately 4 GJ of energy and emits nearly 1 ton of carbon dioxide gas into the atmosphere. Together with the mining of raw materials such as aggregates, limestone and clay, the overall system in production of concrete material is socially, economically and ecologically unsustainable.

Based on standard code of practice in reinforced concrete such as Eurocode 2, the infrastructure built using concrete was designed to have minimum service life of 50 years. Nevertheless, the existing concrete structure in the last few decades might have begun to experience deterioration after withstanding the mechanical loads and the exposure to its service environment. Not to mention that the brittle nature and low tensile strength of concrete cause concrete to be vulnerable to cracking. It is expected that cracks could lead to other types of deterioration, such as steel corrosion, sulphate attack etc. As a result, repair or replacement work are solutions to prevent further deterioration of concrete structure. However, by looking at the downturn of current economic trend, repair work is more suitable than replacing existing concrete structure.

In many countries, the construction of new concrete structure is getting decreasing. As existing concrete structures age, the demand in reparation and maintenance works is increasing. Therefore increasing amount of repair materials such as ettringite based binders, epoxy resin, fibre reinforced polymer (FRP) and etc are being developed and used. However, despite the increasing varieties of concrete repairing material, the rate of success remains low mainly because of inadequate early age performance, long-term durability (Gürkan Yıldırım *et al.*, 2018) or wrong choice of repair material. Therefore, it is important to formulate a concrete repair material that is equipped with good mechanical properties, compatibility and sufficient early age performance so that the failure rate of concrete repairs can be reduced as well as eliminate the need for recurring repairs. Besides focusing on its performance, it is crucial to effectively incorporate by-products or waste material so that more environmentally friendly repair material can be produced.

Of all repair material, fibre reinforced cementitious composites (FRCC) serves as a potential repair material and it is produced adding short fibre into high flowable mortar. Mainly polymeric fibres are being used in FRCC which includes polyvinyl alcohol (PVA) fibre (M. Li & V. C. Li, 2011; Magalhães *et al.*, 2015; Meng *et al.*, 2017), polypropylene (PP) fibre (Pakravan *et al.*, 2016) and polyethylene (PE) fibre (Said & Razak, 2015). To be used in repair application, fibre with high tensile strength, modulus of elasticity and tensile strain capacity is preferred as reinforcement in cementitious composites. Which is why PVA and high-performance PE fibres were used in FRCC for repair application. However, PVA is a more popular option as high performance PE fibre is high in cost (Horikoshi *et al.*, 2006).

In order to have excellent properties in FRCC, the cement matrix of FRCC has much higher cement content (900 – 1300 kg/m^3) compared to conventional concrete (250 – 500 kg/m^3). This is due to the absence of coarse aggregate in FRCC which requires more cement matrix for coating, effective fibre dispersion and matrix toughness control. This high cement content does not merely cause high material cost and heat of hydration but it is also less eco-friendly. To reduce the cement usage, fly ash (FA) is mostly used as cement replacement by researchers (C. Lin *et al.*, 2017; S. X. Wang & Li, 2007; Zhang & Zhang, 2017). For FRCC to be applied as repair material, certain early age performance should be achieved, especially having higher compressive strength than the substrate. Therefore, alternate SCM such as ground granulated blast furnace slag (GGBS) which has higher activity index than FA can be used to improve the early age performance. Besides, GGBS is locally available. Hence, this research will be focusing on using triple blended binder, namely cement, FA and GGBS to formulate PVA-FRCC based repair material with various binder contents.

1.2 Objectives

1. To assess the influence of GGBS, binder content and fibre dosage on workability and compressive strength of PVA FRCC.
2. To evaluate the mechanical properties of ternary blended binder PVA FRCC.
3. To determine the flexural performance of PVA FRCC prepared with ternary blended binder.

1.3 Scope of work

The initial phase of this research began with trial mix of mortar and FRCC with different binder content at 900kg/m^3, 1100kg/m^3 and 1300kg/m^3, different fly ash replacement using GGBS at 0% (as control), 30% and 60% and the fibre dosage at 1.5% and 2.5%. Workability and compressive strength were used as the minimum criteria to proceed with the second phase. The compressive strength was focused on the early phase because it is the only engineering property of concrete that is routinely specified and has a relationship to most other mechanical properties (Bamforth & et al., 2008).

In second phase, the mechanical properties of the ternary blended binder PVA FRCC such as splitting tensile strength, flexural strength, slant shear strength and impact strength were further studied. The flexural performance of the FRCC was also studied in terms of toughness, failure mode and flexural behaviour.

CHAPTER 2: LITERATURE REVIEW

2.1 Introduction

This chapter covers on the following items: 1) types of compatibility in concrete repair material; 2) requirement of concrete repair material specified by relevant engineering standards; 3) introduction of fibre reinforced cementitious composites (FRCC) as repairing material; 4) constituent materials used in FRCC and; 5) effects of fibre on workability and mechanical properties of FRCC to show its suitability as repairing material.

2.2 Types of compatibility for repair material

The compatibility for repairing material is normally correlated to its durability and capability to sustain loading (Morgan, 1996). However, Emmons and Vaysburd (1995) stated that 'compatibility can be defined as a balance of physical, chemical and electrochemical properties and dimensions between a repair material and the existing substrate that will ensure that the repair can withstand all the stresses induced by volume changes and chemical and electrochemical effects without distress and deterioration over a designated period of time.' Figure 2.1 summarized the model for concrete repair design and the importance of compatibility is discussed briefly at the following section.

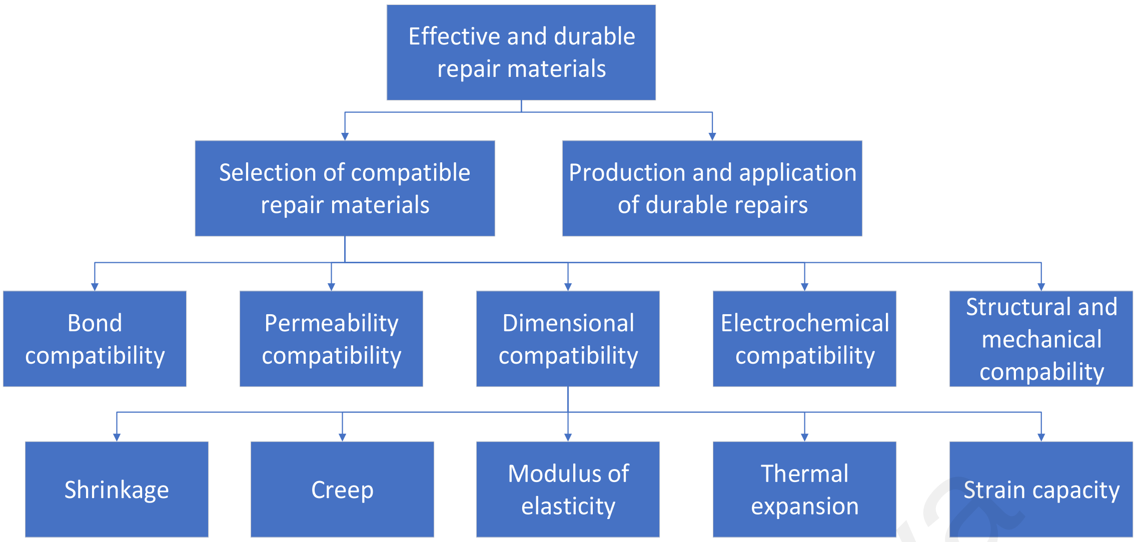

Figure 2.1 Model of concrete repair material (Emmons & Vaysburd, 1995; Morgan, 1996)

2.2.1 Bond compatibility

According to Morgan (1996), bond compatibility is the development and maintenance of a satisfactory level of adhesion between the substrate and repair material. The performance of the remaining material is primarily dependent on its bonding towards the concrete substrate especially for repairs which are not secured mechanically through tying and anchoring. Under normal circumstances, the interface of repair material and substrate form the weakest link, making it the main limitation for the concrete repairing material. Therefore, it is crucial to have excellent bonding between the substrate and repair material in order to have high rate of success in repairing work. There are several methods used to quantify the bonding of repair system by engineering standards (ASTM, 2013; BSI, 1999a, 1999b) and researchers (Bentz *et al.*, 2018; Guo *et al.*, 2018; Zanotti & Randl, 2019), namely, pull-off test (direct tension), slant shear test, direct shear test, splitting tensile strength test (indirect tension). Other than improving the bond compatibility and durability of repair material, surface preparation on the substrate also helps in optimizing the bond compatibility. The concept on surface preparation of existing substrate is basically focusing on its surface roughness, cleanliness and the moisture condition. The surface roughening is usually done mechanically and there are various procedures and methods, namely sand blasting, water jetting, grinding, hammering, wire brushing and etc. In terms of cleanliness, the bond surface must be ensured free of any dust, oil or any contaminants (Austin *et al.*, 1995) as they decrease the friction and prevent the interlocking between substrate and repair material. Upon the placement of repair material, Figure 2.2 indicates the best moisture condition for the surface should be in saturated surface dry (SSD) condition rather than being too dry or too wet (Silfwerbrand, 2009). When it is too dry, the substrate absorbs the moisture from the fresh repair material, causing the interface to be heterogenous and form porous zone. Conversely, free water could exist when the substrate surface is too wet and this creates high water/cement (w/c) ratio at the bond interface which is detrimental to the bond strength.

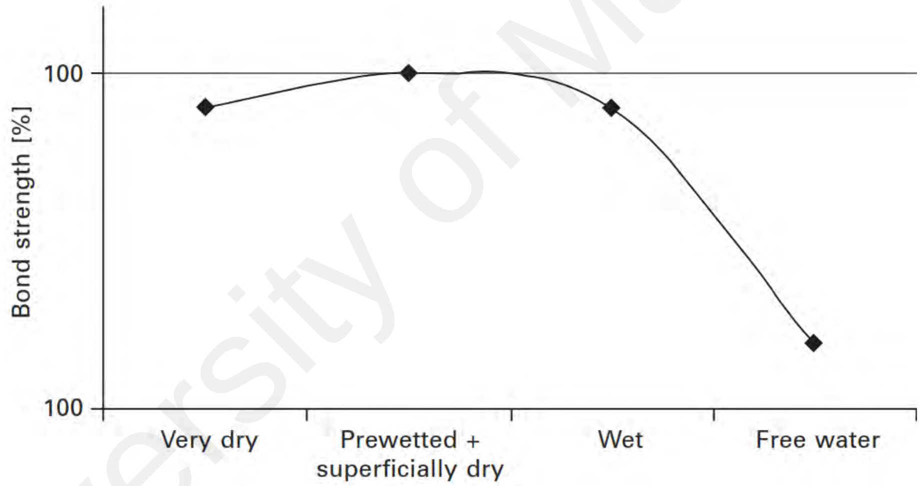

Figure 2.2 Relationship of moisture condition to bond strength between repair material and substrate (Silfwerbrand, 2009).

2.2.2 Structural and mechanical compability

For this compatibility, it is dependent on the application of the repair material whether is for non-structural or structural repair. The requirement for this compatibility is that the mechanical properties of the repair material, namely compression, flexure and tension must exceed the existing substrate material. This requirement is generally set as consideration by engineering standards but the criteria for both non-structural and structural repair are different. For non-structural repair, the mechanical strength requirement is not as stringent as structural repair as stress-carrying capacity is not a major consideration for non-structural repair. Conversely, the requirement for structural repair is more complex and according to Morgan (1996), repair materials with high MOE should be cautious and avoided as excessively high stiffness could cause repaired area to attract undue load.

2.3 Requirement of concrete repair material from engineering standards

To ensure the performance and durability of repair material, minimum requirements have been set up by various engineering standards such as British Standards Institution (BSI), American Society for Testing and Materials (ASTM) International and Florida Department of Transportation (FDOT). According to EN 1504-3, concrete repair material is generally grouped into structural and non-structural (BSI, 2005) which is tabulated in Table 2.1. On the other hand, Section 930 from FDOT (2016) categorizes repair material based on its application for the horizontal and vertical surface as shown in Table 2.2 and Table 2.3. In overall, the minimum requirements are based on the mentioned compatibility.

Table 2.1 Requirement for structural and non-structural repair material (BSI, 2005b).

Performance properties	Requirement			
	Structural		Non-structural	
	Class R4	Class R3	Class R2	Class R1
Compressive strength	≥ 45 MPa	≥ 45 MPa	≥ 15 MPa	≥ 10 MPa
Adhesive bond	≥ 2.0 MPa	≥ 1.5 MPa	≥ 0.8 MPa	

Table 2.2 Minimum requirement of repair material for horizontal surface (FDOT, 2016)

Horizontal surface			
Requirement		Rapid	Very rapid
Compressive strength, MPa	3 hours	N/A	17.3
	24 hours	17.3	34.5
	7 days	34.5	51.8
	28 days	Greater or equal than 7 days	
Mortar flow, %		100	80
Bond strength	24 hours	2.8	3.1
	7 days	Greater or equal than 24 hours	

Table 2.3 Minimum requirement of repair material for vertical surface (FDOT, 2016)

Vertical surface			
Requirement		High performance	Ultra-high performance
Compressive strength, MPa	24 hours	8.6	17.3
	7 days	N/A	43.1
	28 days	43.1	Greater or equal than 7 days
Flexural strength (7 days), MPa		3.4	4.8
Mortar flow, %		100	100
Bond strength	24 hours	3.1	5.2
	7 days	5.2	5.2

2.4 Fibre reinforced cementitious composites

Fibre reinforced cementitious composites (FRCC) is a type of high-performance concrete produced by adding discontinuous short fibres to the cement matrix. As opposed to conventional concrete which is brittle and has localized crack failure, FRCC has superior mechanical properties (tensile and flexural strengths) and ductility which was aided by the ability to exhibit multiple cracking. The function of fibres in the matrix is primarily in the post-cracking stage which induces the fibre-crack interactions, including crack suppression, crack stabilization, crack bridging and fibre-matrix debonding (Bentur & Mindess, 2006). The function of fibre can be schematically shown in Figure 2.3.

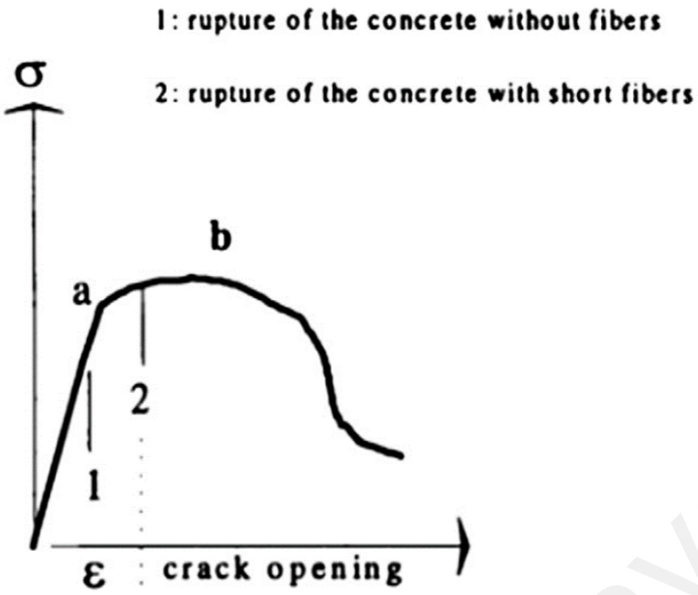

Figure 2.3 Schematic description of short fibre in cementitious composites (Rossi, 2001)

At the pre-cracking stage, the extension of both fibre and the matrix are same. But when cracking happens, the matrix extends more than fibres as stress is built up at the crack tip and through the fibre-matrix interfacial bond, the fibres suppress the matrix to extend more. As a result, the crack initiation stress was increased which also means an increase in the first crack stress. Then, the fibre starts to stabilize the crack by transferring and sustaining the stress from the crack. As cracks widen with increased loading, the fibre will act as a connector bridging across the crack which helps to slow down the rate of crack opening and thus ensuring the integrity of the composite. Ultimately, the bridging fibres will start to debond from the matrix or rupture which result in the failure of the composite.

There are many types of concrete or cementitious material such as polymer modified concrete, fibre reinforced polymer concrete, high early strength mortar, textile reinforced concrete formulated as repair material, however, these repair materials were not substantially benefitted with self-healing ability correspond to FRCC. Also, with the superior enhancement in the mechanical properties and ductility, FRCC shows the potential as repair material. Therefore, many types of research about repair application using FRCC had been done by other researchers (Victor C. Li *et al.*, 2000; X. Li *et al.*, 2017).

2.5 Constituents of FRCC

Basically, FRCC is made of hydraulic cement, mineral admixture, aggregate, discrete, discontinuous fibre, water and superplasticizer.

2.5.1 Cement

Cement is a type of binder which forms a cohesive paste when added with water that can bind all the materials together such as aggregate and fibres to form composites. Also, upon the addition of water, hydration of cement particle takes place and it is exothermic. As illustrated in, illustrated in Figure 2.4, there are 5 phases in hydration process which involve the reaction of tricalcium silicate (C_3S), dicalcium silicate (C_2S), tricalcium aluminate (C_3A) and tetracalcium aluminoferrite (C_4AF) in cement particle (Aïtcin, 2016b). In phase 1 (initial dissolution), the rapid dissolution of different alkali species is highly exothermic and hydration involves C_3S and C_3A which last for a few minutes. which then continue with Phase 2 (induction period) which has low chemical activity and comes with low heat of hydration. Due to the rapid drop in the concentration of silicate, calcium silicate hydrate (CSH) is formed in Phase 2 until they reach a certain critical size that marks the beginning of Phase 3 (acceleration period). Figure 2.4 shows the main peak of heat release due to the dissolution of C_3S and formation of C-S-H and calcium hydroxide (CH). and 4 (deceleration period) where the continuation of hydration of C_3S and C_3A takes place. Lastly, Phase 5 (deceleration period) involves mainly with the hydration of C_2S and C_4AF which induce continuous strength development and densifying process at a low rate.

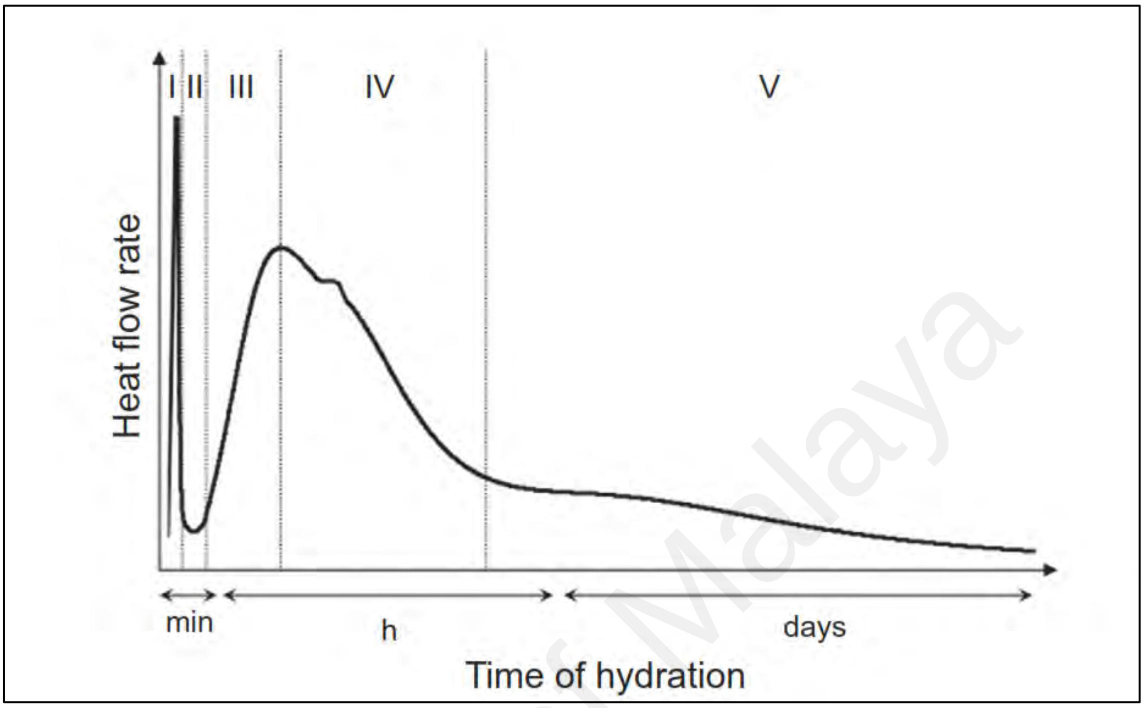

Figure 2.4 Schematic representation of heat release and stage of Portland cement hydration (Marchon & Flatt, 2016).

2.5.2 Supplementary cementitious material

Due to the high surface area of fibres, more paste volume is required to have an easier dispersion of fibre in the matrix. Rather than having high w/b ratio, high binder content is the best way to attain good workability and mechanical properties without compromising the durability and performance of FRCC. Also, the addition of fibres changes the structure of the aggregate skeleton, the packing density is decreased and thus, it requires higher fines content in order to compensate for this effect (Grünewald, 2004). Hence, the binder content used in FRCC is in the range of 800kg/m^3 to 1250kg/m^3 (Said *et al.*, 2015; Sherir *et al.*, 2015). However, when cement content is more than 500kg/m^3, the matrix will be compromised by the rapid high heat of hydration and causing more water required to be hydrated in hardened mortar or concrete which leads to shrinkage cracking (S. X. Wang & Li, 2007). This was also similarly reported by other researchers, whereby high cement content leads to both drying and autogenous shrinkages (Kapelko, 2006; Kosmatka *et al.*, 2011; Yurdakul, 2010). Therefore, in order to reduce the rate and amount of heat of hydration and more environmentally friendly, mineral admixture such as FA, silica fume and slag are used by researchers (J.-K. Kim *et al.*, 2007; Sadrmomtazi *et al.*, 2018; Yu & Leung, 2017). The usage of SCM as cement replacement is reported to be increasing the setting time of concrete due to the less content of C_3A in the mixture of different binder (Dave *et al.*, 2017).

2.5.2.1 Fly ash

Fly ash (FA) is a by-product of the burning of pulverized coal in electric power plant and it consists of silica, alumina, iron and calcium. It is also known as pulverized fuel ash. The particle size of FA varies from 10μm to more than 100μm and in spherical shape. Its surface area is within 300 – 500m^2/kg, specific gravity of between 1.9 – 2.8 and its colour ranges from off-white to light grey. Since the shape of FA is in spherical which is indicated in Figure 2.5, it acts as ball bearing that contributes the lubricating effect in the matrix. Thus, it helps to increase the workability of fresh mortar or concrete and also reduce the water demand in the mixture when in comparison with the same workability (Ikotun *et al.*, 2017; Thomas, 2007).

FA attain pozzolanic reaction which increases the amount of CSH at the expense of CH at later stage which fills up the capillary space in cement. Thus, FA increases the later strength of concrete and enhances durability by reducing its permeability (Thomas, 2007). Other than that, the un-hydrated FA can act as a filler due to its small and smooth spherical shape to densify the fibre-matrix interface (Yu & Leung, 2017) in FRCC. For these reasons, FA is used as supplementary cementitious material in FRCC (C. Lin *et al.*, 2017; S. X. Wang & Li, 2007; Yuan *et al.*, 2013).

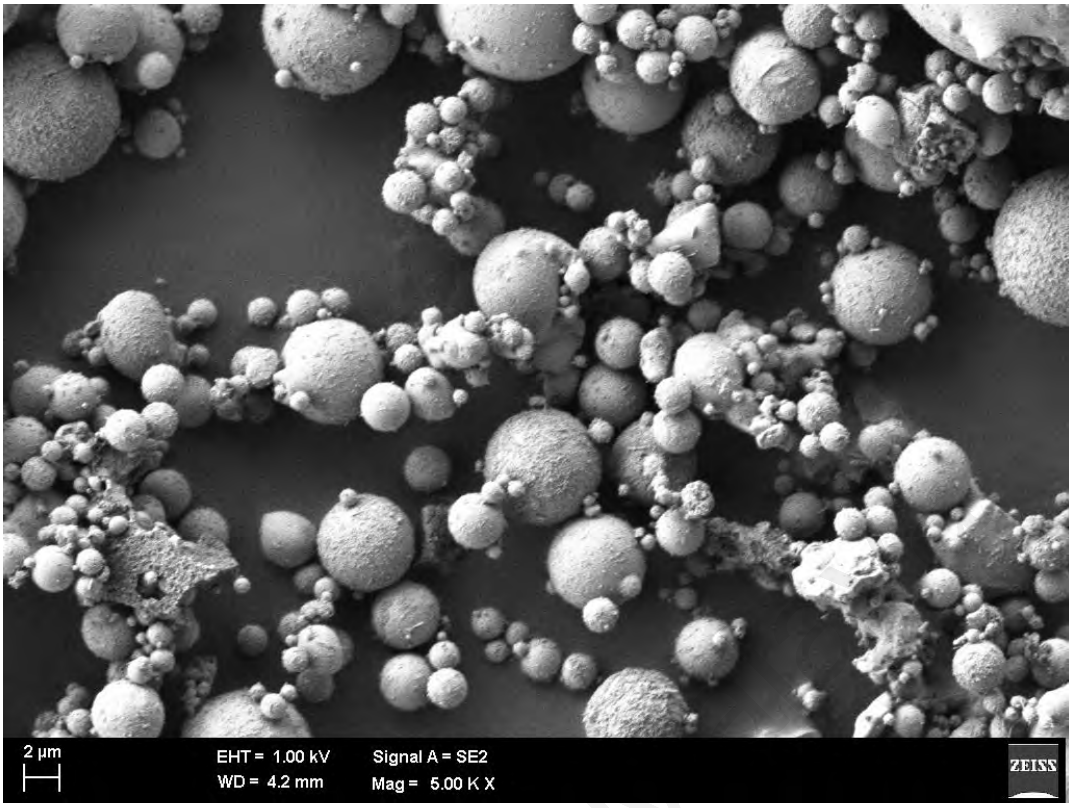

Figure 2.5 Micrograph of FA

2.5.2.2 Ground granulated blast furnace slag

Blast furnace slag is obtained from the by-product in iron and steel industries. Different cooling process blast furnace slag exhibit different behaviour. When it is air cooled, the chemical composition of slag will form crystalline phase which does not have pozzolanic or cementitious property even ground to high fineness. On the other hand, when the silicates and aluminosilicates of calcium-rich molten slag are rapidly chilled, granulated blast furnace slag is produced and it behaves like pozzolan and possesses cementitious properties (Aïtcin, 2016c). In order to be used as a mineral admixture, it is generally ground finer than Portland cement within the range of 10 – 45 microns.

Its glassy surface shown in Figure 2.6 also gives a positive effect on workability that helps to reduce internal friction between the constituting material in concrete and delay chemical reaction. Other than that, GGBS has lower specific gravity than ordinary Portland cement (OPC) which induces more paste volume and less aggregate used which renders better workability (Bilim, 2006). Similar to FA, its pozzolanic reaction helps in improving the later strength and durability of concrete (G. X. Li *et al.*, 2018; Topçu, 2013). Thus, GGBS is accepted to be used as alternate binder in FRCC (J.-K. Kim *et al.*, 2007; Said & Razak, 2015).

Figure 2.6 Micrograph of GGBS

2.5.3 Aggregate

Aggregates generally hold crucial percentage of volume in concrete, and thus it is vital on different aspects of material properties and shrinkage restrain (M. Sahmaran *et al.*, 2009). In FRCC, no coarse aggregate is used as it constrains the matrix toughness of the mortar so that multiple cracking can be formed before reaching maximum bridging stress (S. X. Wang & Li, 2007). Also, the presence of aggregate size larger than fibre causes balling and hinders effective dispersion of fibres which results in poor fibre-matrix interface (De Koker & Van Zijl, 2004). Therefore, as long as the size of aggregate (<2.38mm) do not interfere the dispersion of fibre, the mechanical performance and ductility of FRCC will not be negatively affected (M. Sahmaran *et al.*, 2009).

2.5.4 Superplasticizer

Superplasticizer (SP) is a type of chemical admixture that has the ability to reduce water demand by 30% as compared to normal water reducer which water reduction is in the range of 10% – 15% at a given workability (Ramachandran, 1996). Hence, SP is also known as high range water reducer (HRWR). There are 4 types of superplasticizers, namely lignosulphonates (LS), sulphonated melamine formaldehyde (SMF), sulphonated naphthalene formaldehyde (SNF) and polycarboxylate ether (PCE) (Björnström & Chandra, 2003).

LS is generally regarded as the first generation of SP and it is derived from the by-product of pulp and paper industry (Aïtcin, 2016a). It has the weaknesses of low water reduction effect and high dosage is required in order to increase the water reduction. Other than that, it also causes excessive retardation and air entrainment in concrete. In SMF, it is manufactured from the resinification of melamine – formaldehyde and it is able to provide high initial slump. However, it has poor slump retention, causing SMF to be unsuitable for long-haul applications. On the other hand, from the process of oleum sulphonation, SNF is synthesized through the process of sulphonation of oleum and react subsequently with the formaldehyde to form polymerization. Although SNF is widely used in the world due to low cost, it has compatibility issue with cement. The polymerization of PCE is initiated from the free radical mechanism using peroxide initiators. Among the four types of superplasticizer, PCE is the most effective superplasticizer as it can cause water reduction up to 40% and hence, it is preferred in the production of high or ultra-high-performance concrete where w/b can be as low as 0.2 (P. P. Li *et al.*, 2017). Although PCE is costlier compared with other types of SP, a lower dosage is required to achieve the same workability and ensuring PCE to be cost-effective.

2.5.5 Fibre

Generally, there are two types of fibres used in concrete which are natural and synthetic fibres. Natural fibres are generally categorized into animal based and plant-based fibres. Natural fibres used by researchers in concrete are generally plant based which include bamboo, hemp, straw, bagasse and coconut (Merta & Tschegg, 2013; Reis, 2006; Wahyuni *et al.*, 2014; W. Wang & Chouw, 2017). On the other hand, synthetic fibres are made from metal, polymer and mineral and these fibres are generally manufactured by forming threads through hole extrusion and then chopped into the desired length. For the application in concrete, synthetic fibres are preferred as they have better mechanical properties and chemical resistivity corresponds to natural fibre. The examples of synthetic fibres used by researchers are steel, polypropylene (PP), polyethylene (PE), basalt and polyvinyl alcohol (PVA) fibres (Ezziane *et al.*, 2015; Jiang *et al.*, 2014; Z. Pan *et al.*, 2015; Said & Razak, 2015; Won *et al.*, 2015).

Among the synthetic fibres, PVA fibres are one of the most renowned fibres used in FRCC for research and application. This fibre is made by the polymerisation of vinyl acetate, creating polyvinyl acetate which is then converted into powdered form PVA and extruded as fibres. Other than that, this fibre has unique properties such as high aspect ratio, high tensile strength, high modulus of elasticity, good compatibility with OPC (Choi & Lee, 2015) and relatively low density (1300kg/m^3) compared to cement matrix (2000kg/m^3 – 2500kg/m^3). Also, this fibre has good resistance to chemical attack typically in alkali condition due to the presence of acetate group ($CH_3CO_2^-$) that absorbs calcium hydroxides (M. Li & Li, 2013). For these reasons, PVA fibre induces superior improvement in mechanical properties and ductility of FRCC to correspond to other fibres (Nam *et al.*, 2016; Shafiq *et al.*, 2016).

2.6 Effect of fibre on FRCC

2.6.1 Workability

Generally, the workability of FRCC decreases when added with any type of fibres, (Figueiredo & Ceccato, 2015; M. Li & Li, 2013). According to Bentur and Mindess (2016), there are 3 factors that can affect the workability which are fibre dosage, modulus of fibre and aspect ratio of fibre. When fibre dosage is increased, less lubricant effect from the cement matrix as more cement matrix is used to coat the fibre causing decreasing in workability. This phenomenon can be observed in the research of Figueiredo and Ceccato (2015), where the slump value decreased and Ve-Be time increased when fibre dosage was increased. In the case of fibre modulus, workability of FRCC is lower when the modulus is higher. This is due to the stiffer fibre increases stiffening effect to the concrete mix. However, the stiffening effect can be compensated with vibration and therefore workability test with dynamic effect is more useful (Johnston & Gray, 1978). Aspect ratio is the ratio of fibre length to its cross-sectional diameter and it is important for the fibre-matrix bond. Performance of hardened FRCC can be improved and lower critical fibre volume can be induced by high fibre aspect ratio but also giving a detrimental effect to the workability of FRCC (Bentur & Mindess, 2006). This can be explained by the higher fibre surface area caused by higher aspect ratio fibre which requires more cement matrix to coat the fibre. However, reduction in workability from higher aspect ratio can be compensated by achieving the desired mechanical performance and ductility with less fibre dosage due to lower critical fibre volume.

2.6.2 Compressive strength

Compressive strength is the capacity of a material to sustain compressive load on a certain unit of area. For FRCC, the effect of fibre on compressive strength is controversial as there were different observations made; there were researchers who reported improvement in the compressive strength with certain dosage of fibre addition whereas on the other hand there were findings of lowering compressive strength with fibre addition; insignificant effect was also reported by researchers (Ayub *et al.*, 2014a; Fakharifar *et al.*, 2014; Grantham *et al.*, 2014; Sivakumar & Santhanam, 2007; Yusof *et al.*, 2011). However, this effect varies on different types of fibre and dependent on the workability of FRCC.

Based on the research done by Ayub *et al.* (2014), the effect of fibre volume to compressive strength was insignificant. As listed in Table 2.4, the compressive strength increased until fibre dosage of 2% and then dropped at 3% fibre. The increment in compressive strength could be attributed to the higher modulus of basalt fibre causing the composite to be stiffer and harder. This was due to the 2% of basalt fibre dosage contributed more stiffness than the specimen with 1% fibre dosage. When fibre dosage reached 3%, the workability of fresh basalt-FRC could be insufficient, causing improper compaction and eventually more void is formed. As shown in Figure 2.7, this observation was also reported in steel and alfa fibres by Yusof *et al.* (2011) and Grantham *et al.* (2014).

On the other hand, some researchers observed that fibre has a detrimental effect on compressive strength of FRCC, especially on polymer fibre. Based on previous research, both PVA and polypropylene fibre were reported to reduce the concrete compressive strength which is illustrated in Figure 2.8 (Hossain *et al.*, 2013; A. E. Richardson, 2006). This could be due to the low bond strength between the polymer fibre and cement matrix (A. Richardson, 2005) that causes a break in the calcium silicate hydrate (CSH) bond.

Table 2.4 Mechanical properties of basalt-FRC (Ayub *et al.*, 2014a)

Sample	Compressive strength				Elastic modulus (GPa)	Splitting tensile strength	
	Max strength (MPa)	Percentage increase with respect to P0	Peak strain	Ultimate strain		Max strength (MPa)	Percentage increase with respect to P0
P0	71.87	-	2412	14630	40.76	5.26	-
P1	73.52	2.29	2781	19512	42.01	5.40	-4.78
P2	74.16	3.19	2832	18335	41.88	5.52	-2.24
P3	65.08	-9.45	2969	16662	42.54	6.00	8.62

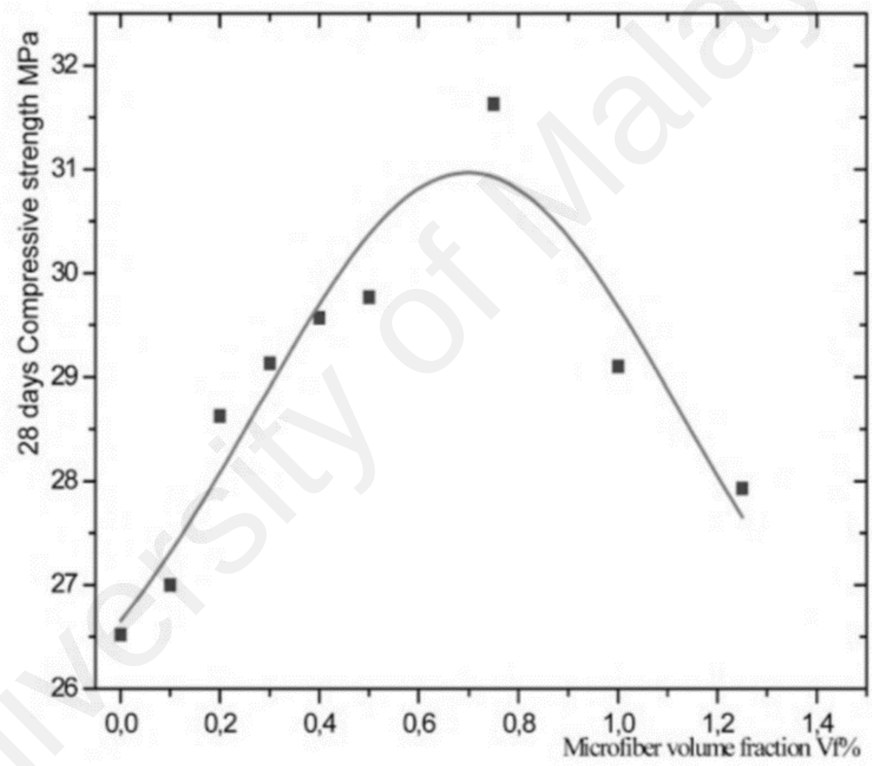

Figure 2.7 Compressive strength of Alfa fibre with different fibre dosage (Grantham *et al.*, 2014).

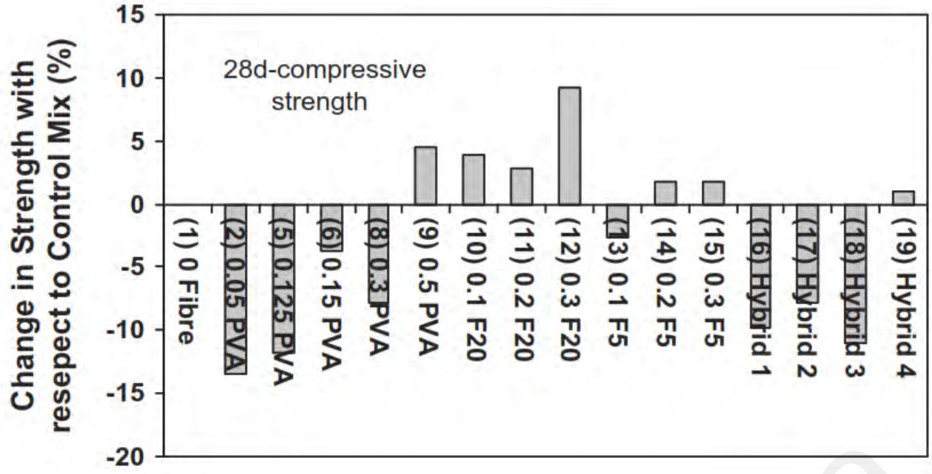

Figure 2.8 Compressive strength of concrete including PVA, steel and hybrid fibres (Hossain *et al.*, 2013)

2.6.3 Tensile strength

When fibre is added, the tensile load sustained by the brittle matrix is transferred to the fibre which helps to increase the tensile strength of the composite. Commonly, previous researchers showed that fibre improves tensile strength and tensile capacity of concrete (Ayub *et al.*, 2014b; Yusof *et al.*, 2011) and it is correlated to the fibre dosage and length of the fibre. Figure 2.9 and Figure 2.10 show the increment in fibre dosage provides higher tensile strength until certain dosage. As reported by previous research, the increment of fibre in the cement matrix able to sustain more tensile loading, resulting in higher tensile strength. However, Yusof *et al.* (2011) reported that as the fibre dosage reached 2%, the tensile strength decreased and this can be explained as high fibre dosage hinders good workability which resulted in ineffective fibre dispersion and cracks bridging. Yusof *et al.* (2011) also found out that longer fibre provides better tensile strength in FRCC. As observed in Figure 2.10, the tensile strength increased until the percentage of long fibre reached 70% as this was the most optimum ratio of long to short fibre.

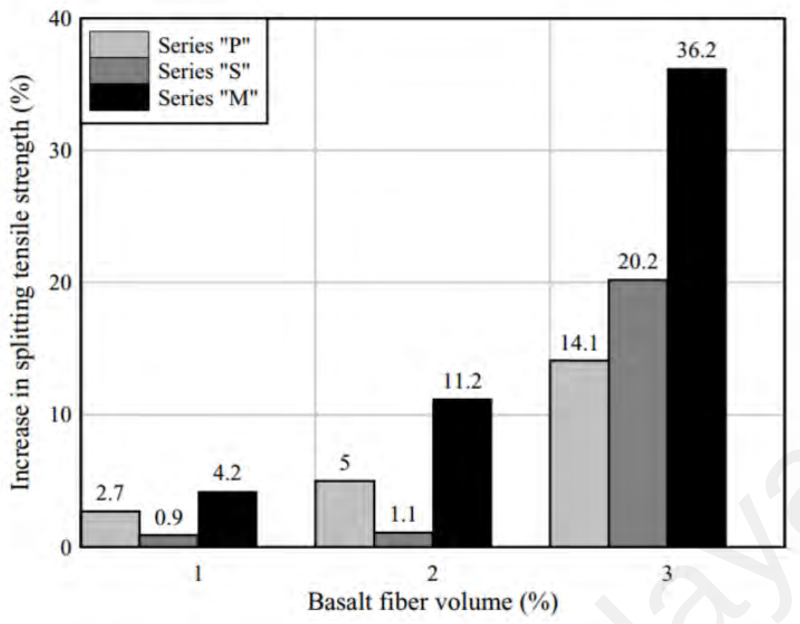

Figure 2.9 Splitting tensile strength of Basalt-FRCC (Ayub *et al.*, 2014b).

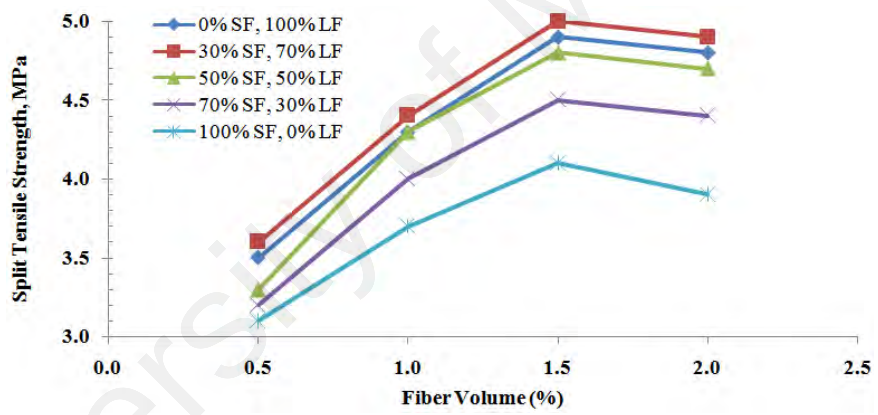

Figure 2.10 Cementitious composite reinforced by long and short steel fibres (Yusof *et al.*, 2011)

However, there is a crucial factor which outweighs the tensile strength of fibre and it is known as the orientation efficiency factor of fibres (Bentur & Mindess, 2006). When the fibre is mixed with the cement matrix, it is assumed that the fibre is randomly orientated and the tensile strength of the fibre varies at different inclination angles. This can be supported by the result of single PVA and basalt fibre pull-out test conducted by Choi *et al* (2015) details in Table 2.5. Although basalt fibre has higher tensile strength than PVA fibre, the strength reduction coefficient which is correlated to the orientation efficiency factor is higher than PVA fibre. Thus, it can be deduced that fibre bridging capacity of PVA fibre is better than basalt fibre.

Table 2.5 Tensile strength of PVA and basalt fibres at different inclination angle (Choi & Lee, 2015)

Fibre	Average fibre tensile strength (MPa)				Strength reduction coefficient
	0^{o}	30^{o}	45^{o}	67.5^{o}	
PVA	1202 ± 132	1114 ± 182	1025 ± 223	1003 ± 161	0.171
Basalt	1773 ± 349	871 ± 247	715 ± 268	302 ± 219	1.535

2.6.4 Flexural behaviour

Generally, it is well known that flexural strength can be improved by adding fibre. When fibre is included in concrete, part of the loading is distributed to the fibre which causes concrete to sustain higher flexural loading and the improvement is correlated with the fibre dosage. This phenomenon can be observed in Figure 2.11 that shows the improvement of flexural strength increases with fibre dosage. According to Pakravan *et al.* (2017), the increase of ultimate flexural strength of FRCC is due to the formation of good chemical bonding between PVA fibres with cement matrix. At higher fibre content, the magnitude of chemical bond is higher. However, the enhancement effect dropped at 3% fibre volume fraction because high fibre dosage induces lower workability which results in the ineffective dispersion of fibre. Nevertheless, the flexural strength of specimens with overdosed fibre volume still has higher flexural strength than concrete without fibre.

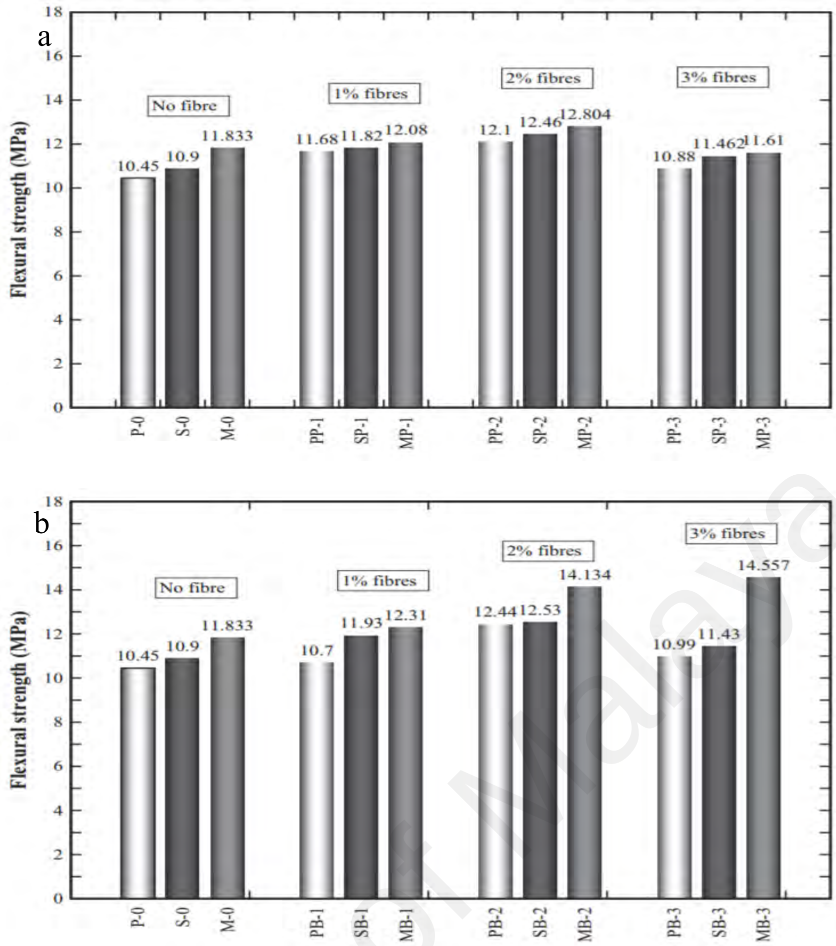

Figure 2.11 Flexural strength of FRCC with different fibre dosage: a) PVA fibre b) basalt fibre (Shafiq *et al.*, 2016)

As conventional concrete cracks and fails instantaneously when loading exceeds its flexural strength, fibres continue to sustain loads by transferring stresses and loads across cracks which help in delaying the failure of composites. This flexural behaviour induced from the inclusion of fibre is known as deflection hardening and softening, as shown in the load-deflection curve in Figure 2.12. To achieve deflection hardening in bending, the bending moment of resistance at the first crack in bending must be greater than the moment resistance in the post-cracking zone (Bentur & Mindess, 2006) and deflection hardening is more beneficial when it comes to energy absorption capacity to a given deflection (Shaikh, 2013). There are a few factors that will determine the flexural behaviour, including fibre volume, mechanical properties and chemical bond of fibre. In order to obtain strain hardening or deflection hardening in FRCC, the fibre content must exceed the critical fibre volume to provide sufficient volume of fibres to sustain the load and bridge the cracked matrix effectively (Bentur & Mindess, 2006). Therefore, to fully enhance the performance of FRCC, the fibre dosage must exceed the critical fibre volume. On the other hand, mechanical properties of fibres, especially in modulus of elasticity, is one of the most crucial properties. When fibre has lower modulus than cement matrix (10 – 45 GPa), dowel action is allowed to take place after first cracking as there was more flexibility for the fibres to bridge across the crack and jamming effect happens inside the matrix, causing slip or deflection hardening of fibre in matrix (Redon *et al.*, 2001). Contradictorily, high modulus fibre is stiff and local flexural stress will be built up in the fibre which superimposed on the axial tensile stress that may cause deterioration of fibre after cracking occurs. As a result, deflection softening happens. However, as illustrated in Figure 2.13 and Figure 2.14, Said & Razak (2015) tested that cementitious composites reinforced with both low and high modulus polyethylene fibre (39 GPa & 82 GPa) could still show deflection hardening behaviour while Pakravan *et al.* (2016) reported that polypropylene fibre induced deflection softening due to low modulus of elasticity (4 GPa).

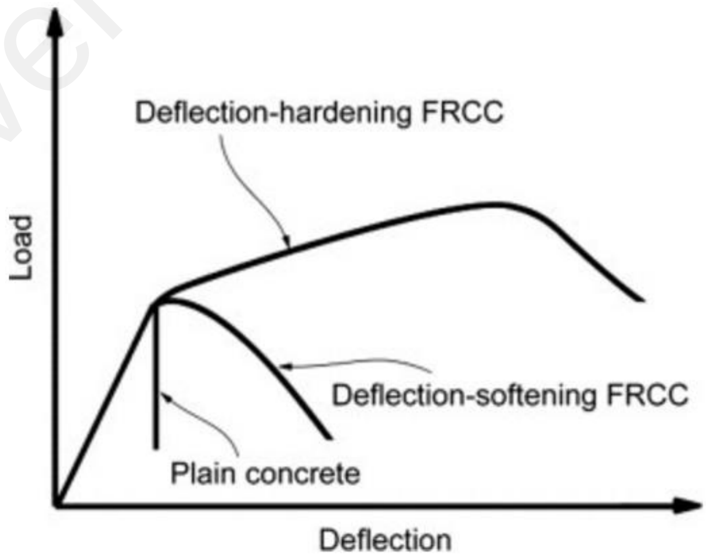

Figure 2.12 Typical load-deflection curve of FRCC in bending (C. Lin *et al.*, 2014)

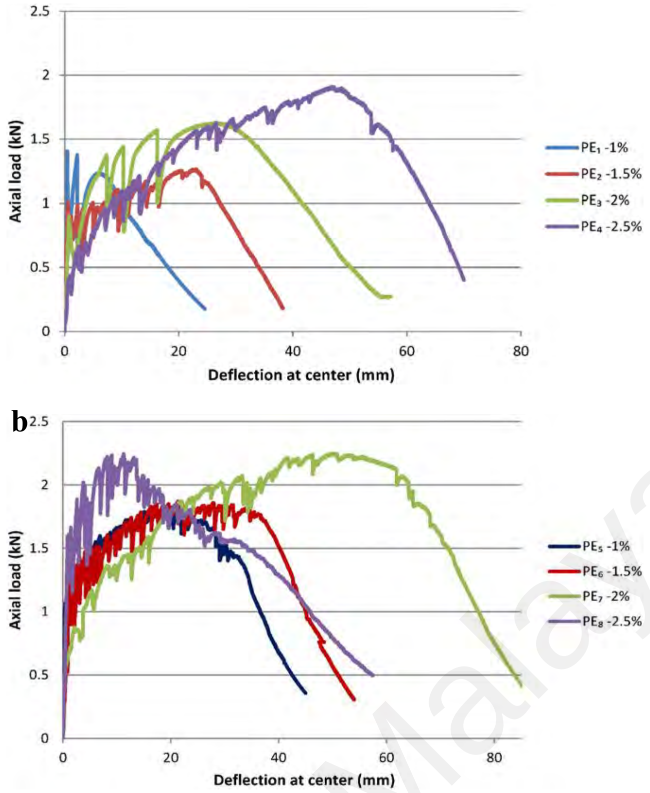

Figure 2.13 Load-deflection curve of cementitious composites reinforced with PE fibre. a) low modulus b) high modulus (Said & Razak, 2015)

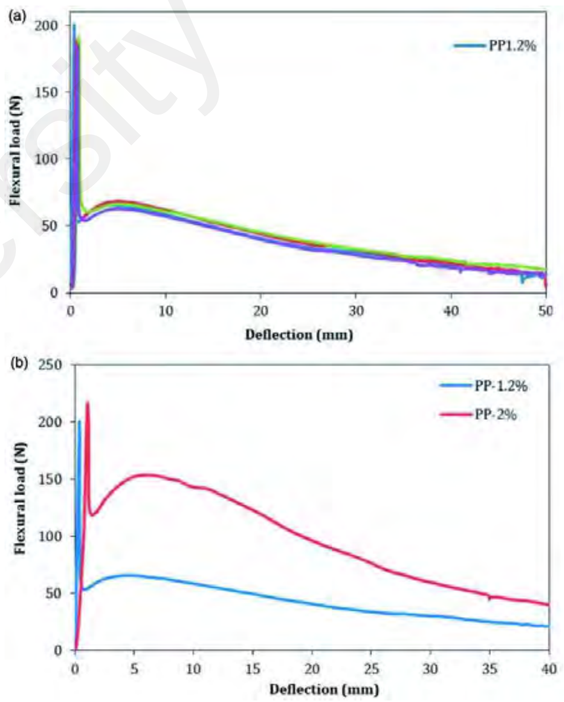

Figure 2.14 Load-deflection curve of cementitious composites reinforced with PP fibre (Pakravan *et al.*, 2016)

Additionally, the load-deflection curve is related to the energy absorption of FRCC as it is obtained by calculating the area under the curve where it is the dissipation of energy from flexure loading through debonding and pull-out of fibres during cracks bridging (Bentur & Mindess, 2006; Yoo *et al.*, 2013). Therefore, good post cracking load with high displacement induced by deflection hardening gives high energy absorption. Based on previous researches, energy absorption is dependent on fibre dosage and fibre-matrix chemical bond. By referring to the load-deflection curve at Figure 2.13a and Figure 2.14, the area under load-deflection curves was larger with increasing fibre dosage. This could be due to higher fibre dosage which could sustain more load and exhibit better crack control. However, when observing the curve at Figure 2.13b, the stiffer PE fibre had a negative influence at 3% dosage. This might be due to the more intense stiffening effect from the higher modulus PE fibre, causing ineffective fibre dispersion at high dosage. This was similarly reported by Pakravan *et al*. (2018). Conversely, higher fibre-matrix chemical bond causes rupture of fibre which causes less ductility compare to fibre pull-out (Redon *et al.*, 2001). For higher chemical absorption or better ductility, it is better for fibre to exert pull-out rather than rupture (Z. Lin & Li, 1997). By comparing the load-deflection curve of Figure 2.15, the curve exerted by PVA fibre had lower displacement than PP fibre's load-deflection curve. This can be explained by the fact that PVA fibre is hydrophilic whereas PP fibre is hydrophobic in nature. The hydrophilic properties, the hydroxyl group from PVA fibre provides a stronger fibre-matrix interfacial bond.

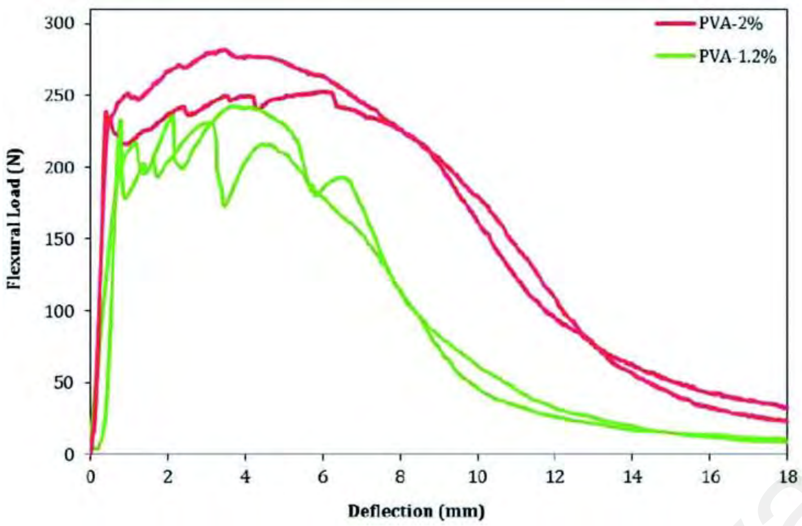

Figure 2.15 Load-deflection curve of cementitious composites reinforced with PVA fibre (Pakravan *et al.*, 2016)

2.6.5 Bonding with concrete substrate

There are many ways to test the bonding of repair system, namely slant shear strength, pull-off test, direct shear test and splitting tensile (Austin *et al.*, 1995, 1999; Gerges *et al.*, 2015; Momayez *et al.*, 2005; Mustafa Sahmaran *et al.*, 2013; G Yıldırım *et al.*, 2015). Among all the methods, the failure mode of the specimen using conventional high strength mortar or micro-silica concrete consistently happen at the interface. However, this did not occur on FRCC-concrete substrate repair system. Also, the design of FRCC requires high amount of binder content it is expected that the bonding between FRCC and the substrate is more superior than certain type of repairing material such as high strength mortar or micro-silica concrete (MSC).

One of the research done by Mustafa Sahmaran *et al.* (2013) was to compare the bond between concrete substrate with engineered cementitious composites (ECC). 2 types of ECC were used, namely F_ECC and S_ECC. The cementitious material used in F_ECC comprised of cement (566 kg/m^3) and FA (680 kg/m^3); whereas cement (593 kg/m^3) and GGBS (712 kg/m^3) was used in S_ECC. Slant shear test was conducted in compliance with ASTM C882, using 100 mm diameter x 200 mm height composite cylinder. The test result tabulated in Table 2.6 shows ECC has better bonding after 7 days and 28 days, whereas MSC was stronger at 1st day. Explanation was given by Sahmaran *et al.* (2013) that ECC used a high amount of mineral admixture, and hence the maturity of ECC was not as good as MSC during 1st day. Other than that, it was found that the bond strength of S_ECC was better than F_ECC, which was due to the hydration and pozzolonic reaction of GGBS was better than FA during the testing age. The most significant advantage of ECC compared to MSC was the failure mode. All specimens in the composite cylinder of ECC only failed at the substrate whereas composite cylinder of MSC experienced interface failure and monolithic rupture.

Table 2.6 Slant shear strength result and failure mode (Mustafa Sahmaran *et al.*, 2013)

Mixture	Bond strength (MPa)			Failure mode
	1 day	7 day	28 days	
F_ECC	7.1	14.7	21.7	Through substrate
S_ECC	8.3	17.4	24.3	Through substrate
MSC	10.4	14.1	15.6	Slanted interface and monolithic rupture

Another testing method used by G Yıldırım *et al.* (2015) in their research about comparing market available repair material (REP) with high early strength ECC (HES-ECC) was direct pull-off test which measures tensile bond. Based on their finding, HES-ECC had slightly better (maximum 30%) tensile bond strength than REP and it was not significant. However, when focusing on the failure mode in Figure 2.16, HES-ECC outperformed the market available repair material as the specimens failed at substrate, unlike REP which failed at the interface.

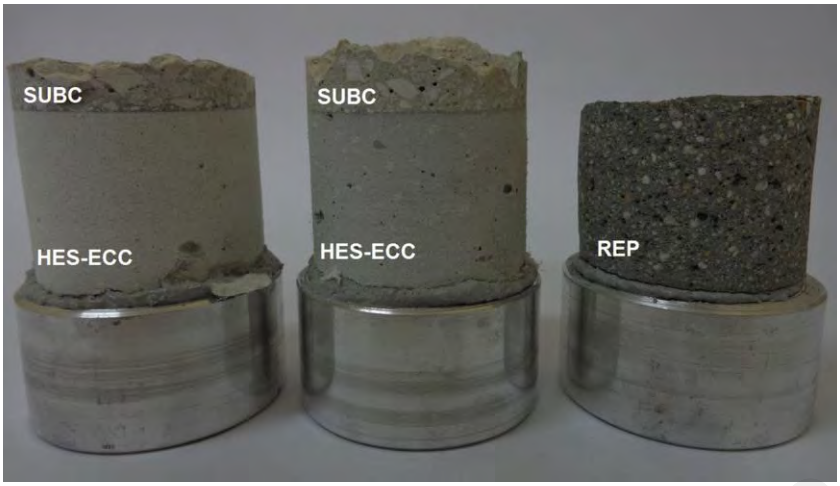

Figure 2.16 Failure modes of HES-ECC and REP specimens after 28 days using direct pull-off test (G Yıldırım *et al.*, 2015)

2.7 Research Gap

Research on FRCC in repairing application has been conducted since year 1997. In general, the repair application is not only limited to structural repair such as reinforced concrete (RC) structure repair, but also non-structural such as overlay and highway repair. Most of the FRCC mixture requires high binder content in order to have sufficient bonding with high volume of fibre. Therefore, Supplementary Cementitious Materials (SCM) were frequently used to partially replace OPC in the research of FRCC for environmental friendly purposes (X. Li, Wang, Bao, & Chen, 2017) and to enchanced the properties of FRCC (Kim, Fischer, Lim, & Li, 2004; Sahmaran, Yücel, Yildirim, Al-Emam, & Lachemi, 2013). Table 2.7 shows the summary of past research on FRCC with different binder combination for repair applications.

The commonly used SCM in FRCC are FA, GGBS, SF and calcium aluminate cement (CAC). There are several reasons in selecting the suitable SCM in the mix design of FRCC. Chen *et al.* (2018) used SF with OPC to develop ultra-high performance repair material with compressive strength higher than 130 MPa. On the other hand, calcium aluminate cement (CAC) was used by Y. Y. Kim *et al.* (2004) to decrease the setting time of FRCC for shotcrete application. Furthermore, FRCC with the use of OPC and GGBS as binder attained larger average bond strength than specimens with OPC and FA or SF (Sahmaran et al., 2013). Sahmaran et al. (2013) found out that GGBS enhance the early and ultimate strength (28 days and 90 days) of FRCC more than FA and even SF. This triggers the interest of using GGBS as binder in this research as good bonding strength with substrate as one of the main requirements for repair materials to perform properly and long lasting. Besides that, the previous research done was more into specific repair application, but the parametric studies on the effect of types of binder were less focused. Therefore, this research will be focusing on investigating the effect of ternary blended binder (OPC, FA and GGBS) on the mechanical properties and flexural perfornace of PVA FRCC which can be used as repair materials.

Table 2.7 Past research on FRCC for repair application

Researcher	Application	Binder content[1]	Binder used	Fibre
Lim and Li (1997)	Old infrastructure repair	1180	OPC, FA and silica fume (SF)	PE
Victor C. Li *et al.* (2000)	Repair and retrofit	Not stated	OPC and SF	PE
Victor C Li (2004)	RC repair	1320	OPC and FA	PVA
Y. Y. Kim *et al.* (2004)	Shotcrete repair application	1260	OPC, FA and CAC	PVA
M. Li and V. C. Li (2011)	Repair	Not stated	OPC (Type III)	PVA
Mustafa Sahmaran *et al.* (2013)	Overlay repair	1246	OPC and FA	PVA
		1305	OPC and GGBS	PVA
Muzenski *et al.* (2015)	Highway repair	Not stated	OPC	PVA
(X. Li *et al.*, 2017)	RC repair	1250	OPC and FA	PVA
Chen *et al.* (2018)	RC structure corrosion repair	1100 - 1600	OPC and SF	PE
Hou *et al.* (2019)	RC structure corrosion repair	1305	OPC, FA and SF	PVA

[1] Calculated based on given mixture proportion from literature

CHAPTER 3: METHODOLOGY

3.1 Introduction

This chapter comprises of the following items: 1) program flow of the research; 2) procedure of mixing and curing method; 3) material used and; 4) method of statement in the conducted test in fresh and hardened FRCC.

3.2 Experimental work

The experimental work was divided into two phases which are Phase I and II. The details of the process on both phases are illustrated in the flowchart shown in Figure 3.1.

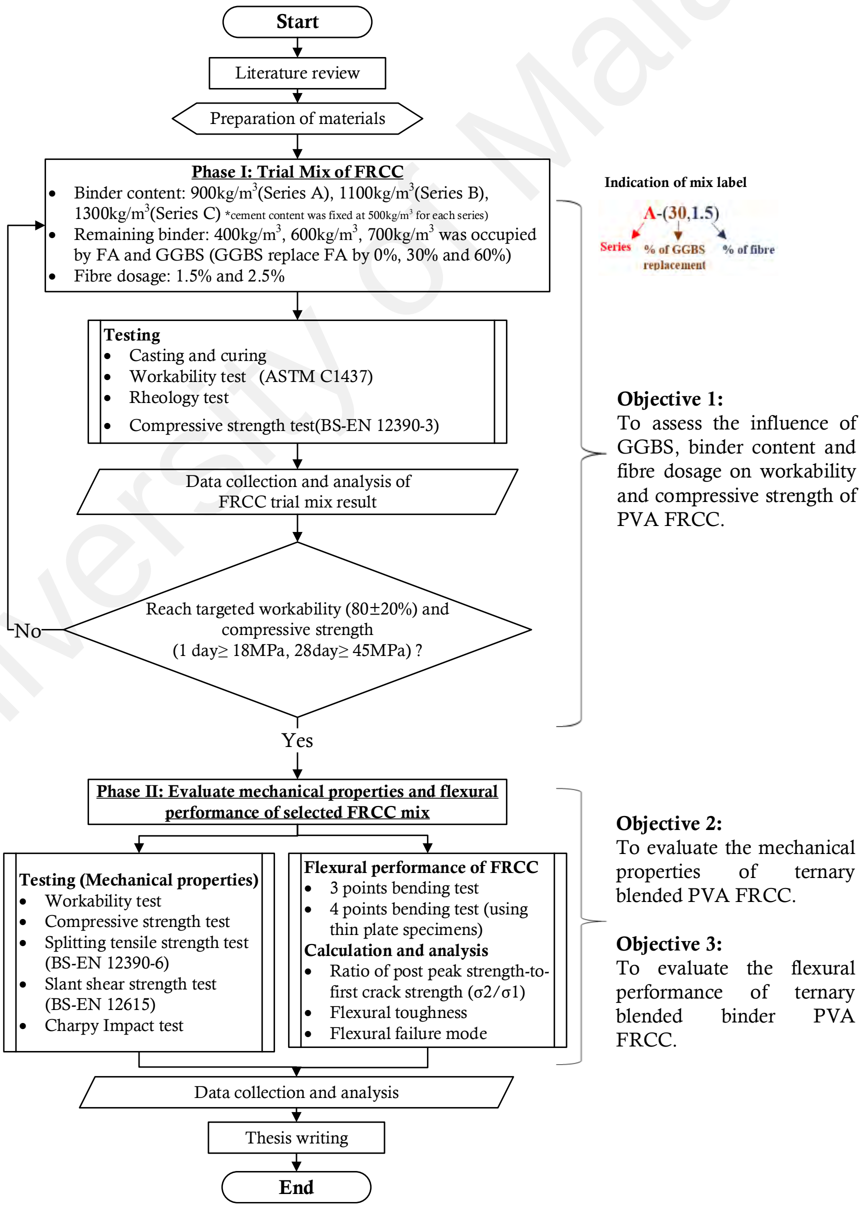

Figure 3.1 Flowchart for work plan

3.2.1 Phase I

This phase focused on the trial mixing of mortar and FRCC with targeted compressive strength (as stated in Table 2.2 and Table 2.3) of 18 MPa in 1 day and at least 45 MPa at 28th day together with flow (80 ± 20%). In the trial mixing process, different parameters namely binder content, percentage of FA replacement with GGBS and PVA fibre dosage were used. The binder content was fixed at 900kg/m^3 (Series A), 1100kg/m^3 (Series B) and 1300kg/m^3 (Series C) but using fixed cement content at 500kg/m^3. This fixed cement content was to lower the matrix toughness and autogenous shrinkage as high cement content induced higher shrinkage strain (M. Li & V. Li, 2011). The remaining binders are either FA or GGBS, it can be fully FA (0% GGBS) or partially replaced with GGBS at a percentage of 30% and 60% as illustrated in Figure 3.2. Lastly, the PVA fibres are dosed at 0%, 1.5% and 2.5%. The detailed proportion ratio of the FRCC mixture can be referred in Table 3.1 and Table 3.2 holds the information of the tests conducted in this phase. The mixtures that had fulfilled the minimum criteria would be selected and continued in Phase II.

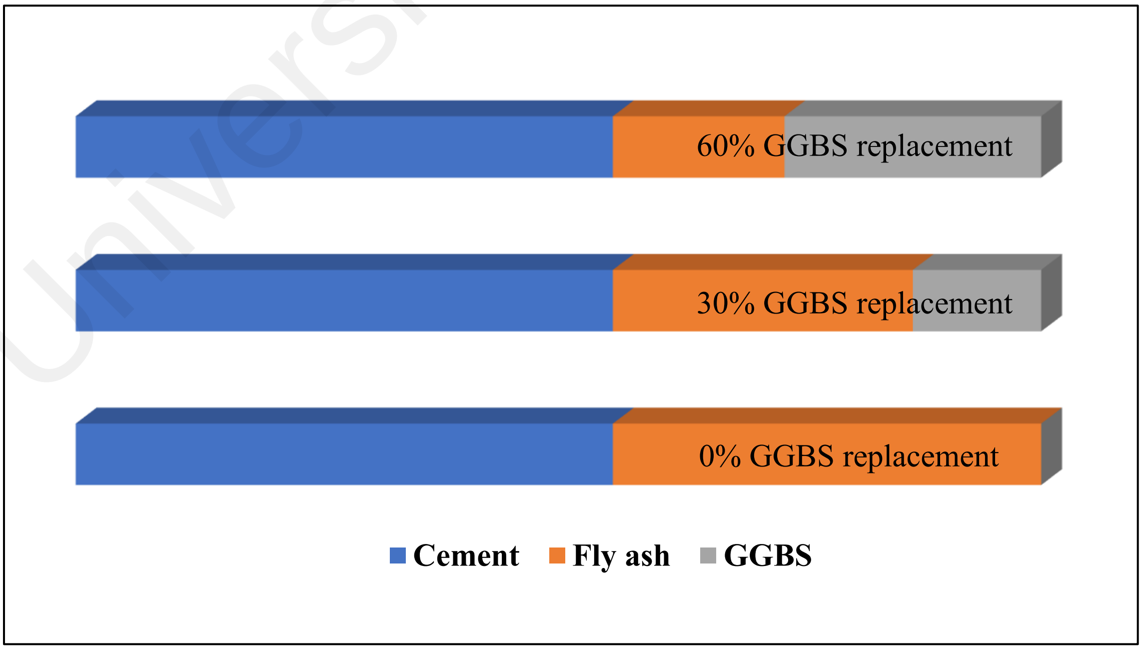

Figure 3.2 Overview of GGBS replacement

Table 3.1 Proportion ratio of mortar and FRCC

Series	Mix[2]	Cement	FA	GGBS	Water	Sand	Fibre, %	SP[3], %
A (900kg/m^3)	A-(0,0.0)	0.56	0.44	0.00	0.28	1.19	0.0	0.65
	A-(0,1.5)	0.56	0.44	0.00	0.28	1.15	1.5	0.65
	A-(0,2.5)	0.56	0.44	0.00	0.28	1.12	2.5	0.65
	A-(30,0.0)	0.56	0.31	0.13	0.28	1.21	0.0	0.65
	A-(30,1.5)	0.56	0.31	0.13	0.28	1.17	1.5	0.65
	A-(30,2.5)	0.56	0.31	0.13	0.28	1.14	2.5	0.65
	A-(60,0.0)	0.56	0.18	0.27	0.28	1.23	0.0	0.65
	A-(60,1.5)	0.56	0.18	0.27	0.28	1.19	1.5	0.65
	A-(60,2.5)	0.56	0.18	0.27	0.28	1.16	2.5	0.65
B (1100kg/m^3)	B-(0,0.0)	0.45	0.55	0.00	0.28	0.65	0.0	0.35
	B-(0,1.5)	0.45	0.55	0.00	0.28	0.62	1.5	0.35
	B-(0,2.5)	0.45	0.55	0.00	0.28	0.59	2.5	0.35
	B-(30,0.0)	0.45	0.38	0.16	0.28	0.68	0.0	0.35
	B-(30,1.5)	0.45	0.38	0.16	0.28	0.64	1.5	0.35
	B-(30,2.5)	0.45	0.38	0.16	0.28	0.62	2.5	0.35
	B-(60,0.0)	0.45	0.22	0.33	0.28	0.70	0.0	0.35
	B-(60,1.5)	0.45	0.22	0.33	0.28	0.67	1.5	0.35
	B-(60,2.5)	0.45	0.22	0.33	0.28	0.64	2.5	0.35
C (1300kg/m^3)	C-(0,0.0)	0.38	0.62	0.00	0.28	0.22	0.0	0.25
	C-(0,1.5)	0.38	0.62	0.00	0.28	0.20	1.5	0.25
	C-(0,2.5)	0.38	0.62	0.00	0.28	0.18	2.5	0.25
	C-(30,0.0)	0.38	0.43	0.18	0.28	0.30	0.0	0.25
	C-(30,1.5)	0.38	0.43	0.18	0.28	0.27	1.5	0.25
	C-(30,2.5)	0.38	0.43	0.18	0.28	0.25	2.5	0.25
	C-(60,0.0)	0.38	0.25	0.37	0.28	0.33	0.0	0.20
	C-(60,1.5)	0.38	0.25	0.37	0.28	0.30	1.5	0.20
	C-(60,2.5)	0.38	0.25	0.37	0.28	0.28	2.5	0.20

Table 3.2 Information of test conducted in Phase I

No.	Test	Specimen type	Testing age		
			1	7	28
1	Workability	Fresh FRCC	-	-	-
2	Rheological	Slurry	-	-	-
3	Compressive strength	Cube (50 mm x 50 mm x 50 mm)	3	3	3

[2] [Series]-([percentage of GGBS replacement], [fibre dosage])

[3] Dosed by weight of the binder

3.2.2 Phase II

This phase was the continuation of the mixtures (Table 3.3) that had fulfilled the minimum requirement stated in Phase I (Section 3.31). These mixtures were analysed with more extensive tests listed in Table 3.4 such as compressive, flexural, splitting tensile and slant shear strength tests. Two flexural strength tests were conducted where one was in accordance to engineering standard whereas the other was to assess the flexural performance that is related to thin overlay application. Microstructure analysis was performed by using Scanning Electron Microscope (SEM) to further support the analysis of results.

Table 3.3 Information of FRCC mix in Phase II

Mix selected from Phase I
A-(30,1.5)
B-(0,1.5)
B-(30,1.5)
B-(60,1.5)
C-(30,1.5)
C-(60,1.5)

Table 3.4 Information of test conducted in Phase II

No.	Test	Specimen type	Dimension	Testing age			
				1	7	28	56
1	Compressive strength	Cube	50 mm x 50 mm x 50 mm	3	3	3	3
2	Splitting tensile strength	Cylinder	100 mm ϕ x 200 mm	-	-	3	-
3	Flexural strength (3-point bending)	Prism	160 mm x 40 mm x 40 mm	-	-	3	-
4	Flexural strength (4-point bending)	Panel	500 mm x 75 mm x 16 mm	-	-	3	-
5	Slant shear strength	Prism	160 mm x 40 mm x 40 mm	3	3	3	-
6	SEM imaging	-	-	-	-	-	-

3.3 Material used

3.3.1 Binder

In this research, the binder shown in Figure 3.3 was CEM I grade 52.5 N ordinary Portland cement (OPC), fly ash (FA) and ground granulated blast furnace slag (GGBS). The properties of the used binder were tabulated in Table 3.5.

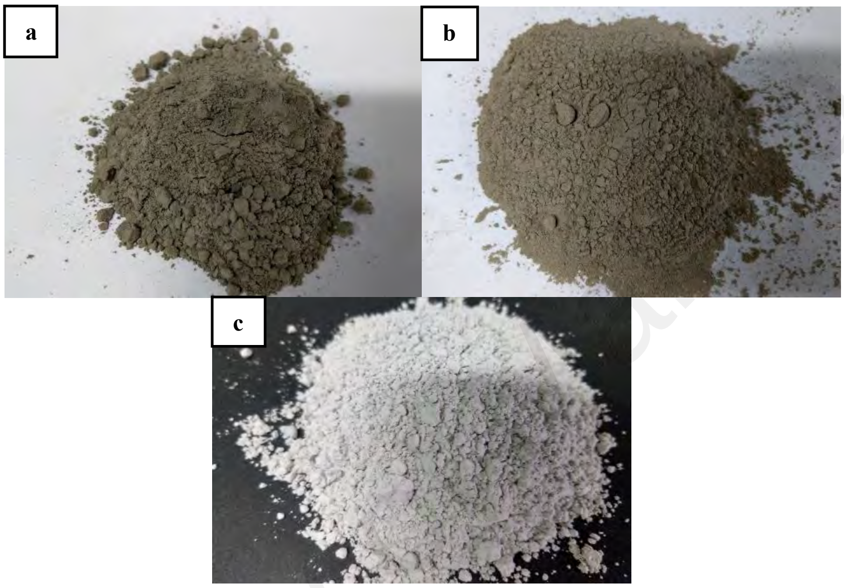

Figure 3.3 Cementitious material: a) OPC; b) FA; c) GGBS

Table 3.5 Properties of OPC, FA and GGBS (as provided by manufacturer)

Properties	Value		
	OPC	FA	GGBS
Fineness, m^2/kg	346	385	477
Moisture content, %	0.36	0.32	0.43
Specific gravity	3.15	2.50	2.89
LOI, %	1.26	1.02	1.41
SiO_2, %	18.96	53.62	36.33
Al_2O_3, %	4.98	26.32	12.57
Fe_2O_3, %	4.76	7.56	0.56
CaO, %	66.56	8.65	38.48
MgO, %	0.96	1.50	7.28
SO_3, %	2.65	0.72	1.86
Total alkali, %	0.71	0.71	0.43

3.3.2 Silica sand

Silica sand with maximum size of 1.18 mm was used as the fine aggregate for fibre reinforced cementitious composites (FRCC) and its particle size distribution was indicated in Figure 3.4. The silica sand is oven dried and kept inside a sealed container to maintain its moisture content.

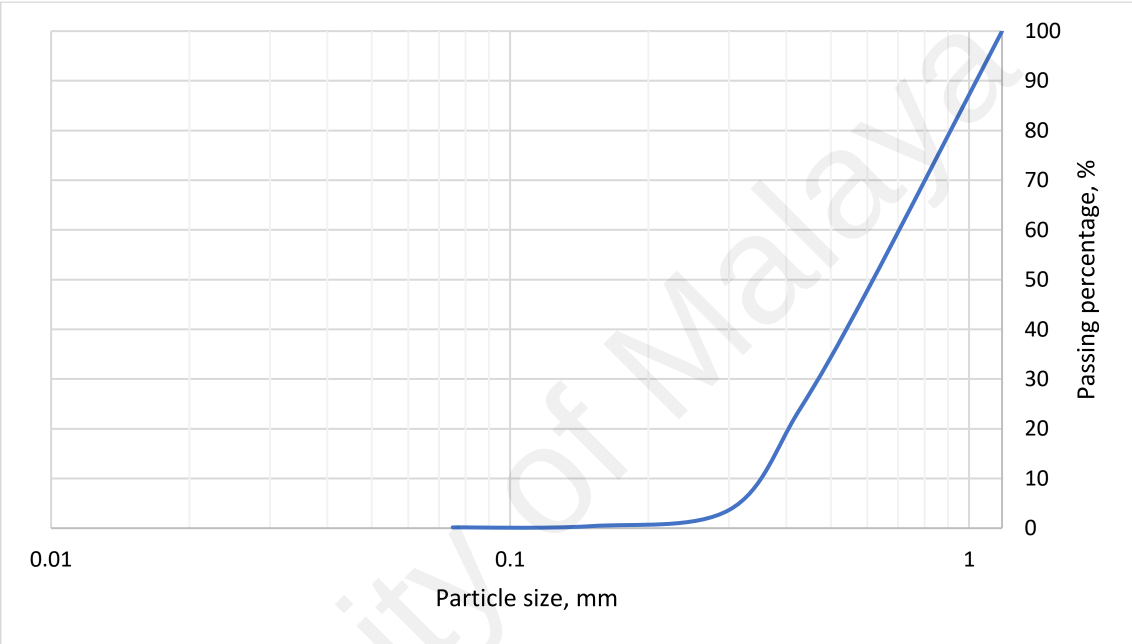

Figure 3.4 Grading of silica sand

3.3.3 Water

The water used is obtained from the tap water. To ensure the purity of the water, a water filter is installed in the lab and thus the water is free from any impurities so that the mechanical strength of the FRCC is not affected.

3.3.4 Superplasticizer

The superplasticizer (SP) used in this experiment was Sika Viscocrete-2044. It is used to reduce the amount of water and produce the desired workability for mixing the fibre with the matrix. It is yellowish-brown liquid and it is polycarboxylate-based SP. It can be premixed with gauging water or straight added to the mixture. The percentage of SP in this research was adjusted accordingly to achieve the targeted workability or before significant bleeding occurs.

3.3.5 Polyvinyl alcohol fibre

The polyvinyl alcohol (PVA) fibre used shown in Figure 3.5 and its properties are tabulated in Table 3.6. The dosage of fibre was fixed at 1.5% and 2.5% to the volume of mortar by aggregate replacement throughout the experiment.

Figure 3.5 PVA fibre

Table 3.6 Properties of PVA fibre used (as provided by manufacturer)

Properties	Value
Tensile strength	1.3GPa
Modulus of elasticity	41GPa
Length	13mm
Diameter	40µm
Colour	White
Aspect ratio	300

3.4 Casting, curing and testing

The materials were mixed in a mortar-mixing machine and procedure shown below was used to produce FRCC:

i. Dry mixing of powder material (OPC, FA, GGBS and silica sand) for 1 minute.

ii. Addition and mixing of liquid material (water and SP) in low revolution for 1 minute and high revolution for 1 minute.

iii. Addition and mixing of PVA fibres until the mixture is homogenous and no balling of fibre is observed.

The fresh FRCC was then casted into oiled steel moulds and stored in a sealed room within 24 hours until demould. Then, the specimens were cured in a water tank until testing age.

3.5 Fresh Fibre Reinforced Cementitious Composites

3.5.1 Flow test

The workability test conducted for FRCC was the flow table test. This test was conducted by referring the standard ASTM C1437 (ASTM, 2007). The apparatus used is a truncated conical mould with 60 mm in height and diameter of 100 mm at the bottom and 70 mm at the top, a flow table, trowel, tamper and Vernier calliper. The principle of this test is measuring the mean diameter of the fresh mortar or FRCC on a flow table disc inside a defined mould and delivers vertical impacts by raising the flow table and free fall at a given height.

The procedure of determination of flow starts with moistening the flow table and placing the mould at the centre. About 25 mm thick of fresh FRCC layer was placed in the mould and tamped for 20 times for uniform filling. The process continued until the mould was fully occupied. The excess FRCC was cut off to a plane surface and the mould is lifted. Twenty-five strokes were applied in 15 seconds and the diameter of the spread mortar was measured by using Vernier calliper. The percentage value of the spread was calculated by using Equation (3.1)

$$A = \frac{average\ of\ 2\ readings - original\ inner\ base\ diameter}{original\ inner\ base\ diameter} \times 100 \qquad \textbf{(3.1)}$$

Where,

A = Flow, in %

3.5.2 Rheology test

The rheological properties of the cementitious matrix such as plastic viscosity and shear stress were measured using Anton Paar's modular compact rheometer as shown in Figure 3.6 at controlled shear rate or angular velocity. Generally, FRCC mortar (without fibre) is used for the rheological measurement. As the rheometer rotated the parallel plate (shown in Figure 3.7), a set of data and graph of viscosity over time were generated by the rheometer's software. Since constant shear rate was used, shear stress was determined at the plateau of the graph as shown in Figure 3.8 or when the viscosity was almost at constant (refer Appendix A). The computation of shear stress was done by using Newton's Law of Viscosity in Equation (3.2) when the measured torque maintained at constant over time. Due to the limitation of the rheometer, the shear rate was set at 0.05/s and slurry (without aggregate) was used instead of mortar. The mixture proportion of slurry was mainly binder and water as given in Table 3.1 but with constant dosage of SP at 0.35%. The slurry was mixed at same mixing sequence, speed and time at relative humidity of 60 ± 5%. Then, slurry was maintained at temperature 25°C by placing on a temperature-controlled dish and the measurement was taken as the parallel plate contacted with the slurry (Figure 3.7).

$$\tau = \eta \times shear\ rate \tag{3.2}$$

Where,

τ = Shear stress, in Pa

η = Viscosity, in Pa.s

Figure 3.6 Modular Compact Rheometer

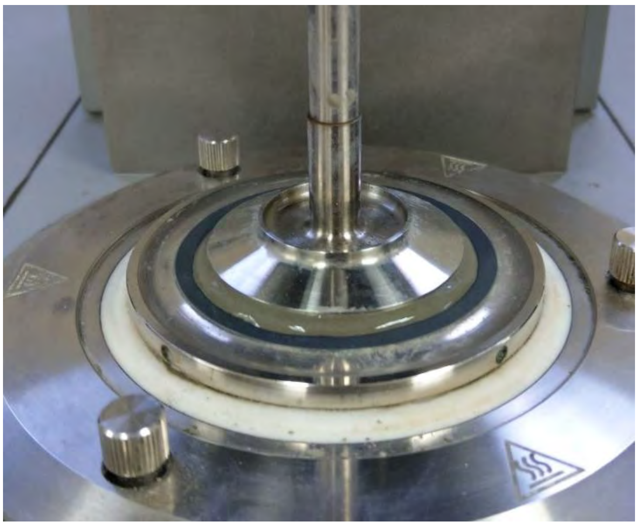

Figure 3.7 Rheological measurement of slurry

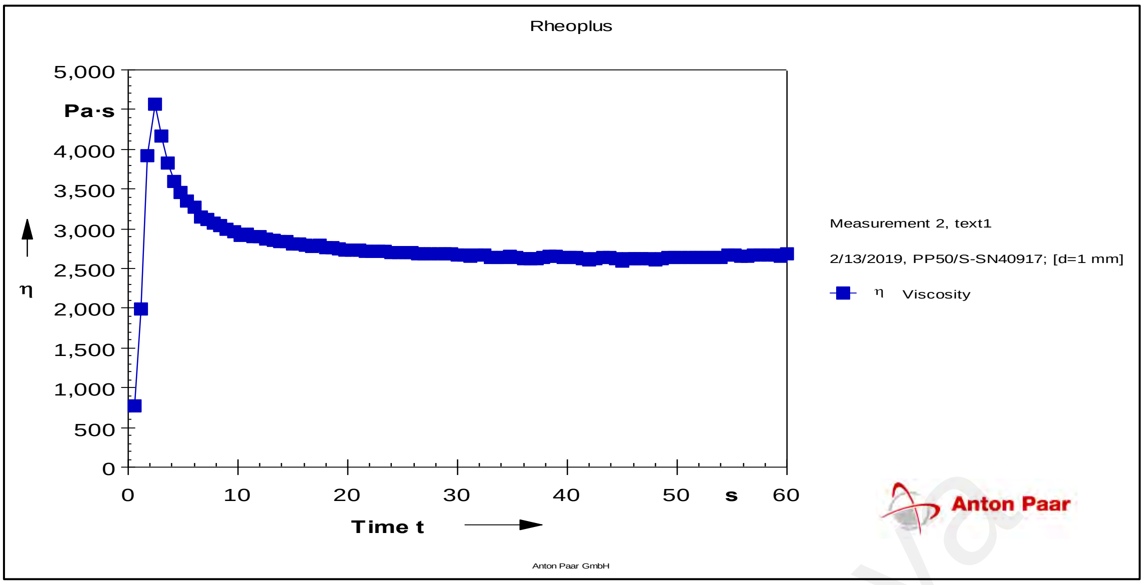

Figure 3.8 Obtained viscosity vs time graph

3.6 Hardened Fibre Reinforced Cementitious Composites

3.6.1 Compressive strength test

In this research, the compressive strength of specimens with dimension of 50 mm x 50 mm x 50 mm was conducted as stipulated in BS EN 12390-3 (BSI, 2009a). Engineering Laboratory Equipment testing machine with loading capacity of 2000kN and a loading frame as shown in Figure 3.9 was used in this test. The specimens were tested at the desired age and loading was applied until specimens failed. Compressive strength was computed using Equation (3.3).

Figure 3.9 Placement of cubic specimen in loading frame

$$f_c = \frac{F}{A_c} \quad \textbf{(3.3)}$$

Where,

f_c = Compressive strength, in MPa

F = Maximum load in failure, in kN

A_c = Cross sectional area of specimen under load, in mm^2

3.6.2 Splitting tensile strength test

The splitting tensile strength conducted at 28th day was in compliance with the standard BS-EN 12390-6 (BSI, 2009b). The testing machine used was ELE testing machine with a load capacity of 2000kN. Before loading, the cylindrical specimen was placed centrally in the testing machine using a jig as shown in Figure 3.10. The plywood packing strips were placed carefully on top and underneath the specimens before placing a steel loading pieces along the top plane of loading of specimen. The loading rate was set to 1.57kN/s and the specimen was tested until failure. The maximum load, F attained from the ELE testing machine was used to calculate the splitting tensile strength using Equation (3.4).

Figure 3.10 Placing of cylinder sample in jig

$$f_{ct} = \frac{2 \times F}{\pi \times L \times d} \quad \textbf{(3.4)}$$

Where:

f_{ct}	=	Tensile splitting strength, in MPa
F	=	Maximum load, in kN
L	=	Length of specimen, in mm
d	=	Diameter of specimen, in mm

3.6.3 Flexural strength test

There were two different types of specimen used in the flexural strength test and their dimension were 160 mm x 40 mm x 40 mm and 500 mm x 75 mm x 16 mm. The former specimen size was required by engineering standards in order to conduct flexural test. Whereas the latter is one of the characteristic tests done by other researchers (Pakravan *et al.*, 2016; Z. F. Pan *et al.*, 2015) to assess the flexural behavior of FRCC through the analysis of load-deflection curve. Besides, FRCC is suitable for thin overlay (Mustafa Sahmaran *et al.*, 2013; Yucel *et al.*, 2013) in repair application, therefore the flexural behaviour of the thinner specimen was studied.

3.6.3.1 Three-point bending test

The flexural strength of the FRCC was tested by using three-point bending test and the dimension of the specimens was 160mm x 40mm x 40mm by referring to BS EN 196-1-2005. Due to the setting ELE testing machine in the laboratory was not suitable, INSTRON displacement-controlled testing machine with load capacity 100 kN was used. Before loading, the specimens were marked at the side to indicate the position of supporting span and loading point. Then, the specimens will be placed in a frame as shown in Figure 3.11. The specimens were tested until failure by using displacement rate of 1.5mm/min. The ultimate flexural strength was computed by using Equation (3.5) and load-displacement graph was plotted for further analysis.

Figure 3.11 Setup of three-point bending test

$$R_f = \frac{1.5 \times F_f \times l}{b^3} \quad \textbf{(3.5)}$$

Where,

R_f	=	Flexural strength, in MPa
b	=	Side of the square section of the prism, in mm
F_f	=	Load applied to the middle of the prism at fracture, in N
l	=	Distance between the supports, in mm

3.6.3.2 Four-point bending test

The four-point bending test was done using INSTRON displacement-controlled testing machine with 250kN loading capacity at 1.5mm/min displacement rate. The specimen sample used by researcher Z. F. Pan *et al.* (2015) on four-point bending test was 350 mm x 50 mm x 15 mm. However, in order to suit the available testing facility in the laboratory, the specimen size used in this research was modified to 500 mm x 75 mm x 16 mm. Specimens were marked at the rear to indicate the position of supporting span and loading span and its setup are indicated in Figure 3.12. Bending test was conducted until the specimen's loading reached 50% of its ultimate load. The raw data was retrieved, and load-deflection graph was plotted for further analysis. By using Equation (3.6), the flexural strength is computed. After test, the bottom surface of the flexural specimen was gently tap with moist paper towel to reveal the crack line more easily. Figure 3.13 and Figure 3.14 show the difference between dry and moistened flexural specimen.

$$\sigma_f = \frac{FL}{bd^2} \tag{3.6}$$

Where:

σ_f	=	Flexural strength, in MPa
F	=	Maximum load, in N
L	=	Length of supporting span, in mm
b	=	Width of specimen, in mm
d	=	Depth of specimen, in mm

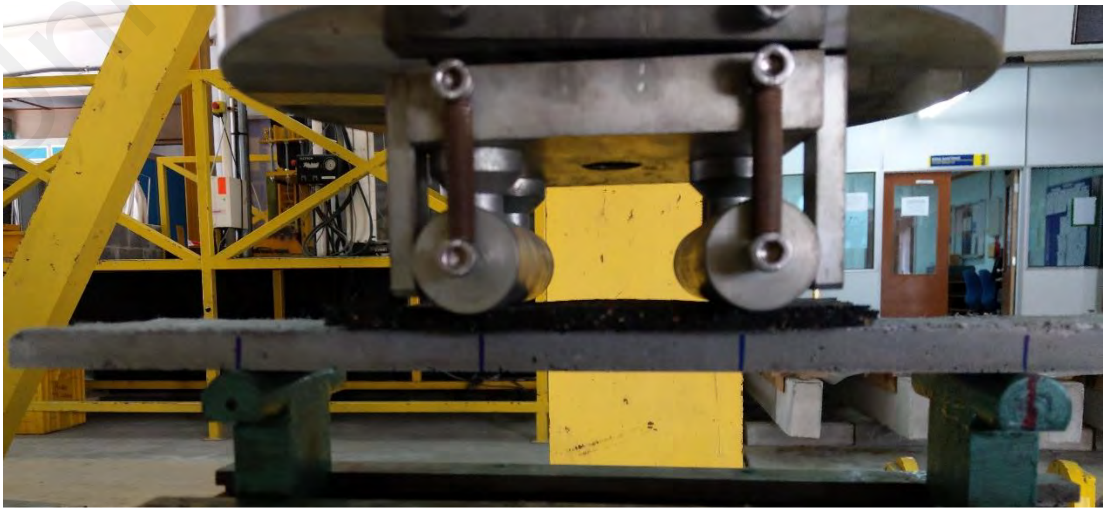

Figure 3.12 Setup of four-point bending test

Figure 3.13 Tension zone of tested flexural specimen (dry)

Figure 3.14 Tension zone of tested flexural specimen (after moistened)

3.6.4 Flexural toughness

During loading, energy is absorbed by the specimen and it is an alternate indication of ductility. The energy absorption was determined by computing the total area under the load-deflection curve and this was similarly done by Pakravan *et al.* (2017). The energy absorption of the specimens was calculated from the total area under the curve up to the point where the load was reduced to 50% of the ultimate load. As illustrated in Figure 3.15. the total energy absorption would be the area under the curve from segment OABCDE. Then, the computation of flexural toughness was in accordance to Equation (3.7).

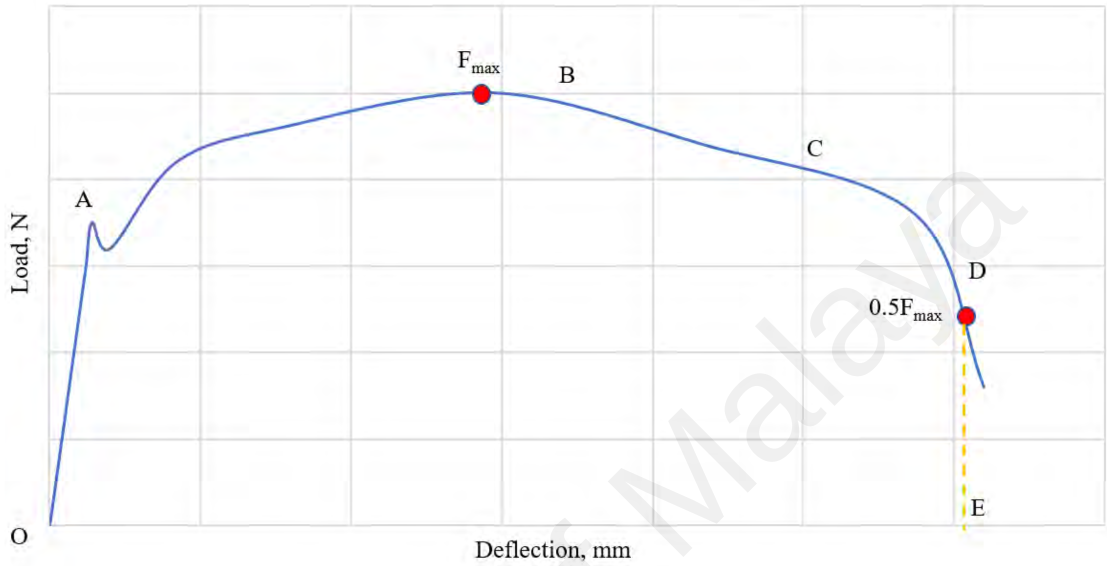

Figure 3.15 Typical load-reflection graph of FRCC

$$Flexural\ toughness = \frac{Energy\ absorbed}{cross\ section\ area} \quad \textbf{(3.7)}$$

3.6.5 Slant shear strength test

The slant shear strength test was conducted in accordance to BS-EN 12615 (BSI, 1999a). Table 3.7 shows the mixture proportion of concrete substrate with 30 MPa compressive strength (cubic strength). The inclination angle (30º) and the dimension of concrete substrate were prepared accordingly to the schematic shown in Figure 3.16. There are a few methods in surface preparation for slant shear strength specimen, namely, sand blasting, mechanical grooving, hand brush and drilling. Based on the research done by Tayeh *et al.* (2013), sand blasting had the best bonding strength, followed by mechanical grooving. However, due to facility limitation, mechanical grooving method was used. By considering the limited slant cross sectional area of substrate, 'X' mark was the most suitable pattern to be mechanically grooved on the surface of substrate. The substrates were pre-wetted to saturated surface dry (SSD) condition before placing onto steel mould. The steel mould was then carefully assembled without damaging the substrate and the inclined surface of the substrate was once again made sure in SSD condition before casting the fresh FRCC to form composite prisms. The composite prisms were de-moulded after 24 hours and water cured until testing age which was at 1st, 7th and 28th days. The sample was orientated at FRCC on top part and substrate at bottom part and then placed on top the loading frame as demonstrated in Figure 3.17. After testing, the slant shear strength was calculated based on Equation (3.8) and the failure mode of the specimens was observed and analysed.

$$f_b = \frac{F\sqrt{3}}{6400} \tag{3.8}$$

Where,

f_b = Shear bond strength, in MPa

F = Failure load, in N

Table 3.7 Mix ratio and compressive strength of concrete substrate

Material	Ratio to cement
Cement	1
Water	0.6
Fine aggregate	3.7
Coarse aggregate	2.5
Compressive strength	30.9 MPa

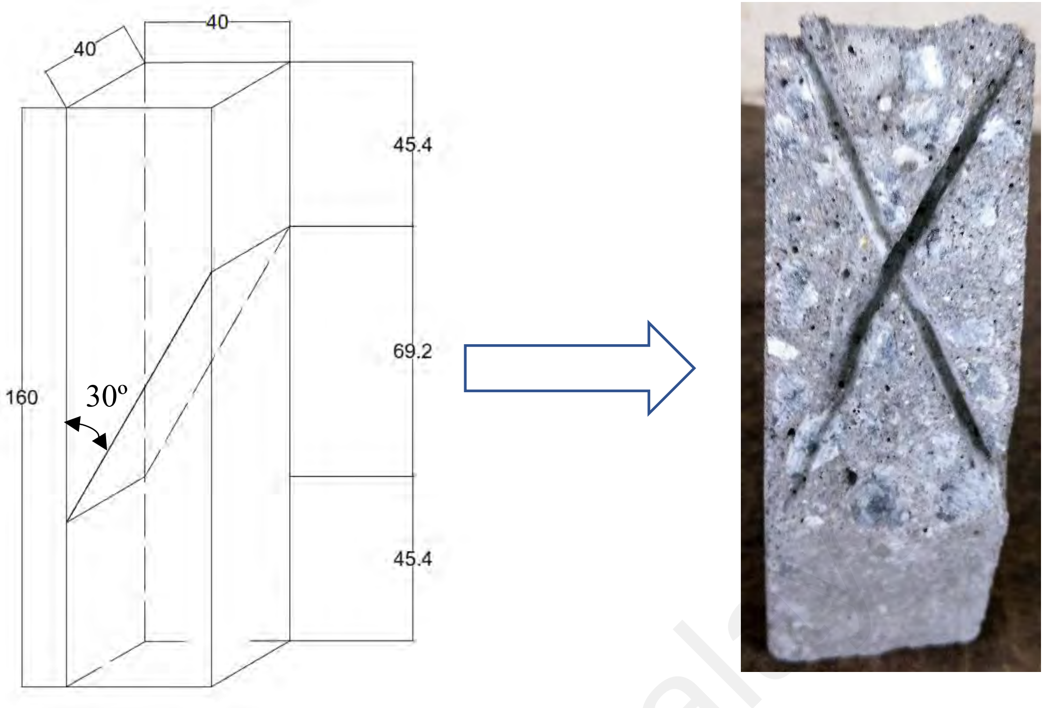

Figure 3.16 Geometry and shape of concrete substrate (left); after surface preparation (right)

Figure 3.17 Placement of slant shear specimen

3.6.6 Charpy impact test

In this test, the six selected mixtures in Phase II were prepared together with an additional control mixture without fibre, B-(30,0) in order to provide comparison between specimens with and without fibre. The dimension of the specimen was 60 mm x 14 mm x 14 mm to suit the existing support as shown in Figure 3.18. The fresh specimens were casted into a 10-gang polyurethane mould and cured for 28 day before impact test. The Charpy impact test machine was adjusted to be free of zero error by lifting the pendulum to the max height and release the pendulum without test specimen. After adjustment, the specimens were carefully positioned on the support as illustrated in Figure 3.19 and the pendulum was released to conduct the impact test. The impact energy recorded was used in calculating the impact strength by using Equation (3.9) and this method was also used by Hakamy *et al.* (2015).

$$Impact\ strength = \frac{Impact\ energy}{Cross\ sectional\ area} \quad \textbf{(3.9)}$$

Where,

Impact energy	=	MPa
F	=	Failure load, in N

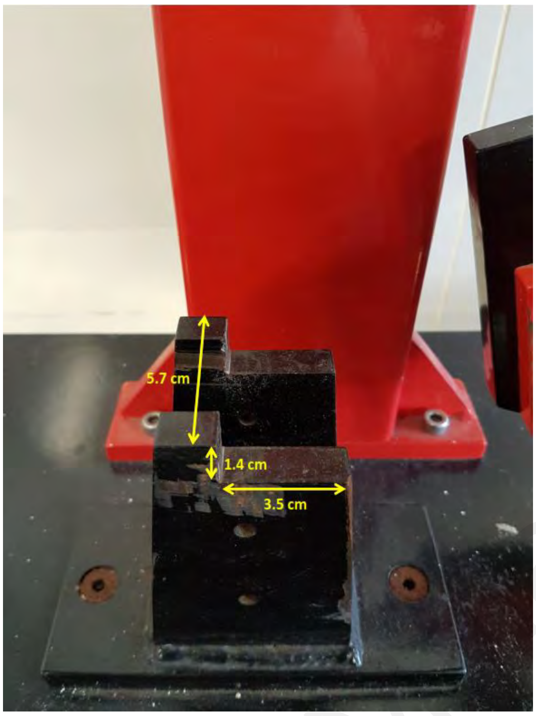

Figure 3.18 Support of Charpy impact test machine

Figure 3.19 Positioning of specimen on support

CHAPTER 4: RESULTS AND DISCUSSION

4.1 Introduction

This chapter gives an overview on the result and analysis done in the experimental work on these properties: 1) workability; 2) rheology; 3) compressive strength; 4) splitting tensile strength; 5) flexural strength; 6) flexural performance of thin plate specimen; 7) slant shear strength and 8) impact strength.

4.2 Phase I

4.2.1 Workability

The workability of the fibre reinforced cementitious composites (FRCC) in this research of different series, fibre content and fly ash (FA) replacement with ground granulated blast furnace slag (GGBS) is tabulated in Table 4.1. The workability decreased with the increasing fibre volume fraction and this phenomenon was similarly reported by Li *et al*. (2013). This was due to the increased fibre content that had higher fibre surface area which demanded more cementitious matrix for coating and dispersion (Bentur & Mindess, 2006). However, when comparing among the three series, the workability of Series C was significantly better than Series A and B since it had the highest binder content (1300kg/m^3). For an example, A-(30,0), B-(30,0) and C-(30,0) were high workable mortar with flow 150%. When 1.5% of polyvinyl alcohol (PVA) fibre was added, the flow of Series A, B and C dropped to 32%, 70% and 100%. Meanwhile, it was noted that at 2.5% fibre dosage, the deviation in the workability of fresh mixes was lower at decreasing binder content. For an instance, the standard deviation was 6.6% in Series C, 3.0% in Series B and 0.6% in Series A when the mixes were incorporated with 2.5% PVA fibre dosage. This happens because the cementitious paste in Series A was very limited for 2.5% PVA fibre dosage and no extra cementitious paste was available for lubrication and therefore exhibited similar workability. As a comparison among the three series, Figure 4.1 displays the texture of the fresh FRCC of A-(30,1.5), B-(30,1.5) and C-(30,1.5). Starting with the lowest binder content, the fresh A-(30,1.5) was rough and stiff with visible fibre balling. Continue with B-(30,1.5), the dispersion of the fresh FRCC was better. Lastly, the highest binder content, C-(30,1.5) had the smoothest and creamiest texture with largest spread. This shows that adequate binder content is pivotal for workability and fibre dispersion.

When observing the effect of GGBS in FRCC, it was noticed that higher content in GGBS induced slightly lower workability in Series A and C. This is due to the higher specific gravity of GGBS (2.89) used in this research than the FA (2.50). This led to lower paste volume and higher aggregate content. However, Series B showed otherwise as the workability of B-(30,1.5) was 10% higher than B-(0,1.5) and B-(60,1.5); and B-(30,2.5) was 3% higher than B-(0,2.5) and 6% higher than B-(60,2.5). This could be due to 30% GGBS replacement being the optimum proportion in the particle packing and provided more effective paste volume in Series B. Lastly, only five mixes which were B-(0,1.5), B-(30,1.5), B-(60,1.5), C-(30,1.5) and C-(60,1.5) fulfilled the desired workability (80 ± 20%).

Table 4.1 Workability of FRCC in Phase I

Series A		Series B		Series C	
Mix	Flow (%)	Mix	Flow (%)	Mix	Flow (%)
A-(0,0)	150	B-(0,0)	150	C-(0,0)	150
A-(0,1.5)	43	B-(0,1.5)	60	C-(0,1.5)	118
A-(0,2.5)	21	B-(0,2.5)	41	C-(0,2.5)	67
A-(30,0)	150	B-(30,0)	150	C-(30,0)	150
A-(30,1.5)	32	B-(30,1.5)	70	C-(30,1.5)	100
A-(30,2.5)	22	B-(30,2.5)	44	C-(30,2.5)	59
A-(60,0)	150	B-(60,0)	150	C-(60,0)	150
A-(60,1.5)	41	B-(60,1.5)	60	C-(60,1.5)	80
A-(60,2.5)	21	B-(60,2.5)	38	C-(60,2.5)	54

Figure 4.1 Fresh FRCC after flow table test: a) A-(30,1.5); b) B-(30,1.5) and c) C-(30,1.5)

4.2.2 Rheology

The bar chart illustrated in Figure 4.2 shows the shear stress of the slurries from Series A, B and C. It was found that the slurry from Series A had highest shear stress (25.9 – 132.4 Pa) than those from Series B (1.8 – 15.2 Pa) and Series C (1.8 – 25.3 Pa). This was most likely due to the lowest content of supplementary cementitious material (SCM) in Series A, at only 44%. Other than that, the fixed dosage of superplasticizer (SP) at 0.35% was inadequate to reduce the viscosity of slurry in Series A. As listed in Table 3.1, 0.65% of SP dosage was required to achieve high flowable mortar.

Meanwhile, when comparing the effect of GGBS, slurry specimen in Series A with 30% GGBS replacement had the highest shear stress, 132.4 Pa followed by A-(60,0) and A-(0,0). This observation corresponded with the workability results listed in Table 4.1. On the other hand, the least viscous slurry in Series B and C was the slurry with 30% GGBS replacement, namely B-(30,0) and C-(30,0) which recorded shear stress of 1.8 Pa and 1.9 Pa respectively. This suggests that there is an optimum proportion of cement, FA and GGBS in terms of the rheological properties provided there is sufficient flow. Hence, it can be concluded that the viscosity of slurry varies on the proportion ratio of the binder materials.

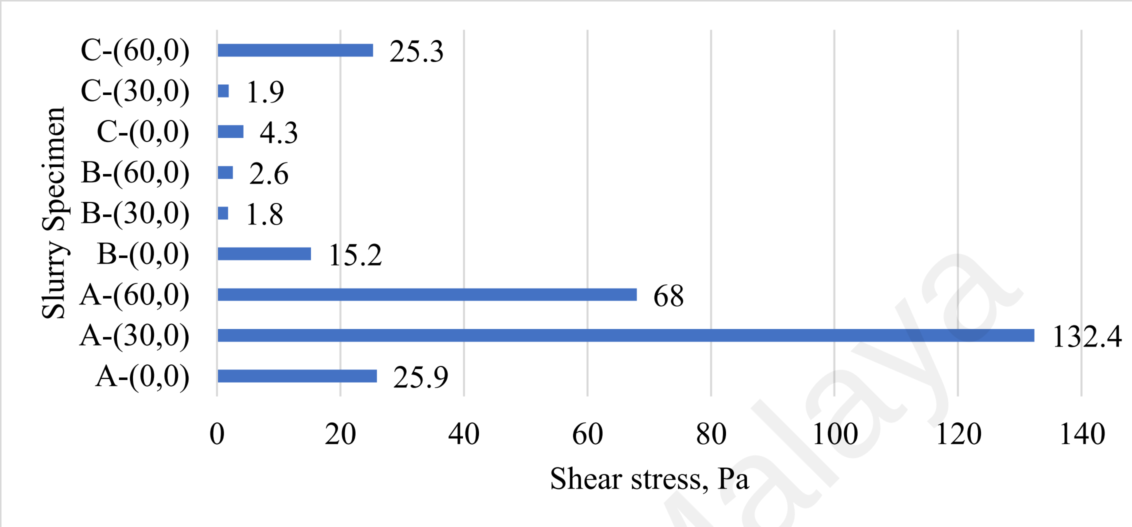

Figure 4.2 Shear stress of slurry

4.2.3 Compressive strength

After curing for up to 28 days, the specimens of all series were tested and the results are tabulated in Table 4.2, Table 4.3 and Table 4.4. Based on the results, the compressive strength of all series had common trend which was the increase in strength over time.

Generally, the compressive strength at all ages for all three series of the FRCC decreased in the presence of PVA fibre. The compressive strength decrease in Series A was in the range of 2.5 – 22.4%, in Series B was 2.6 – 20.1% while in Series C was 2.2 – 16.1%. This could be due to PVA fibres which are relatively soft than the aggregate and matrix, hence slightly compromised the compressive strength. Other than that, the stiffening effect from the fibre decreased the workability which could lead to less effective compaction. In terms of failure mode, the specimens without PVA fibres underwent typical brittle compression failure as shown in Figure 4.3a. On the other hand,

Figure 4.3b indicates the crack bridging ability from PVA fibres as the tested specimen was intact while exhibiting minor crack lines (Kanda & Li, 1999).

Table 4.2 Compressive strength of A-series PVA-FRCC

Series A	Compressive strength, MPa		
	1 day	7 day	28 day
A-(0,0)	32.9 ± 0.5	52.9 ± 0.9	86.7 ± 3.0
A-(0,1.5)	31.8 ± 0.9	51.2 ± 2.1	75.2 ± 1.8
A-(0,2.5)	30.9 ± 2.9	52.6 ± 2.2	71.8 ± 2.3
A-(30,0)	40.6 ± 1.1	64.8 ± 0.3	80.9 ± 1.2
A-(30,1.5)	31.5 ± 0.4	57.9 ± 2.3	70.2 ± 0.7
A-(30,2.5)	32.3 ± 0.8	56.5 ± 2.7	70.3 ± 4.1
A-(60,0)	37.8 ± 0.7	64.0 ± 2.4	72.3 ± 2.9
A-(60,1.5)	33.2 ± 1.5	59.2 ± 1.4	69.0 ± 0.7
A-(60,2.5)	35.0 ± 1.4	57.2 ± 1.1	70.5 ± 1.1

Table 4.3 Compressive strength of B-series PVA-FRCC

Series B	Compressive strength, MPa		
	1 day	7 day	28 day
B-(0,0.0)	26.3 ± 1.1	49.5 ± 2.0	67.9 ± 5.0
B-(0,1.5)	23.4 ± 0.3	42.3 ± 0.4	64.7 ± 2.5
B-(0,2.5)	23.9 ± 0.6	46.5 ± 1.5	63.6 ± 1.7
B-(30,0.0)	31.8 ± 1.2	56.5 ± 1.4	78.8 ± 4.4
B-(30,1.5)	27.3 ± 0.8	54.1 ± 0.9	68.5 ± 2.3
B-(30,2.5)	25.4 ± 0.6	52.4 ± 0.7	66.1 ± 2.6
B-(60,0.0)	27.4 ± 0.2	58.3 ± 0.9	74.4 ± 1.7
B-(60,1.5)	26.7 ± 0.4	55.7 ± 0.4	71.1 ± 1.4
B-(60,2.5)	25.8 ± 0.7	55.8 ± 0.6	71.2 ± 0.6

Table 4.4 Compressive strength of C-series PVA-FRCC

Series C	Compressive strength, MPa		
	1 day	7 day	28 day
C-(0,0)	18.4 ± 0.4	34.9 ± 1.2	46.6 ± 1.2
C-(0,1.5)	16.7 ± 1.0	32.0 ± 1.1	43.5 ± 2.2
C-(0,2.5)	16.1 ± 0.7	30.8 ± 1.3	44.7 ± 0.6
C-(30,0)	20.9 ± 0.7	43.7 ± 0.9	62.1 ± 2.6
C-(30,1.5)	19.1 ± 0.1	41.9 ± 1.5	57.0 ± 1.8
C-(30,2.5)	20.0 ± 0.8	41.3 ± 1.6	56.9 ± 1.9
C-(60,0)	22.3 ± 0.2	51.5 ± 0.3	72.7 ± 0.9
C-(60,1.5)	21.8 ± 0.4	49.0 ± 2.4	62.1 ± 0.9
C-(60,2.5)	21.4 ± 0.7	47.9 ± 2.7	61.0 ± 0.6

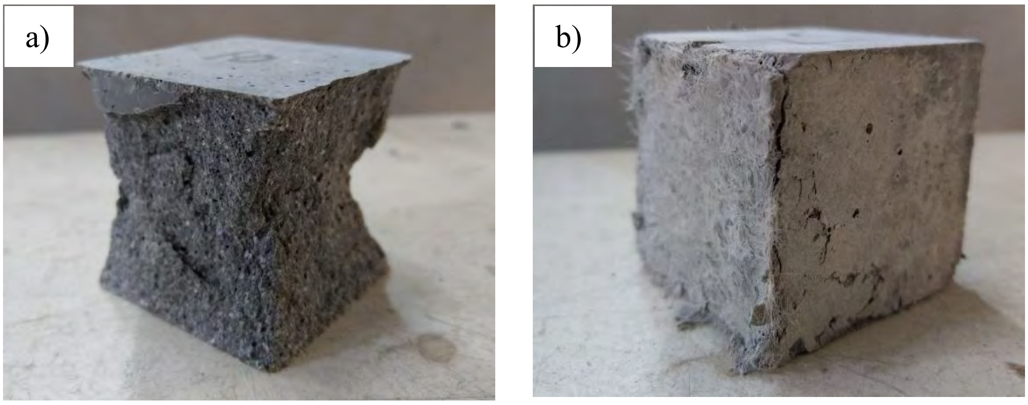

Figure 4.3 Failure pattern of 50mm cube sample: a) without fibre; b) with fibre

In all series and regardless of PVA fibre dosage, the graphs illustrated in Figure 4.4 until Figure 4.9 show a very significant finding that the early age compressive strength decreased along with binder content. In Figure 4.4, Figure 4.5 and Figure 4.6, it was found that the 1-day compressive strength decreased almost linearly from 900kg/m^3 to 1100kg/m^3 binder content. Similarly, the 7-day compressive strength indicated in Figure 4.7, Figure 4.8 and Figure 4.9 also decreased almost linearly especially at 0% and 1.5% fibre dosage. Series A was the most dominant in early compressive strength (1-day: 30.9 – 40.6MPa & 7-day: 51.2 – 64.8MPa), followed by Series B (1-day: 23.4 – 31.8MPa & 7-day: 41.9 – 64.6MPa) and lastly Series C (1-day: 16.1 – 21.8MPa & 7-day: 30.8 – 51.5MPa). These were mainly due to Series A having the lowest w/c ratio of 0.504, whereas Series B and Series C had w/c ratio of 0.616 and 0.728 respectively. Since FA and GGBS were pozzolan, the early age compressive strength was primarily contributed by the w/c ratio as the first hydrates was developed on the surface of cement particles (Aïtcin, 2016a). Other than that, as shown in Figure 4.4 – Figure 4.9, the mixes that contained GGBS had significantly higher early age compressive strength. This finding was also similarly reported by Zhou *et al.* (2012). This was due to GGBS having higher early stage activity index than FA and therefore the early age compressive strength is theoretically higher with greater GGBS content.

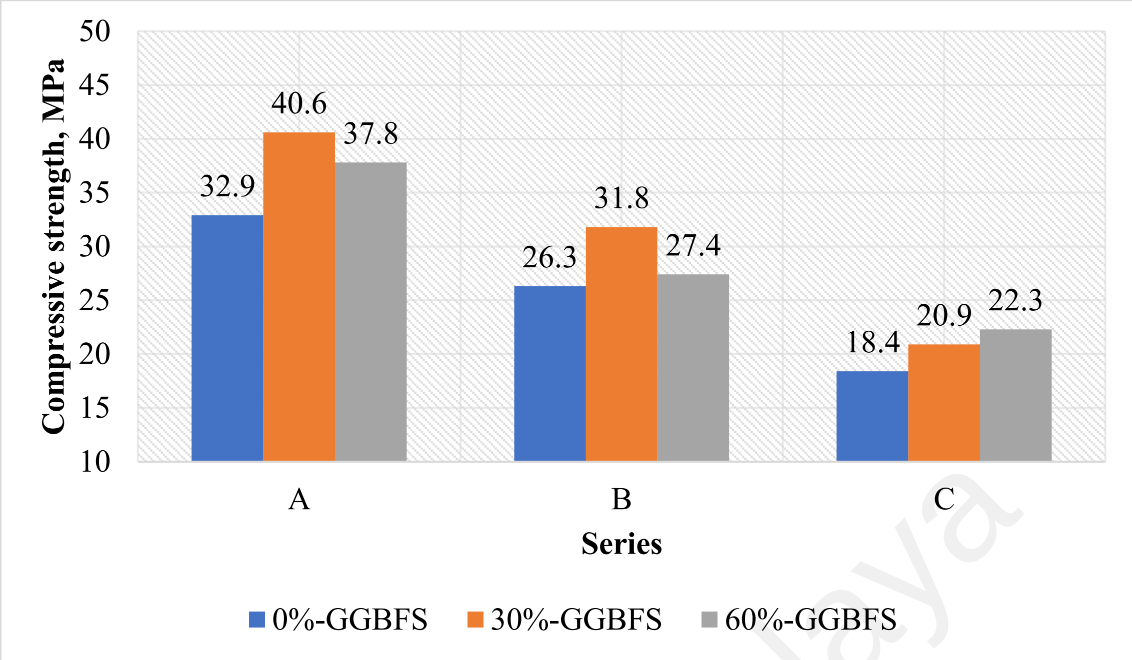

Figure 4.4 Graph of 1-day compressive strength of mortar in different series

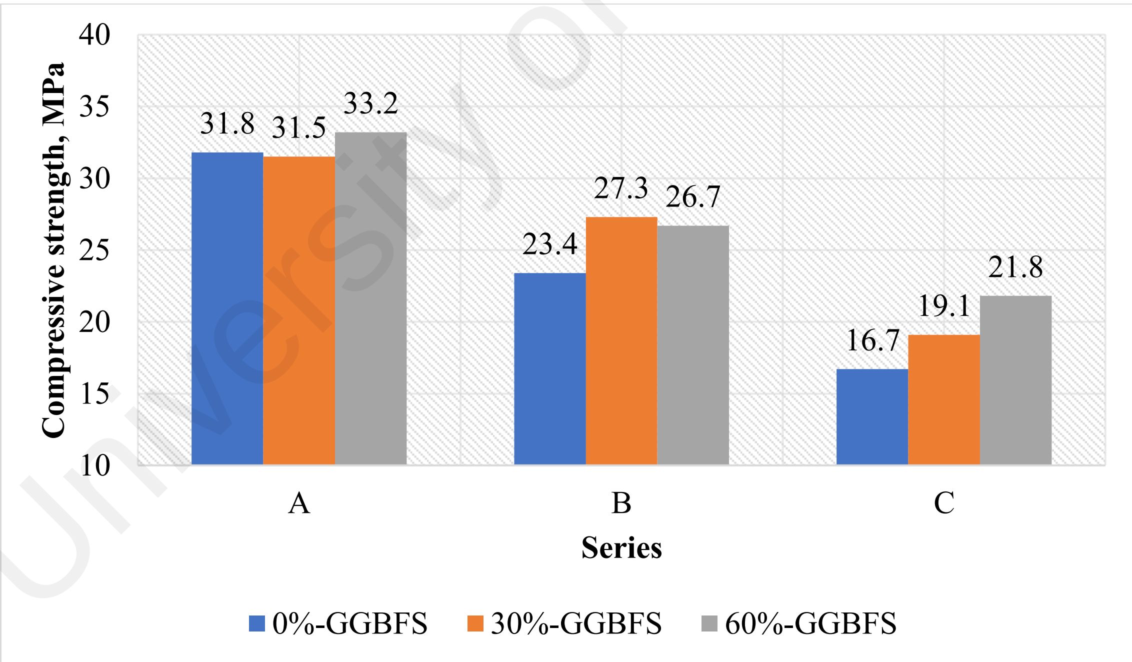

Figure 4.5 Graph of 1-day compressive strength of FRCC (1.5% fibre) in different series

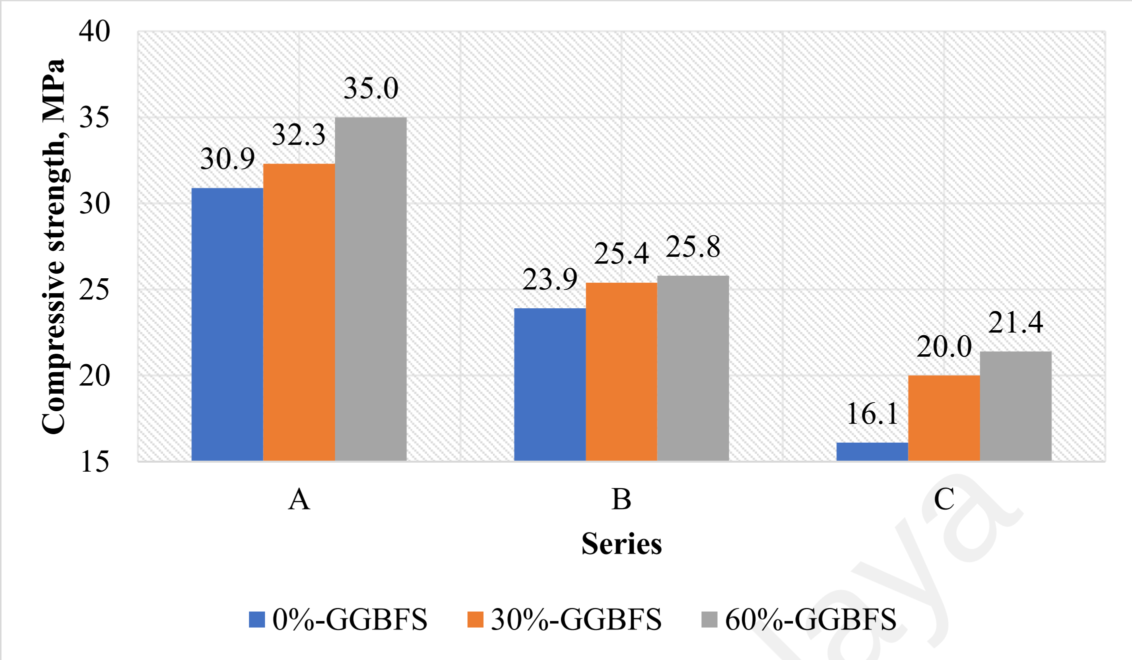

Figure 4.6 Graph of 1-day compressive strength of FRCC (2.5% fibre) in different series

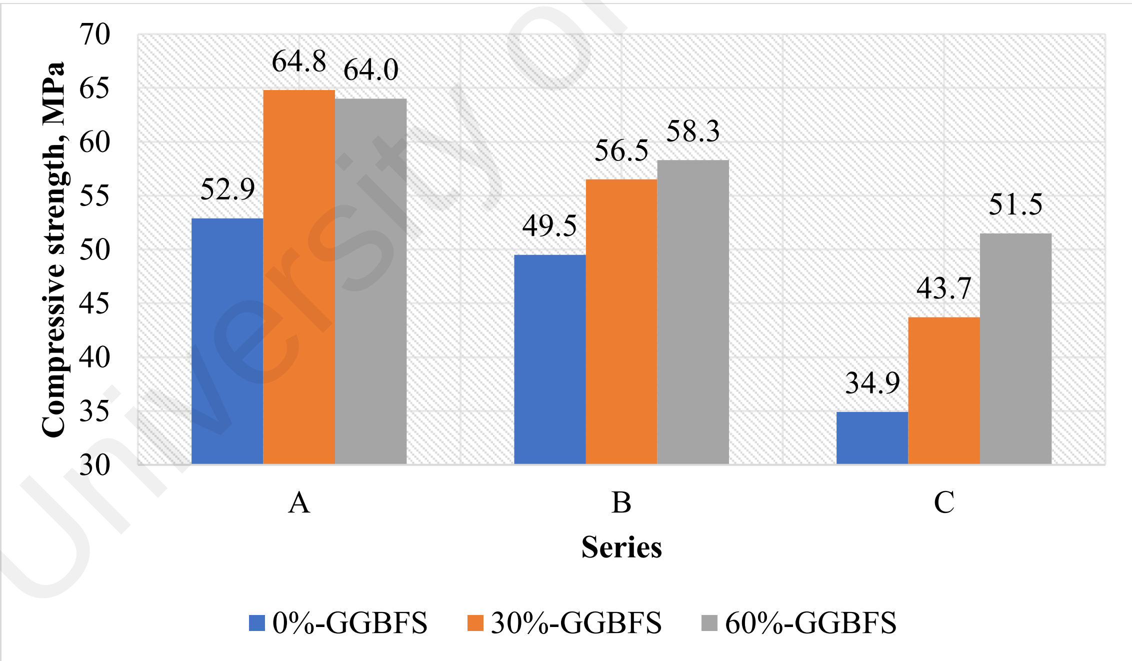

Figure 4.7 Graph of 7-day compressive strength of mortar in different series

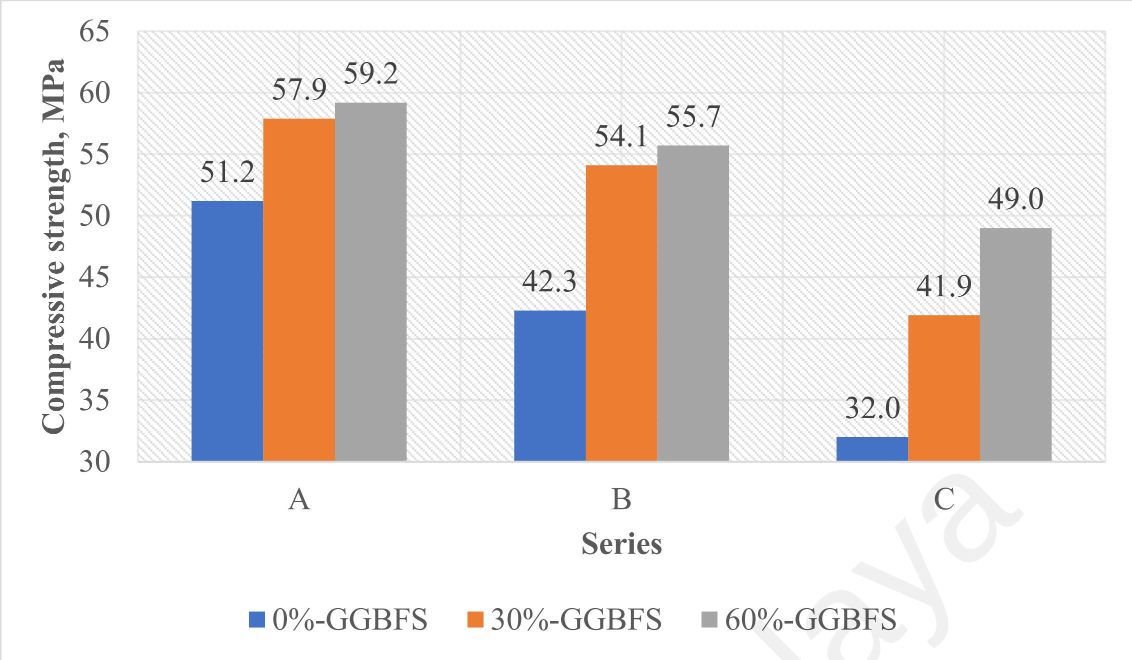

Figure 4.8 Graph of 7-day compressive strength of FRCC (1.5% fibre) in different series

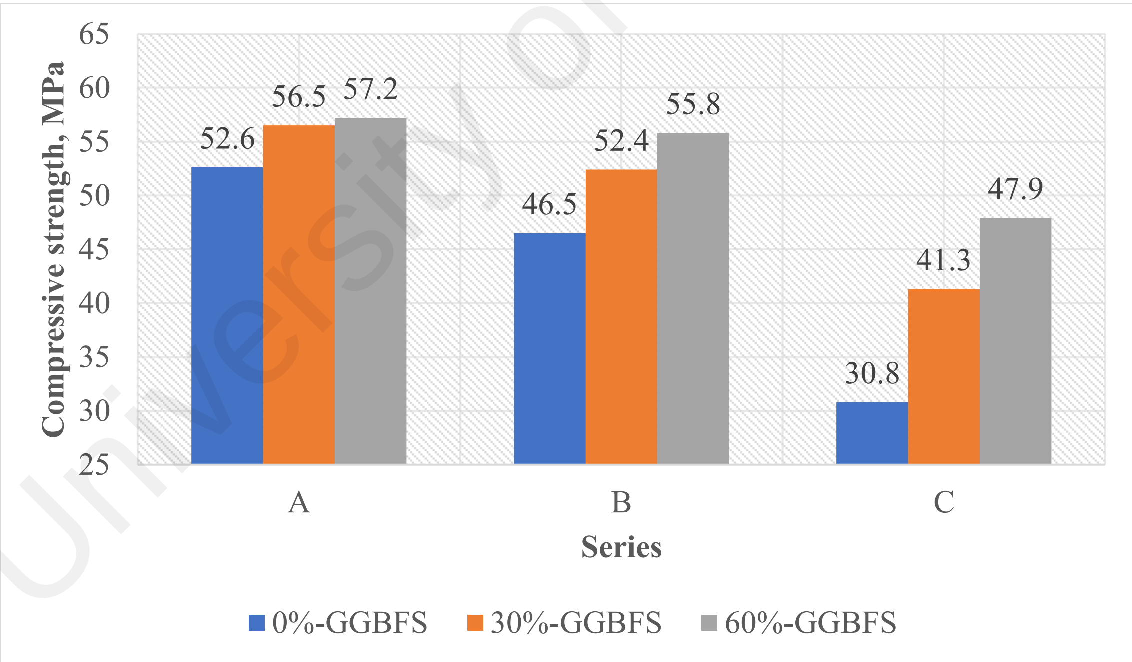

Figure 4.9 Graph of 7-day compressive strength of FRCC (2.5% fibre) in different series

Other than that, the 28-day compressive strength for all series was found to be 69.0 – 86.7 MPa for Series A, 63.6 – 78.8 MPa for Series B and 43.5 – 72.7MPa for Series C. It was noticeable that Series A had the highest 28-day compressive strength compared to others. The graphs in Figure 4.10, Figure 4.11 and Figure 4.12 clearly show most of the Series A points were higher than B and C at all of the fibre dosages. This could be explained by the fact that as all series were having low w/b ratio of 0.28 and in the Series B and C mixes where there was greater amount of SCM, incomplete hydration could occur (Ferrara *et al.*, 2016). The 28-day compressive strength could also be determined by the aggregate content. Based on the research conducted by Yurdakul (2010), at fixed w/c ratio, the compressive strength of concrete did not improve at higher cement content (beyond approximately 300 kg/m^3). Instead, the compressive strength of concrete reached a maximum value. In this research, the binder content used was ranging from 900 – 1300 kg/m^3 and containing high volume of SCM. Hence, the aggregate could have affected the compressive strength and the calculated aggregate volume in Series A, B and C was 46 – 47%, 31 – 32% and 15 – 18% correspondingly. Since Series A had the highest aggregate volume and the lowest w/c ratio as mentioned earlier, it correlated with the highest range in 28-day compressive strength.

By looking at the content of GGBS, the effect of GGBS on compressive strength varied in the early (1 & 7 days) and late (28 days) stages. Without considering the effect of PVA fibres, the graph in Figure 4.12 shows the trend of different combinations of cement, FA and GGBS. For 0% GGBS, a decreasing trend could be observed as the compressive strength dropped 18.8MPa from Series A to B and then 21.3 MPa from Series B to C. Reason for this was FA required longer time than 28 days to fully hydrate. Since the cement content was fixed, higher binder content had more incomplete hydrated FA. Whereas for 30%-GGBS, its compressive strength showed a slight decrement of 2.1 MPa from A to B and then reduced by about 16.7 MPa from B to C. This showed that 30%-GGBS was sufficient to have minor change in the compressive strength from Series A and B. However, the higher reactivity from the 30-% GGBS was not enough to compensate for the strength reduction caused by incomplete hydrated FA in Series C. When it comes to the mix with 60%-GGBS, in Figure 4.10 as the difference of compressive strength among A to B and B to C was minor at 2.1MPa and 1.7MPa, respectively. This concurred that maintaining the 28-day compressive strength of ternary blended mortar across different binder content was possible, provided that the percentage replacement with GGBS was adequate. As mentioned earlier, the presence of GGBS helped in boosting the early age compressive strength. However, different content of GGBS reacted differently in the mix at later stage. Figure 4.10 shows the optimum percentage of FA replacement with GGBS, which were: 0% for Series A, 30% for Series B and lastly; 60% for Series C. It can be explained that the content of GGBS was not effective in Series A since there was no improvement at all. Instead, higher content in GGBS induced more less decrement in the 28-day compressive strength of mix with both 30%-GGBS (-6.7%) and 60%-GGBS (-16.6%). In mortar of Series B, the possible explanation for 30%-GGBS being the most optimum as it exhibited better workability compared to 0% and 60%-GGBS upon inclusion of PVA fibres. The 60%-GGBS in mortar of Series C could have contributed to more complete hydration products as GGBS has greater reactivity. Lastly, the inclusion of PVA fibres did not alter the trend in 28-day compressive strength as the graphs in Figure 4.11 and Figure 4.12 show similar pattern as Figure 4.10.

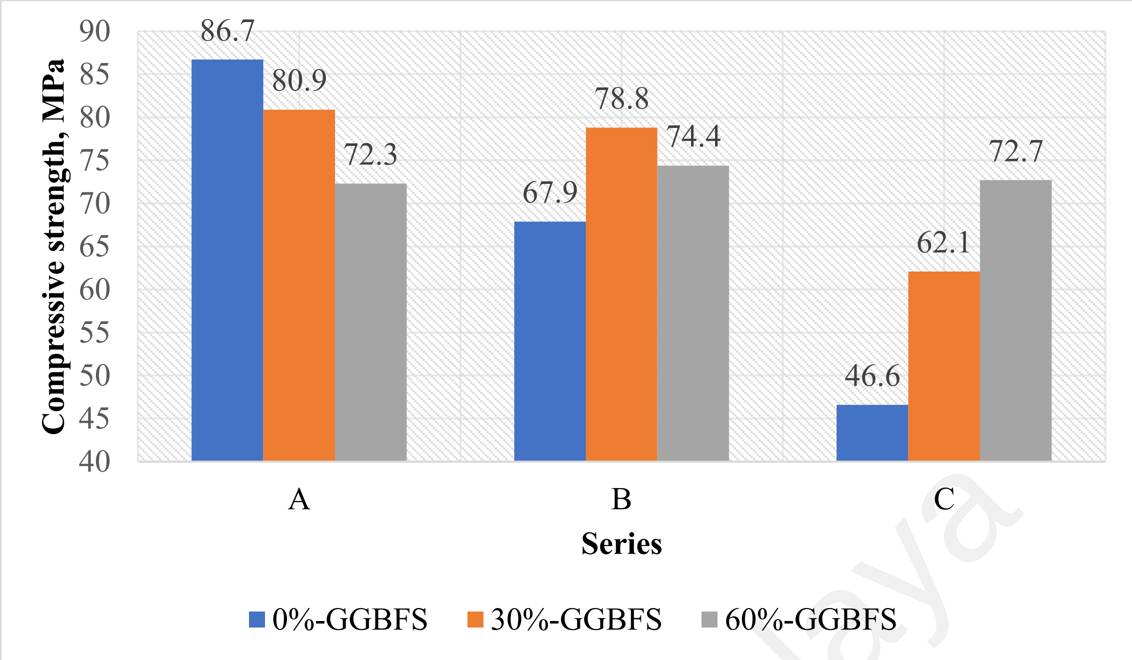

Figure 4.10 Graph of 28-day compressive strength of mortar in different series

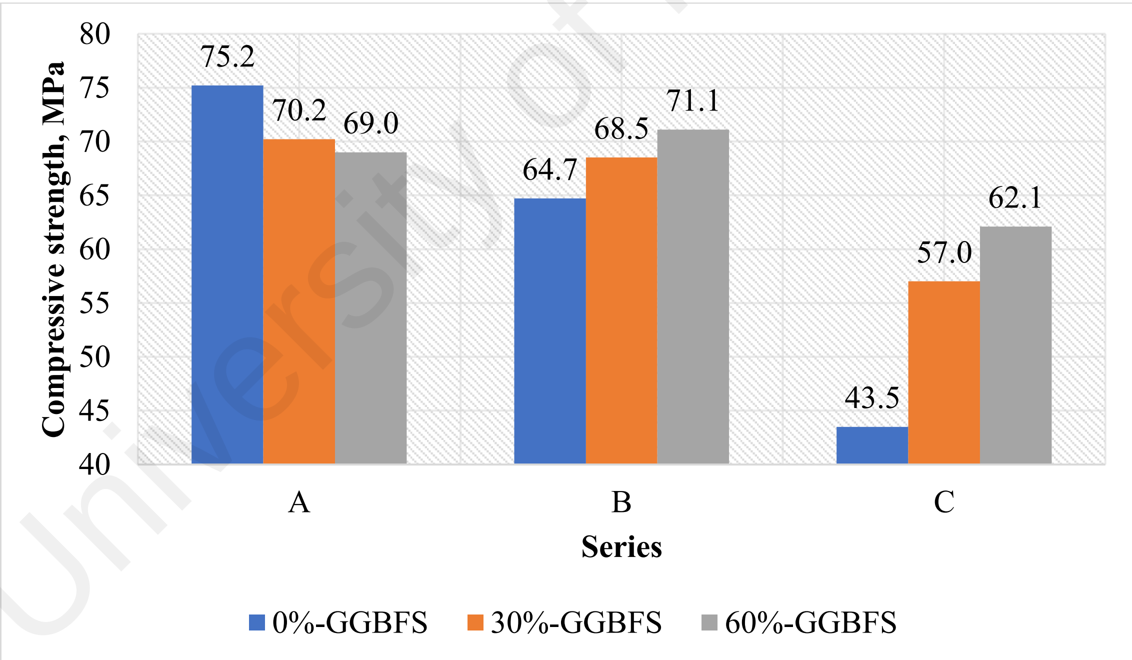

Figure 4.11 Graph of 28-day compressive strength of FRCC (1.5% fibre) in different series

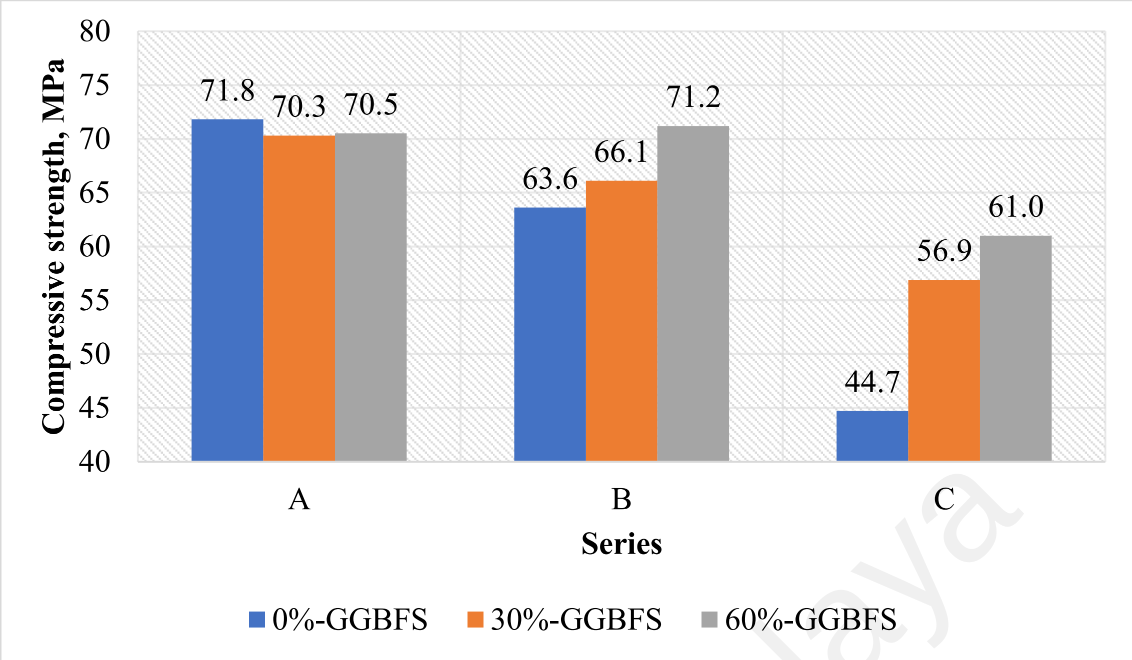

Figure 4.12 Graph of 28-day compressive strength of FRCC (2.5% fibre) in different series

As FA and GGBS are pozzolanic material, the hydration of its particle is relatively slower than cement. Therefore, even after 28 days, the presence of unhydrated pozzolanic material is imminent, especially the high content of SCM in FRCC, which is evidently displayed in Figure 4.13 and Figure 4.14. The micrograph in Figure 4.13 clearly shows that A-(30,1.5) with lower binder content and the presence of GGBS induced more hydration products such as CSH gel and portlandite (cluster of hexagonal crystal). On the other hand, Figure 4.14 shows most of the FA remained smooth and spherical, which implied the low degree of hydration (Xu & Shi, 2017).

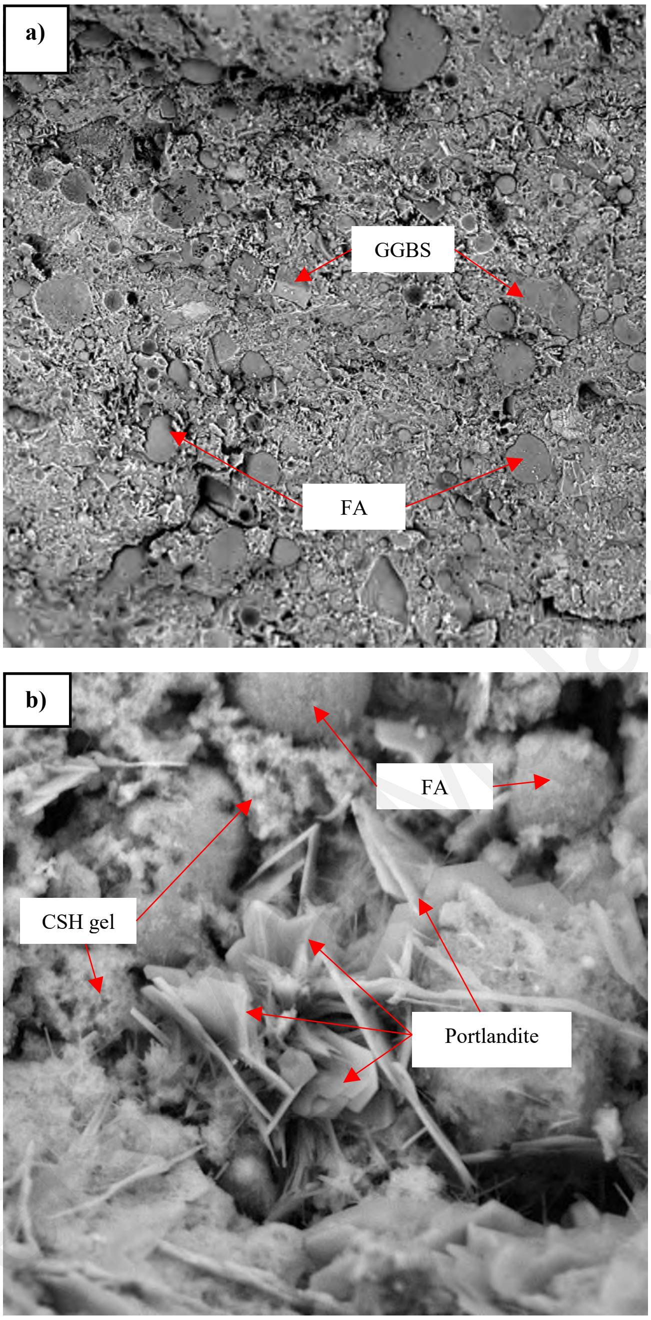

Figure 4.13 Micrograph of A-(30,0) at 28th day: a) at 700 magnification; b) at 7700 magnification

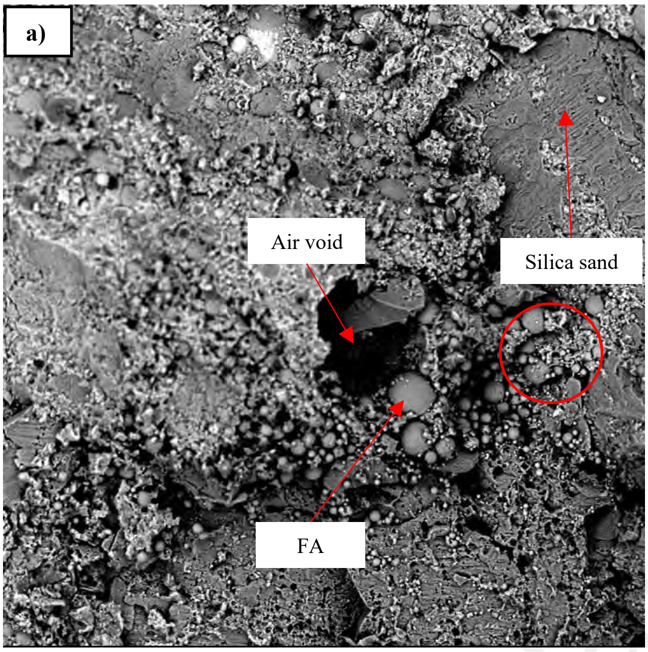

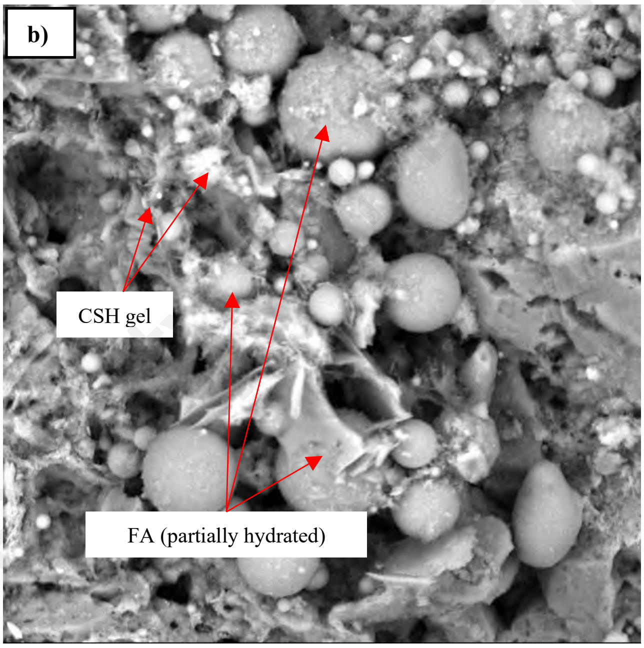

Figure 4.14 Micrograph of B-(0,0) at 28th day: a) at 900 magnification; b) at 5600 magnification

4.3 Phase II

4.3.1 Compressive strength

The 56-days compressive strength of FRCC displayed in Figure 4.15 shared similar trend as the compressive strength at the age of 28th day (Section 4.1.3) which was mainly dependent on the w/c ratio. Based on the combined chart, the compressive strength growth was in the range at 2.3% to 11.9% and it was significant that the growth was least effective at 60%-GGBS. This could be due to the pozzolanic activity of FA is more dominant than GGBS at later stage and the content of FA was lowest in the mixes with 60%-GGBS.

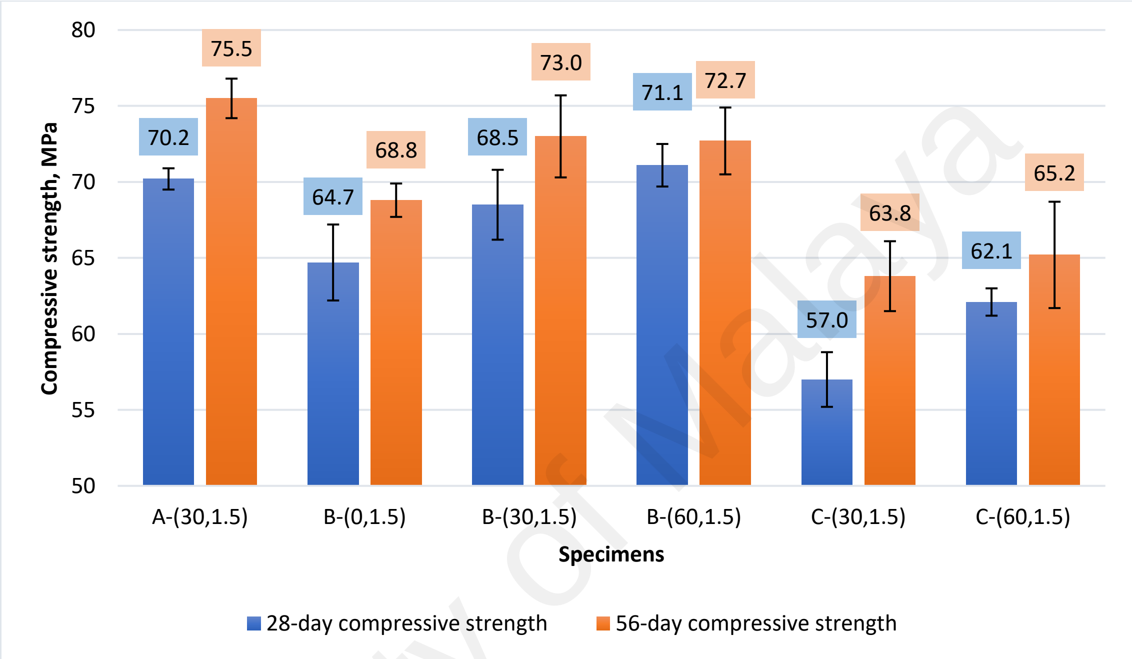

Figure 4.15 56-day compressive strength

4.3.2 Splitting tensile strength

The splitting tensile strength results plotted in the bar chart (Figure 4.16) was found to be in the range between 5.65 – 6.80 MPa, which was 8.6 – 10.2 % of their respective 28-day compressive strength. In overall, the PVA fibres helped in preventing the tested specimens from splitting apart instead of the typical splitting failure mode for control specimens without fibres (Figure 4.17). In terms of the effect of binder content, the FRCC's tensile strength can be correlated to their respective compressive strength. The compressive strength of A-(30,1.5), B-(30,1.5) and C-(30,1.5) was 70.2 MPa, 64.7 MPa and 57.0 MPa respectively; whereas the corresponding splitting tensile strength was

6.80 MPa, 6.65 MPa and 5.65 MPa. Similarly, B-(60,1.5) and C-(60,1.5) displayed the same trend.

On the other hand, the compressive strength of FRCC improved as the content of GGBS increased. However, its effect on the splitting tensile strength was dissimilar. In Series B, the splitting tensile strength without GGBS was 5.95 MPa which was then improved to 6.65 MPa at 30%-GGBS but then decreased to 6.15 MPa at 60%-GGBS. Likewise, C-(60,1.5) had lower splitting strength of 5.65 MPa than the mix C-(30,1.5) with 5.80 MPa. Similarly, this observation was reported by Güneyisi *et al.* (2008) where high volume GGBS (more than 50% cement replacement) had lower splitting tensile strength than the control (0% GGBS). This showed that GGBS improved the splitting tensile strength, but the improvement will be lower at high dosage (60%-GGBS).

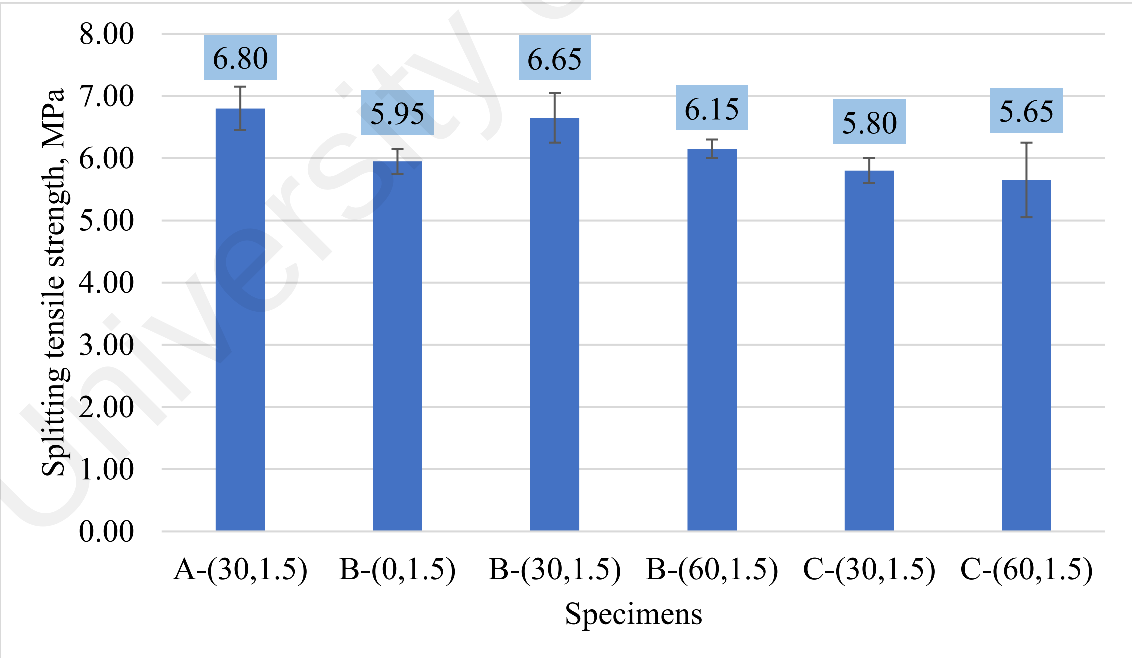

Figure 4.16 28-day splitting tensile strength result

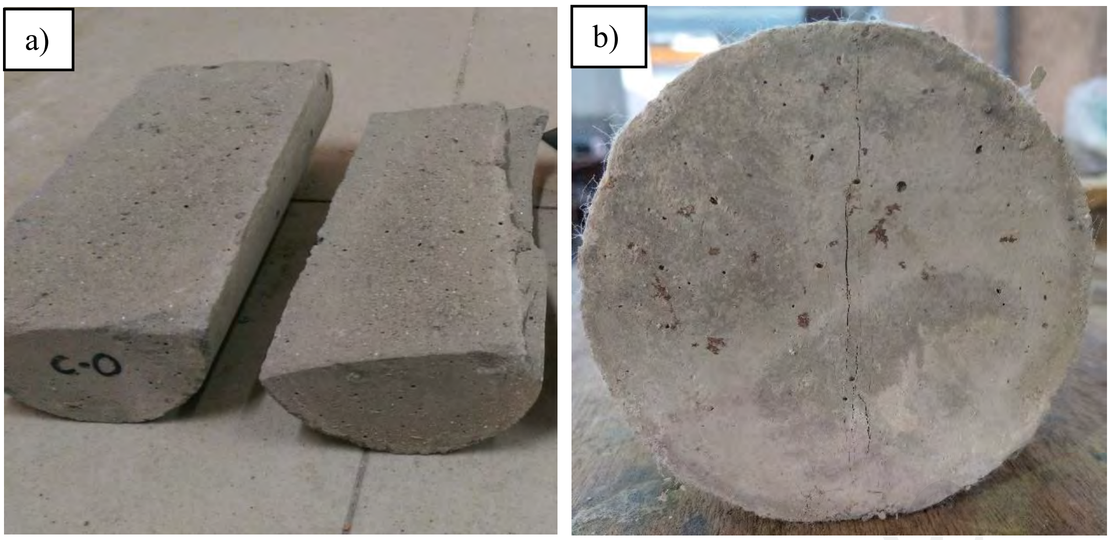

Figure 4.17 Failure mode of splitting tensile specimen: a) typical concrete or mortar; b) FRCC

4.3.3 Flexural strength

Figure 4.18 shows the flexural strength results of prismatic FRCC specimens using three-point bending test. The flexural strength increased along with the binder content which was observed in specimen A-(30,1.5), B-(30,1.5) and C-(30,1.5) by having flexural strength of 13.5 MPa, 20.2 MPa and 22.1 MPa respectively. This might be due to the better dispersion of fibre at higher content of cementitious matrix as reflected from its workability in Table 4.1. It is significant that the GGBS content is inversely proportional to the flexural strength. In Series B and C, the flexural strength of FRCC decreased from 21.6 to 18.9 MPa and 22.1 to 19.8 MPa, respectively as the content of GGBS increased. This phenomenon can be linked with the splitting tensile strength results in Section 4.2.2.

Meanwhile, the flexural strength of thin plate FRCC specimen shown in Figure 4.19 did not share the same trend as those observed for the prismatic specimen. Only A-(30,1.5) had the lowest flexural strength in both thick (13.5 MPa) and thin (5.6 MPa) section specimens which is hypothetically due to poor fibre dispersion (which can be reflected from poor workability as shown in Figure 4.1a) that originated from insufficient cementitious matrix. B-(0,1.5) and B-(30,1.5) had significantly higher flexural strength (8.6 MPa and 8.9 MPa) compared to all other specimens especially in Series B whereby B-(60,1.5)'s thin plate flexural strength was only 6.6 MPa. Likewise, the flexural strength of C-(30,1.5) and C-(60,1.5) was in similar range which was 6.4 MPa and 6.7 MPa.

Other than that, the flexural strength of the prismatic specimen had significantly higher flexural strength (13.5 – 21.6 MPa) compared to thin plate's specimen (5.6 – 8.9 MPa). This is very likely due to the second moment of area (I) in prismatic FRCC (2.13 x 10^6 mm^4) specimen being higher than the thin plate (0.26 x 10^6 mm^4). In theory, structure with higher I have more resistance to bending, therefore, with higher bending resistance, the flexural strength of the prismatic specimen is expected to be greater.

Knowing that fibres are randomly orientated in FRCC, it was expected that the coefficient of variation (COV) will be slightly higher in FRCC's specimen. From Figure 4.18, the COV of prismatic specimen was in the range of 3.47 – 10.65 %; whereas Figure 4.19 indicates the COV of thin section specimen was in between 0.77 – 29.69 %. The lower COV observed for the prismatic specimen was most likely due to the more uniform particle (inclusive of binder, aggregates and fibre) packing of fresh FRCC whereas there was limited space in the thinner specimen which cause greater inhomogeneity.

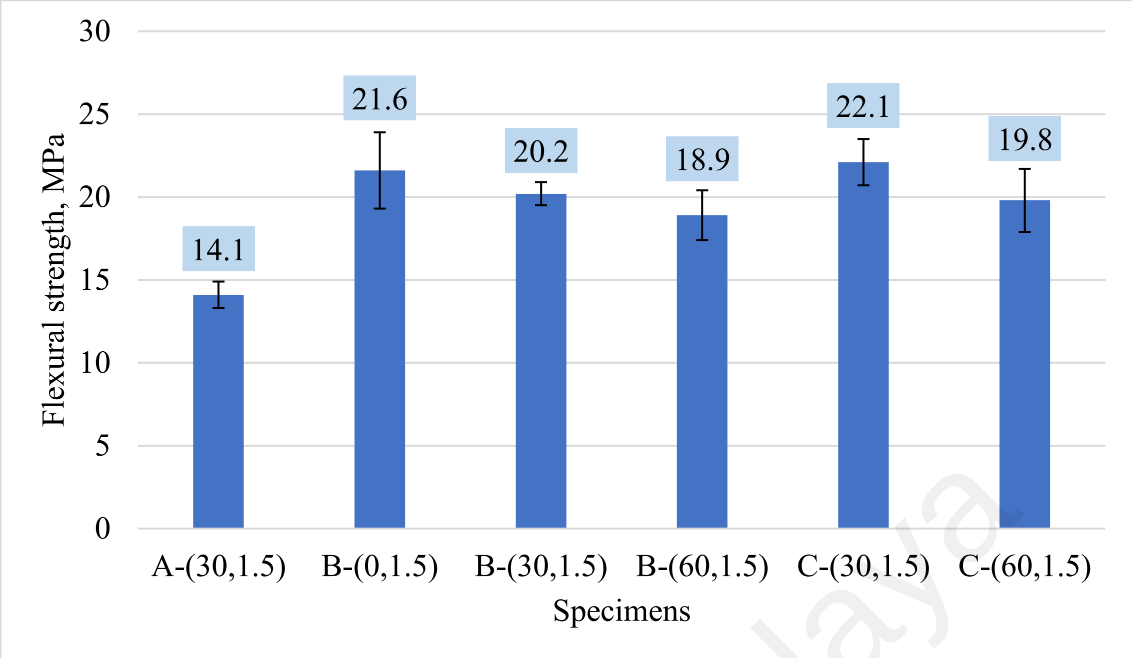

Figure 4.18 Flexural strength of prismatic specimen (three-point bending)

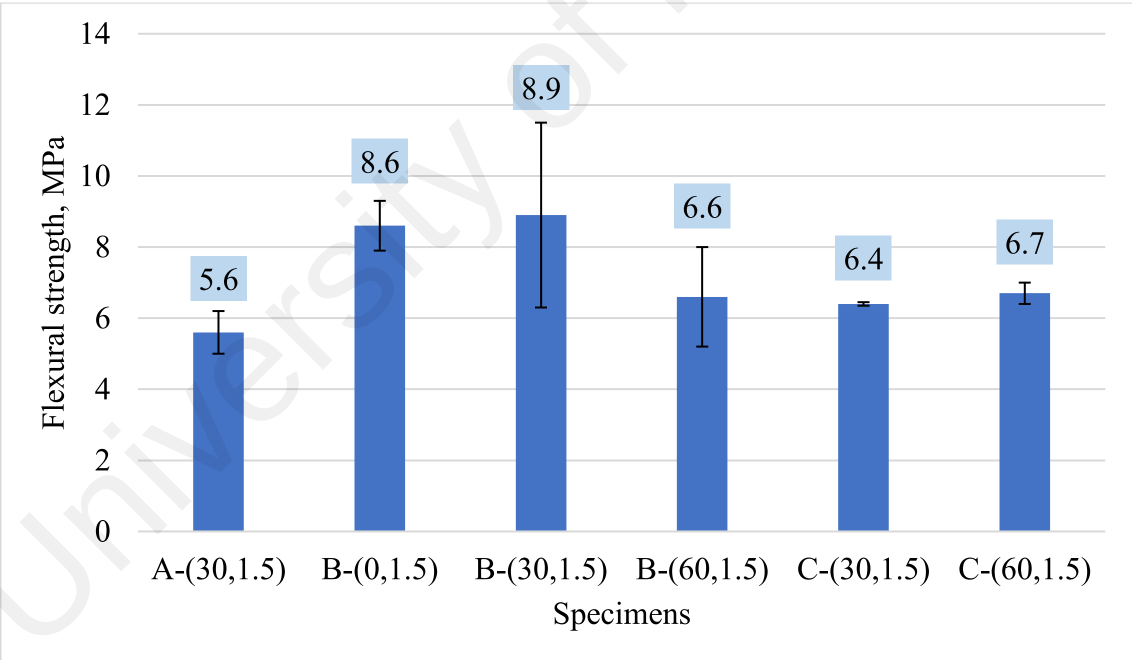

Figure 4.19 Flexural strength of thin plate specimen (four-point bending)

4.3.4 Flexural load-extension curve

4.3.4.1 Prismatic specimen

The flexural load-extension curves of FRCC specimens with cross section of 40 mm x 40 mm were plotted in Figure 4.20 to Figure 4.25. Based on the shape of the curves, PVA fibre was able to prevent instantaneous failure by delaying the fracture failure shortly for about 0.59 mm to 0.89 mm as shown in Figure 4.26.

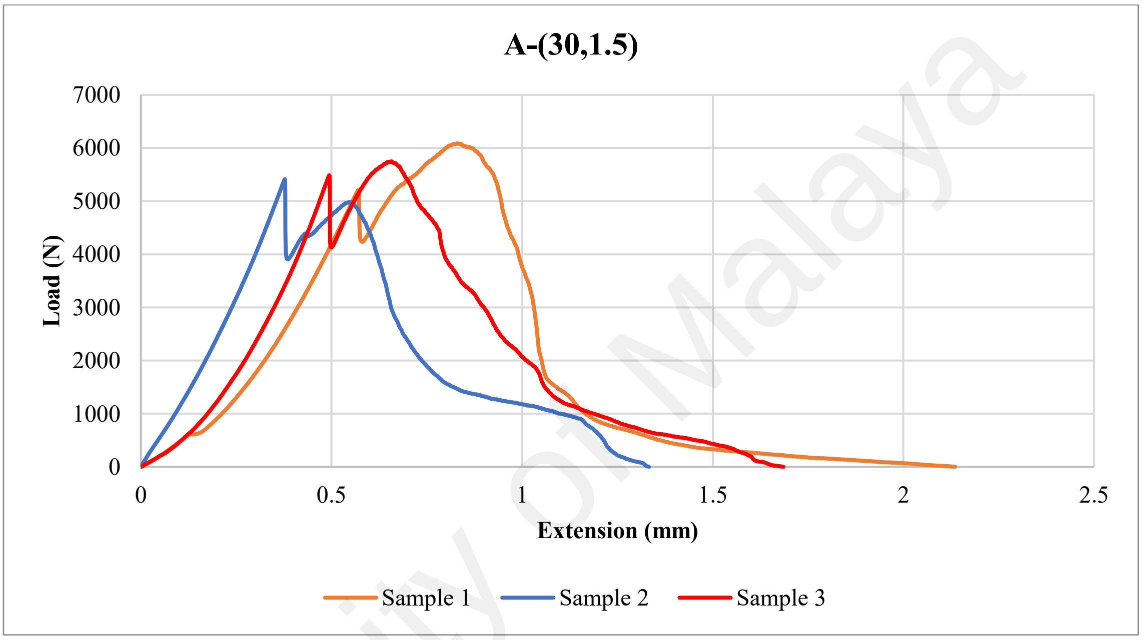

Figure 4.20 Load-extension curve of A-(30,1.5) (prismatic specimen)

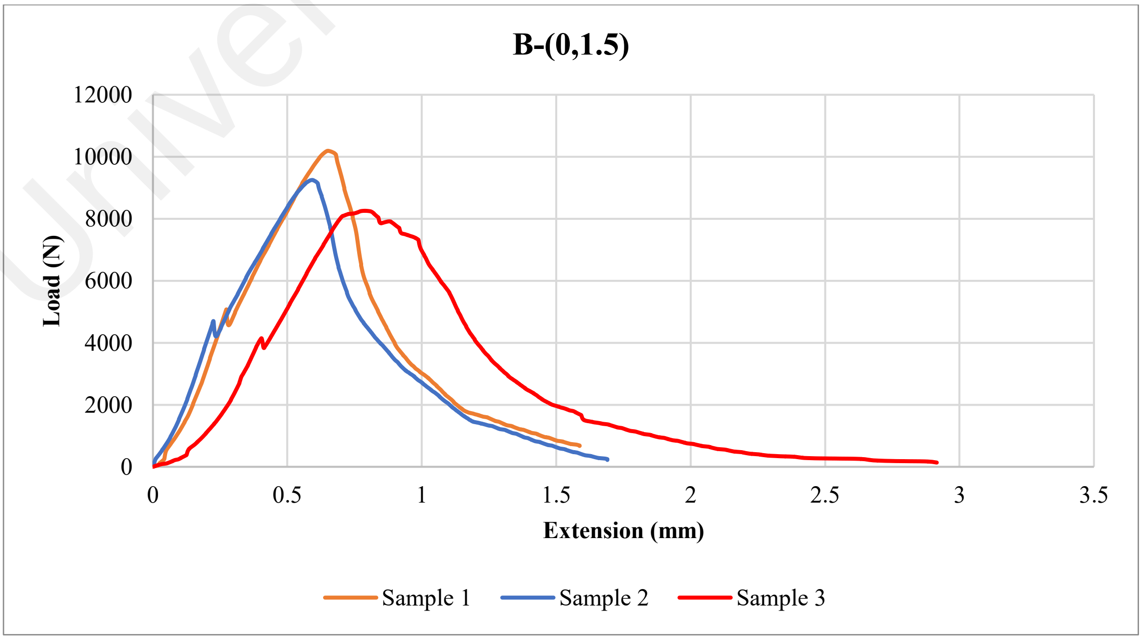

Figure 4.21 Load-Extension curve of B-(0,1.5) (prismatic specimen)

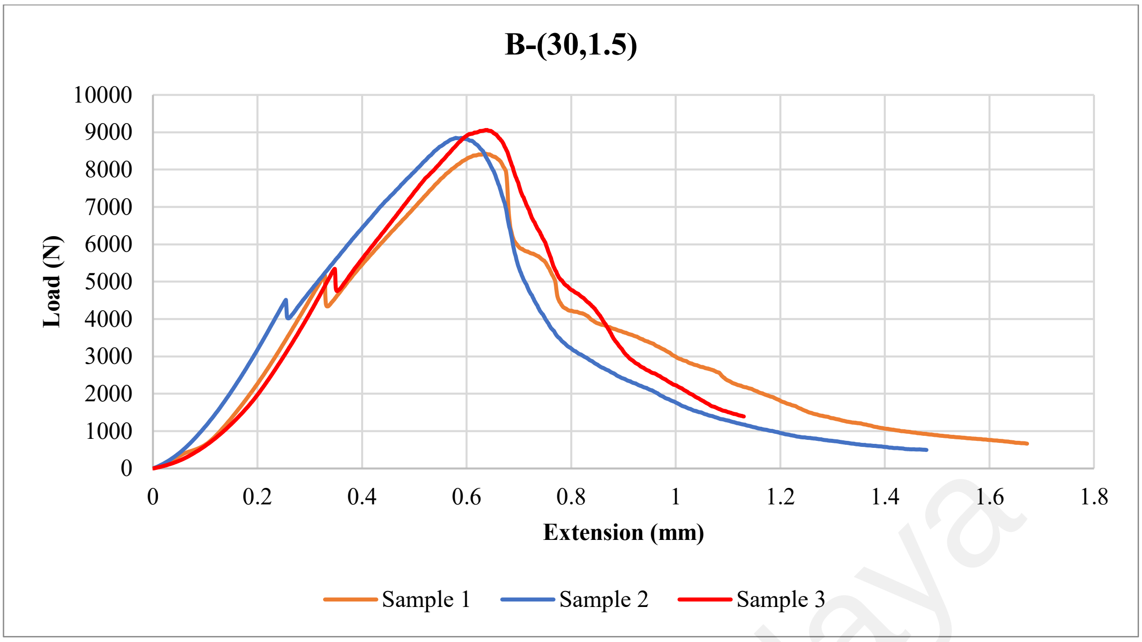

Figure 4.22 Load-extension curve of B-(30,1.5) (prismatic specimen)

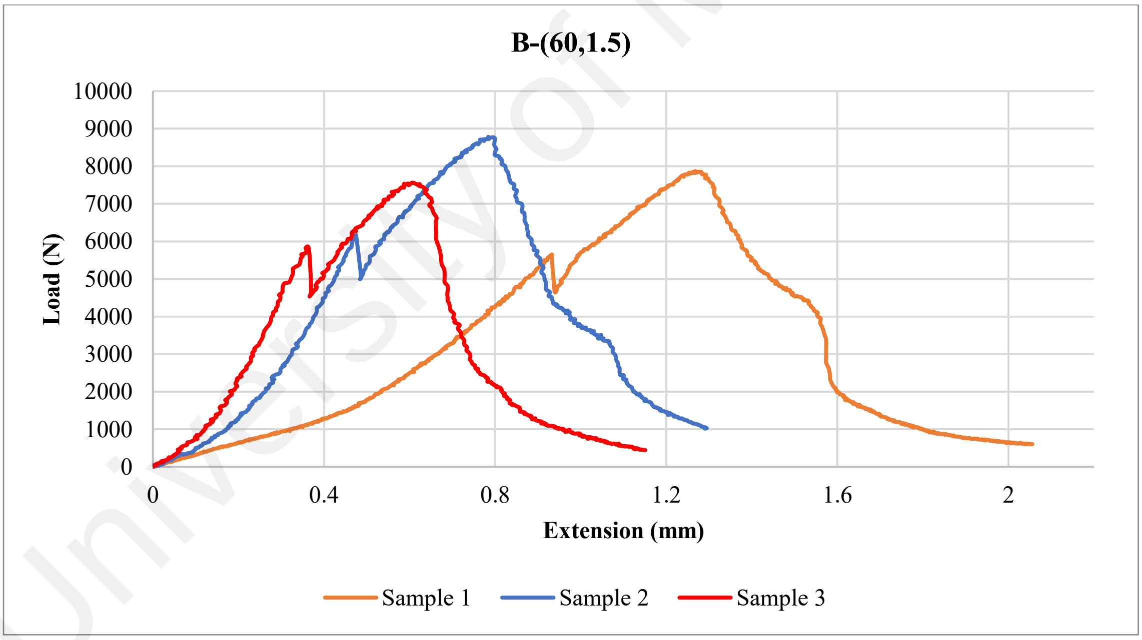

Figure 4.23 Load-extension curve of B-(60,1.5) (prismatic specimen)

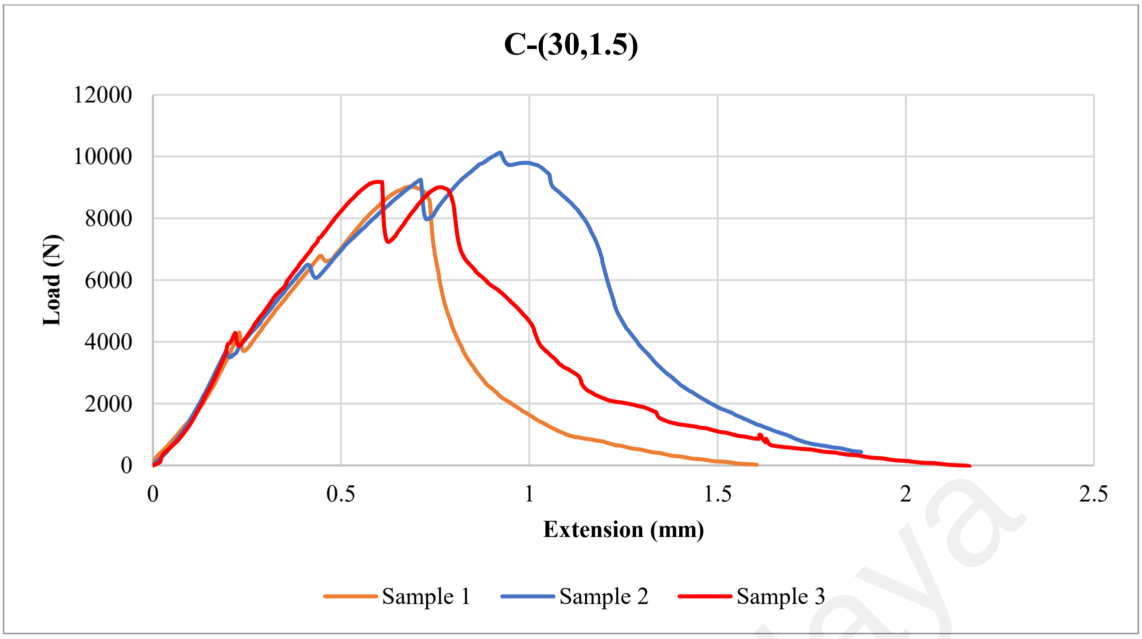

Figure 4.24 Load-extension curve of C-(30,1.5) (prismatic specimen)

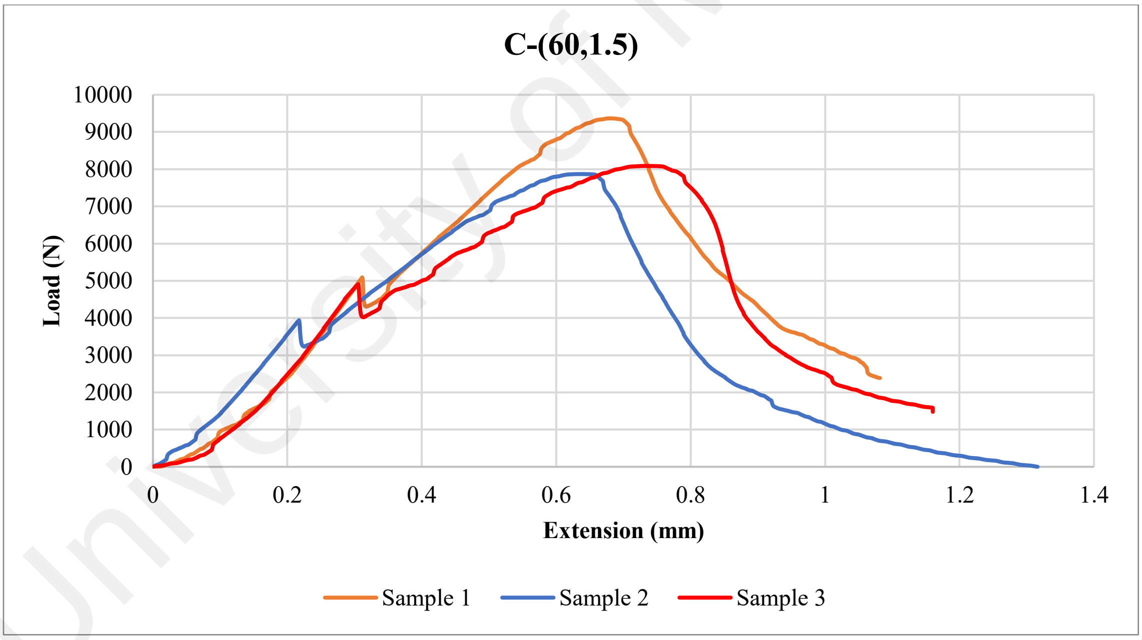

Figure 4.25 Load-extension curve of C-(60,1.5) (prismatic specimen)

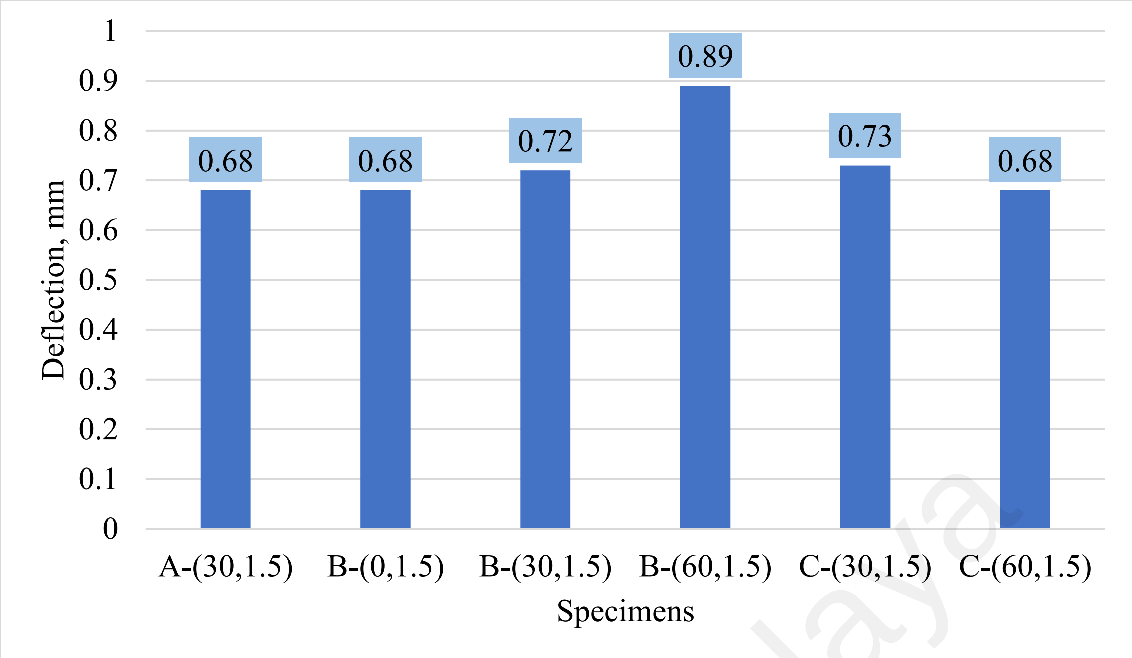

Figure 4.26 Average deflection of prismatic FRCC specimens at maximum load

4.3.4.2 Thin plate specimen

When comparing the deflection of both thin plate and prismatic FRCC specimens, it is obvious that the thin plate specimens exhibited relatively higher deflection. The deflection at maximum load recorded was in the range of 3.27 mm and 9.37 mm. This was most likely due to the difference in second moment of area (I). As I is inversely proportional to the maximum deflection, lower magnitude in I induce higher deflection. Therefore, the curves shown in Figure 4.27 to Figure 4.32 extended longer at the axis of deflection.

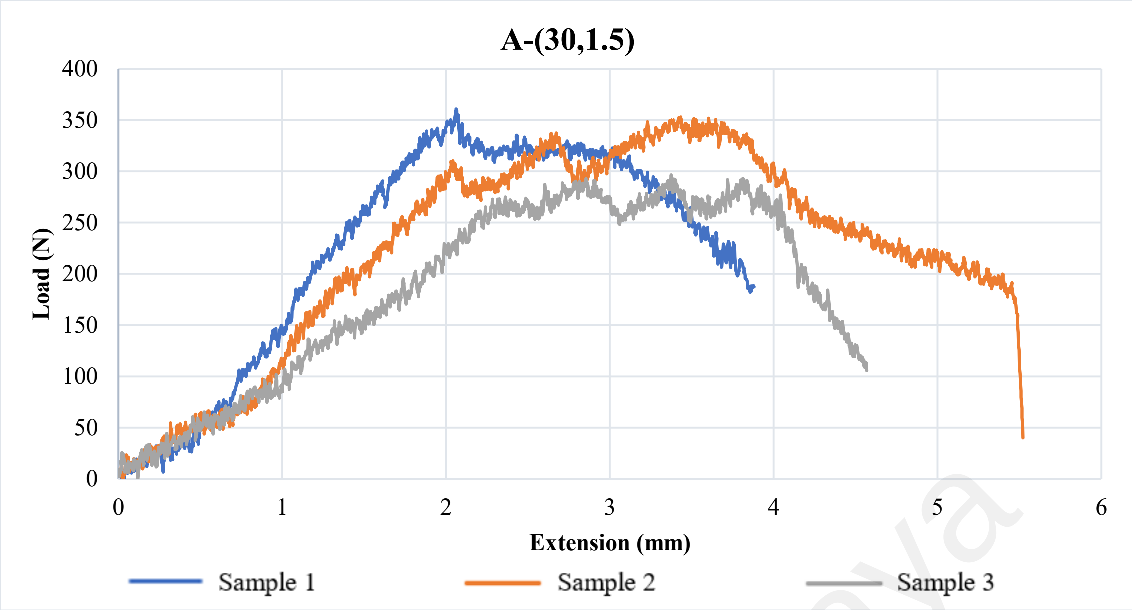

Figure 4.27 Load-extension curve of A-(30,1.5) (thin plate specimen)

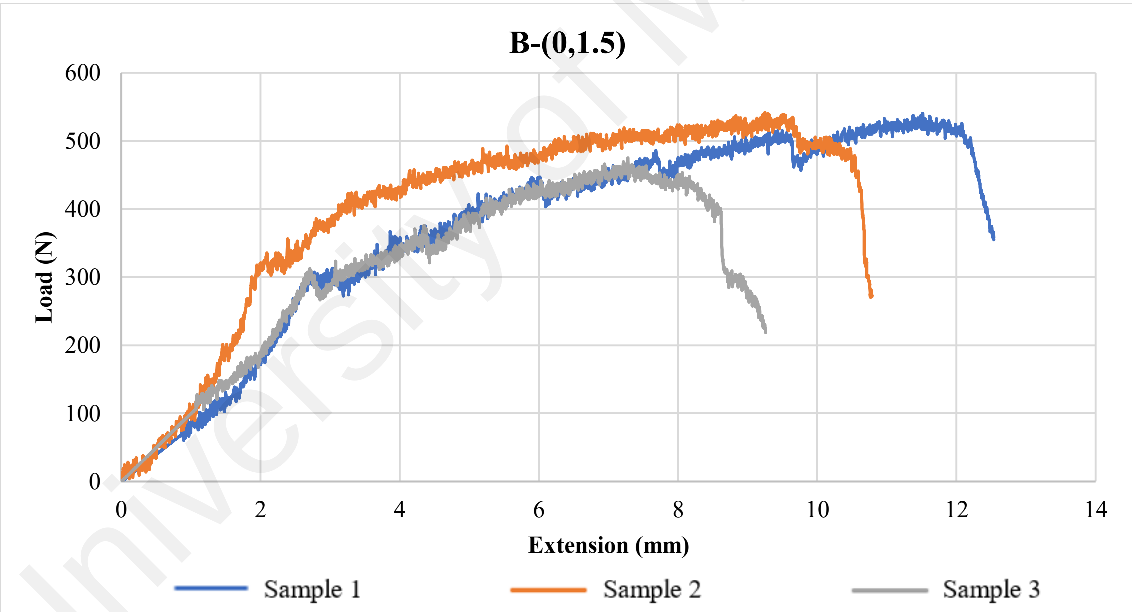

Figure 4.28 Load-extension curve of B-(0,1.5) (thin plate specimen)

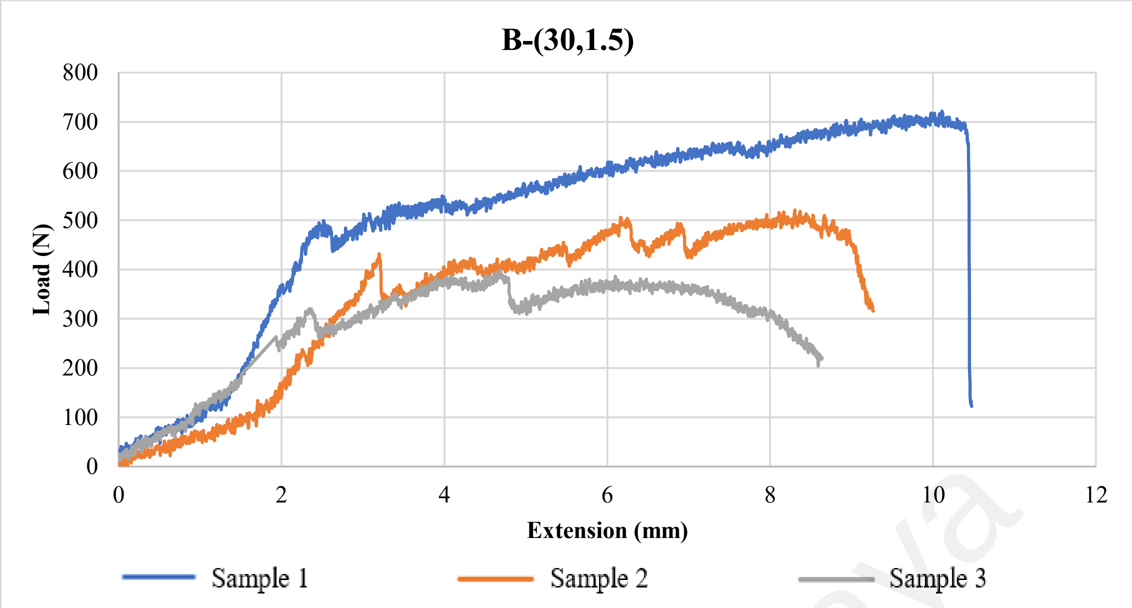

Figure 4.29 Load-deflection curve of B-(30,1.5) (thin plate specimen)

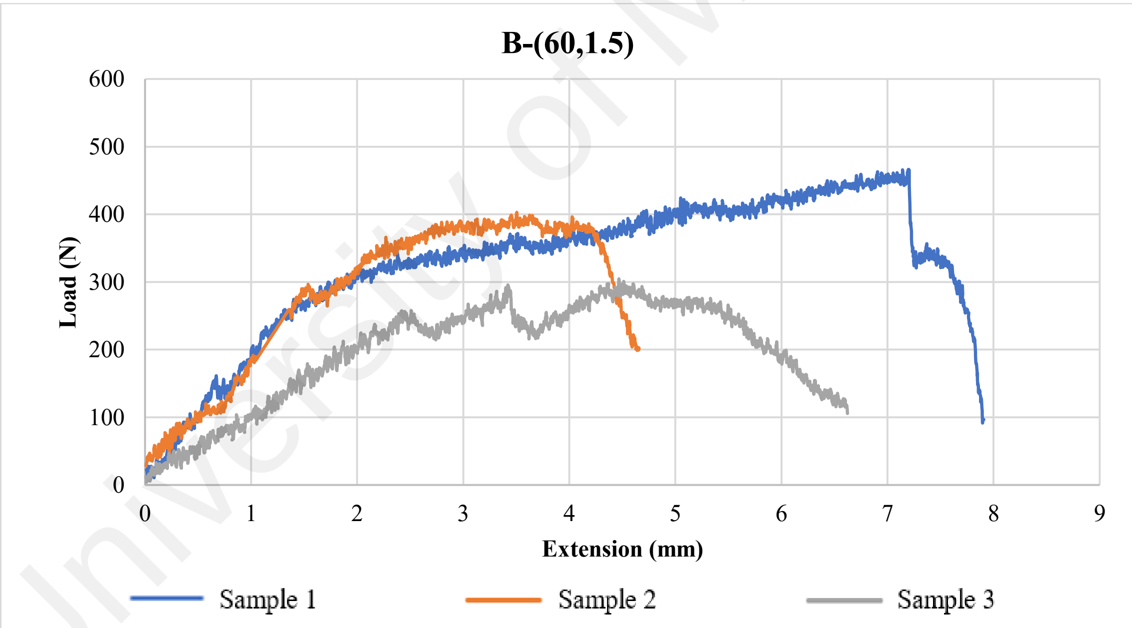

Figure 4.30 Load-extension curve of B-(60,1.5) (thin plate specimen)

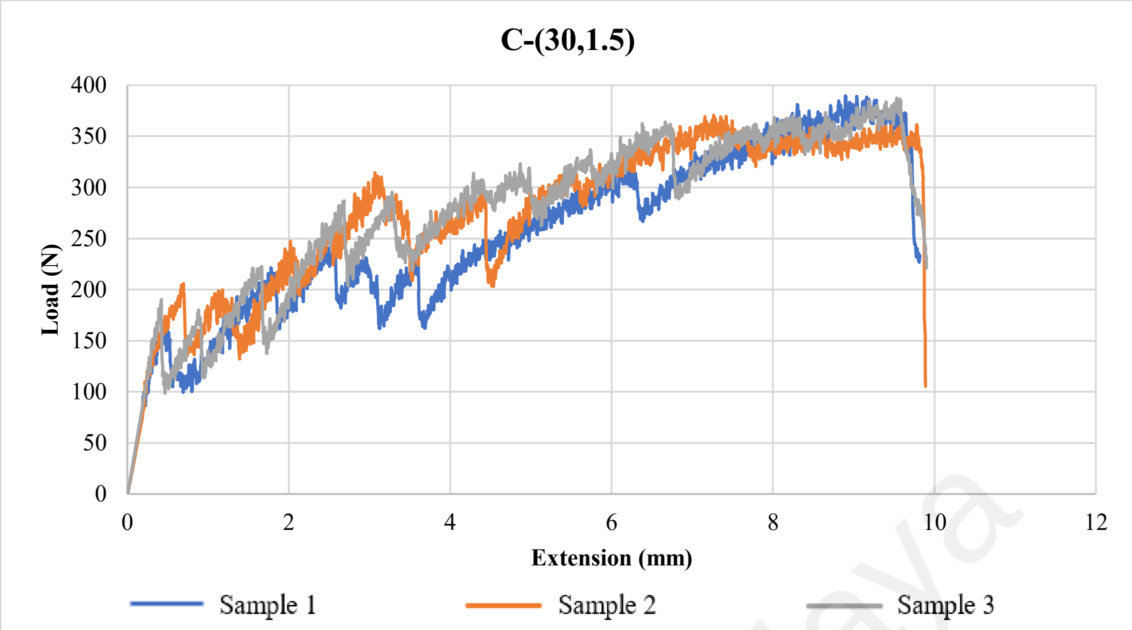

Figure 4.31 Load-deflection curve of C-(30,1.5) (thin plate specimen)

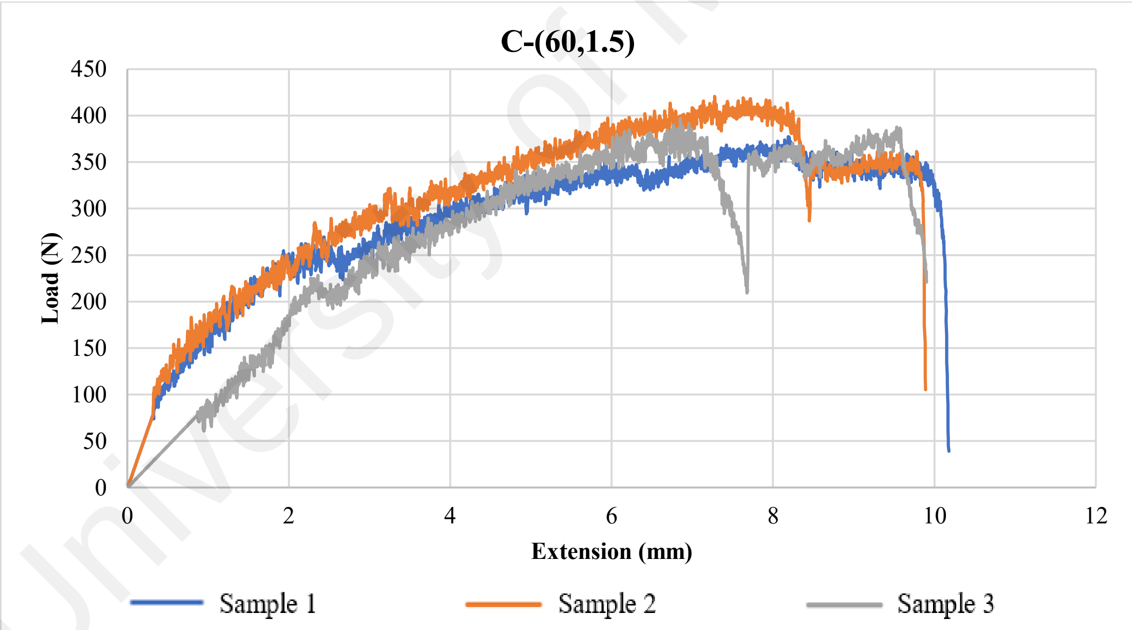

Figure 4.32 Load-deflection curve of C-(60,1.5) (thin plate specimen)

The average maximum deflection of the thin plate FRCC specimens is shown in Figure 4.33. This chart shows the effect of binder content and percentage of GGBS replacement is significant as expected. Deflection increased along with the binder content; whereas deflection decreased as the content of GGBS increased. Both observations can be linked to the matrix strength which was correlated to its compressive strength. Consequently, the specimens were stiffer and deflected less. In overall, the deflection for both Series B and C was similar when the percentage of GGBS replacement was same.

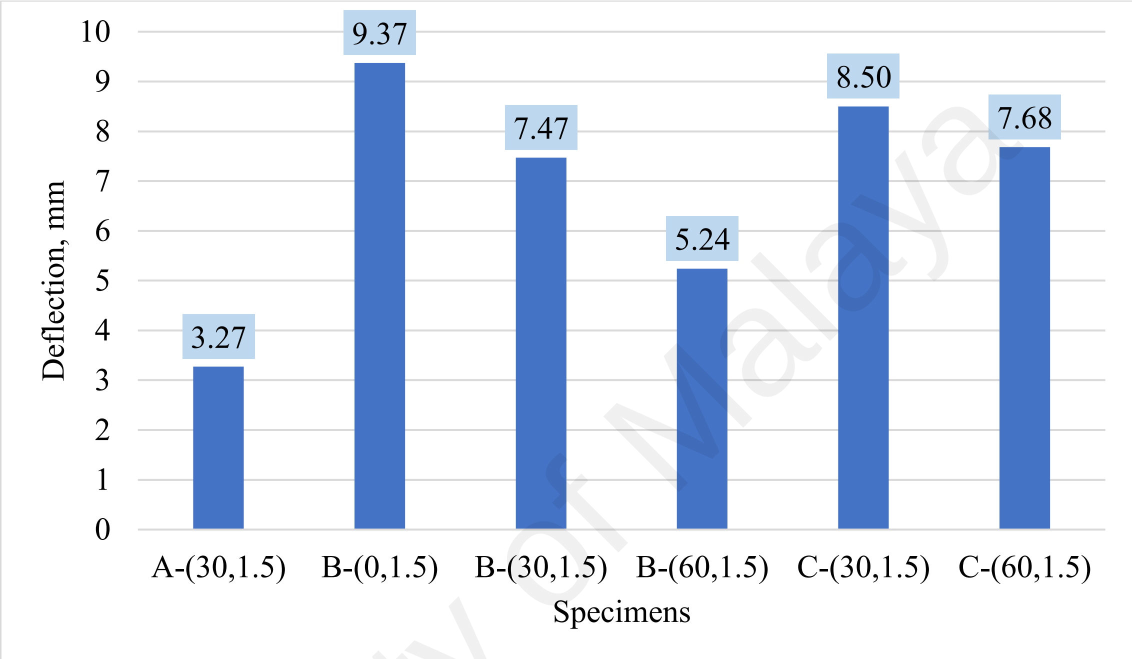

Figure 4.33 Average deflection of thin plate FRCC specimens at maximum load

4.3.4.3 Summary

As summary, the intermediate load-extension curves of each mix from prismatic and thin plate specimens were combined in the graph shown in Figure 4.34 and Figure 4.35.

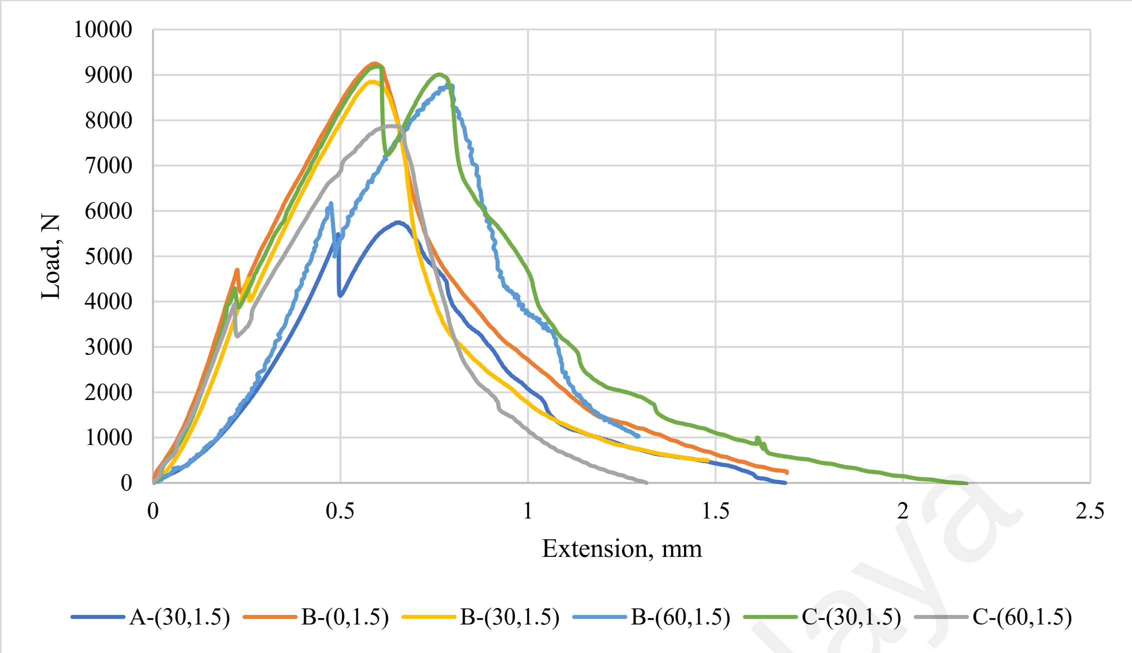

Figure 4.34 Combined load-extension curve of prismatic specimens

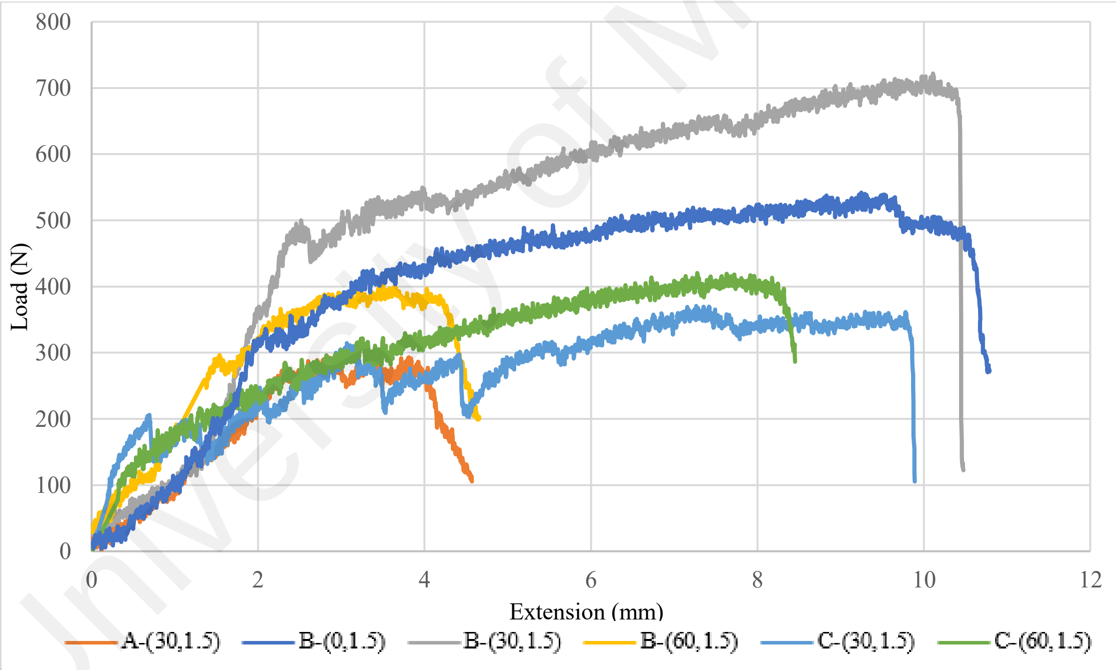

Figure 4.35 Combined load-extension curve of thin plate specimens

4.3.5 Ratio of post peak strength-to-first crack strength (σ_2/σ_1)

Overall, the ratio of post crack to first crack load is higher in prismatic specimen as compared to thin plate specimen which is shown in Table 4.5. This is most likely due to prismatic specimens which allowed the PVA fibres to bridge the specimens after first crack to a greater extent. Meanwhile, since the thickness in thin plate specimens was 16 mm and the fibre used was 13 mm in length, the performance of the FRCC in post-cracking stage was limited. The most significant observation made was that the mix C-(30,1.5) had the highest ratio in both prismatic and thin plate at 2.32 and 2.05 respectively; whereas A-(30,1.5) had the lowest ratio at 1.04 and 1.05 correspondingly. As fibres main contribution is in the post-cracking stage, the ratio was likely to be affected by the fibre dispersion associated with its workability. The workability results in Table 4.1 evidently shows that C-(30,1.5) had the highest flow diameter whereas A-(30,1.5) had the lowest flow diameter. On the other hand, Table 4.5 shows the ratio of post peak strength to first crack strength decreased as the content of GGBS increased. This could be due to the increasing content of GGBS improved the matrix toughness by having higher first crack strength which was associated with its compressive strength (Said & Razak, 2015).

Table 4.5 First crack, post peak strength and the ratio of FRCC specimens

Specimen	Prismatic specimen (160 mm x 40 mm x 40 mm)			Thin plate specimen (500 mm x 75 mm x 16 mm)		
	σ_1 (MPa)	σ_2 (MPa)	Ratio	σ_1 (MPa)	σ_2 (MPa)	Ratio
A-(30,1.5)	12.6	13.5	1.04	5.1	5.6	1.05
B-(0,1.5)	10.9	21.6	1.99	5.6	8.6	1.54
B-(30,1.5)	10.8	20.2	1.76	6.7	8.9	1.30
B-(60,1.5)	13.8	18.9	1.37	5.0	6.6	1.32
C-(30,1.5)	9.6	22.1	2.32	3.2	6.4	2.05
C-(60,1.5)	10.4	18.9	1.83	3.9	6.7	1.72

4.3.6 Flexural toughness

Table 4.6 shows the flexural toughness of both prismatic and thin plate specimens. As deflection was relatively low in prismatic specimen, the computed flexural toughness was primarily from the flexural load. Thus, the trend in thick section was insignificant. Conversely, the flexural toughness from thin plate specimen exhibited a significant trend. Based on previous observation, GGBS was able to enhance the matrix strength, but this was offset by the reduced deflection of the specimens which consequently led to decrease in flexural toughness. For instance, the flexural toughness of specimen from the mix B-(30,1.5) and B-(60,1.5) was reduced by 4.5% and 47.9%, respectively compared to B-(0,1.5) and similarly for C-(60,1.5) in which the toughness decreased by 19.3% compared to C-(30,1.5). It should be noted that among the 3 series, Series B exhibited the highest toughness. This could be due to Series B had the optimum binder content which provided high matrix strength without compensating much in deflection, provided GGBS content did not exceed 60% in FA replacement.

Table 4.6 Flexural toughness

Specimens	Prismatic specimen (160 mm x 40 mm x 40 mm)	Thin section (500 mm x 75 mm x 16 mm)
	Flexural toughness, N/m	Flexural toughness, N/m
A-(30,1.5)	1800	750
B-(0,1.5)	3120	3320
B-(30,1.5)	2390	3170
B-(60,1.5)	3480	1730
C-(30,1.5)	3820	2740
C-(60,1.5)	2630	2210

4.3.7 Flexural failure mode

4.3.7.1 Prismatic specimen

After flexural test, the number of crack lines in prismatic specimens was visually inspected and tabulated in Table 4.7. Specimen A-(30,1.5) showed single crack, whereas B-(60,1.5) and C-(30,1.5) exhibited the highest number of crack lines of 5. The single localized failure of A-(30,1.5) shown in Figure 4.36 indicated that the PVA fibre in the mix did not effectively contribute in post-cracking stage. This happened because bundled PVA fibres were observed at the failure plane as shown in Figure 4.37. Furthermore, the low σ_2/σ_1 ratio (1.04) of A-(30,1.5) corroborated that the PVA fibre in this mix imparted only limited post-crack ductility after the initial crack occurred. However, instead of smooth line, the crack path shown in A-(30,1.5) was tortuous and this indicated the PVA fibres could still impart some degree of ductility in A-(30,1.5).

Table 4.7 Observed number of crack lines on prismatic FRCC specimens

Specimens	Average number of crack line(s)
A-(30,1.5)	1
B-(0,1.5)	3
B-(30,1.5)	2
B-(60,1.5)	5
C-(30,1.5)	5
C-(60,1.5)	3

Figure 4.36 Failure mode of prism specimen, A-(30,1.5)

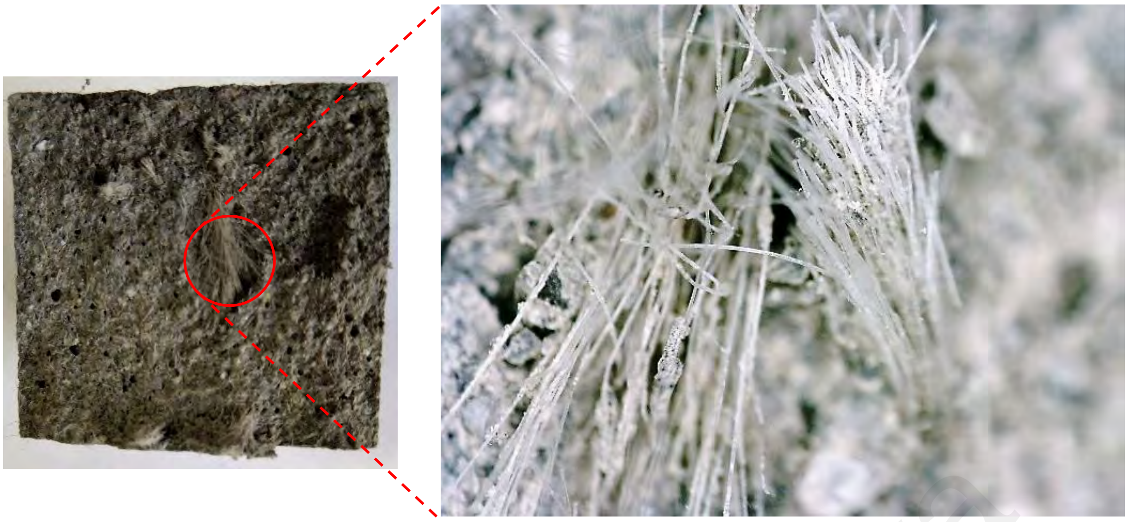

Figure 4.37 Tested A-(30,1.5) prism specimen at failure plane

On the other hand, the other specimens exhibited multiple surface cracking, which are shown in Figure 4.38. However, B-(60,1.5) had distinctive failure mode from the others. As displayed in Figure 4.39, besides transverse cracks at the bottom surface, internal crack lines were revealed after dampened the specimens with water. There were fewer undispersed PVA fibre in the other specimens as shown in Figure 4.40 especially in Series C, due to higher paste content. When inspecting the fracture surface of the specimens, it was found that the PVA fibres were mostly ruptured (Figure 4.41). This could be due to the lower tensile strength of the fibre compared to the matrix strength. Nonetheless, the micrograph in Figure 4.42 shows that the undispersed PVA fibre was pulled out from the matrix during fracture by having smooth edge at the tip of the fibre. This happened because the undispersed PVA fibre was able to resist higher load compared to single strand fibre and this prevented the specimen from rupturing.

Figure 4.38 Typical failure mode of prismatic FRCC specimens

Figure 4.39 Failure mode of prismatic specimen, B-(60,1.5)

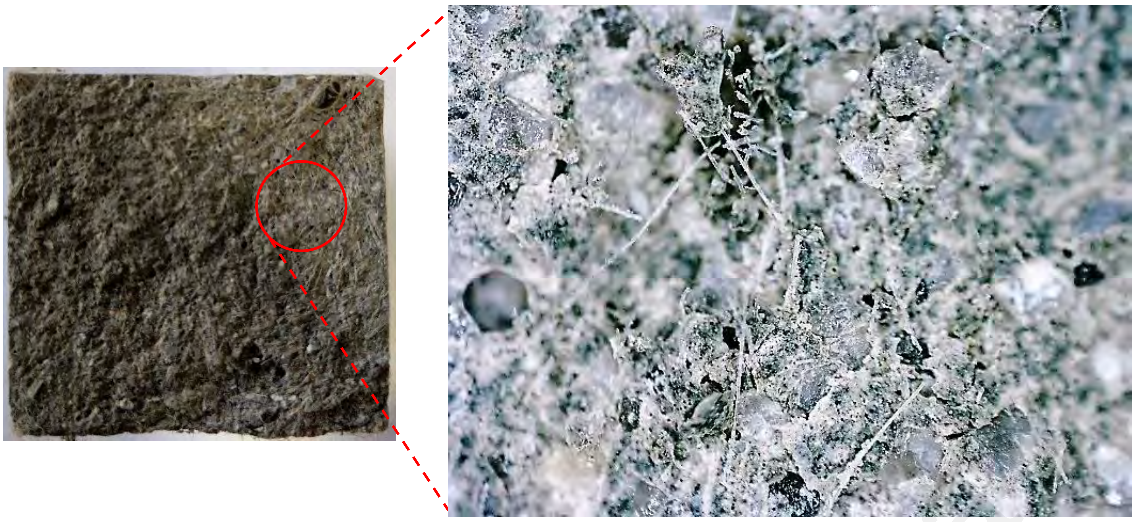

Figure 4.40 Failure plane of FRCC prism

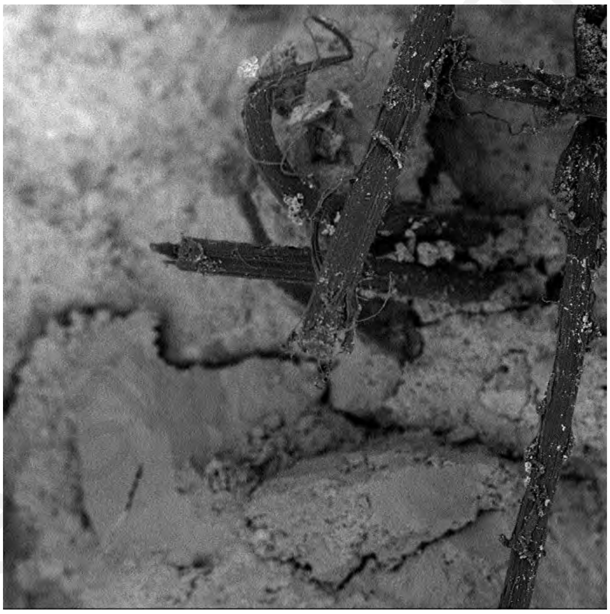

Figure 4.41 Micrograph of fracture surface of prismatic FRCC specimen

Figure 4.42 Micrograph of fracture surface at prismatic A-(30,1.5) specimen (undispersed fibre)

4.3.7.2 Thin plate specimen

In overall, Figure 4.43 shows typical failure mode of tested thin plate FRCC specimen. The PVA fibres at the fracture surface were observed to have ruptured, similar to prismatic specimens seen from Figure 4.41. By comparing Table 4.7 and Table 4.8, it was significant that the number of crack lines in thin section were higher than those found in the prismatic specimens. This could be due to the higher span to depth ratio in thin section FRCC which allowed more cracks to form. As PVA fibres did not disperse well in specimen A-(30,1.5), it was expected that the PVA fibres could only have limited contribution during the post-cracking stage. As a result, the least number of crack lines recorded was in A-(30,1.5) which also experienced the lowest deflection of 3.27 mm. Conversely, for the specimen, B-(0,1.5) that had the highest deflection of 9.37 mm, the highest number of crack lines was found. Interestingly, B-(60,1.5) had the second lowest deflection value but exhibited the second highest number of crack lines. This was most likely due to the distinctive cracking pattern in B-(60,1.5) as illustrated in Figure 4.44. The plausible reason for the distinctive cracking pattern was the high fibre-matrix interfacial bond contributed from the high GGBS content. Whereas the observed number of crack line in the remaining specimens increased as the deflection was greater. Thus, it can be concluded that the deflection is directly proportional to the number of crack lines.

Table 4.8 Number of surface crack lines on thin plate FRCC specimens

Specimens	Average number of crack lines
A-(30,1.5)	9
B-(0,1.5)	25
B-(30,1.5)	15
B-(60,1.5)	20
C-(30,1.5)	19
C-(60,1.5)	17

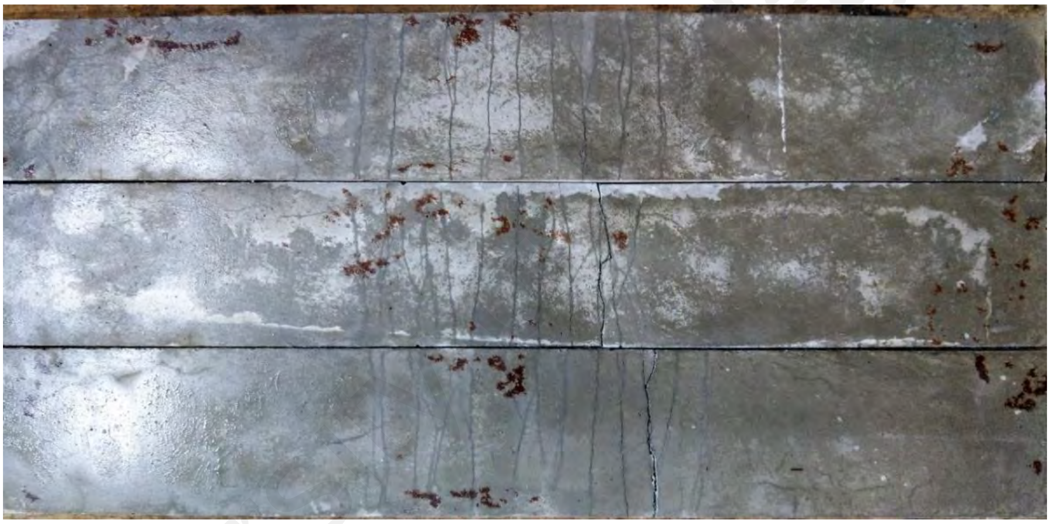

Figure 4.43 Typical failure mode of FRCC thin section specimens

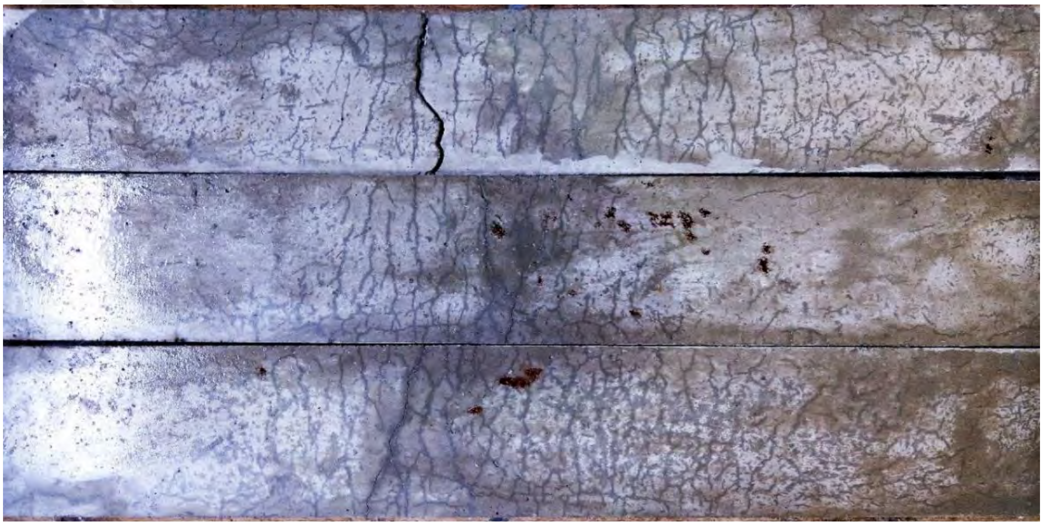

Figure 4.44 Failure mode of thin section specimen, B-(60,1.5)

4.3.8 Slant shear strength

The bar chart in Figure 4.45 shows that the slant shear strength of the composite prism specimens had good bond compatibility to the substrate by fulfilling the minimum requirement as stated in Table 2.2 and

Table 2.3; which was 3.1 MPa for horizontal surface and 5.2 MPa for vertical surface. In general, it seems that the slant shear strength increased along with the compressive strength of the FRCC in the composite prism at the 1st day. However, the magnitude of compressive strength was not necessary directly correlated with the value of slant shear strength, which was also stated by Gürkan Yıldırım *et al.* (2018). Instead, it was governed by mechanical compatibility. For instance, composite prism C-(30,1.5) had the lowest 28-day compressive strength (57.0 MPa) among the other specimens but acquired highest slant shear strength. This was due to the lowest difference in compressive strength between the mix C-(30,1.5) and the substrate (30 MPa) compared to other mixes, and this difference was about 27.0 MPa. Overall, the effect of binder and GGBS content was not significant on the slant shear strength.

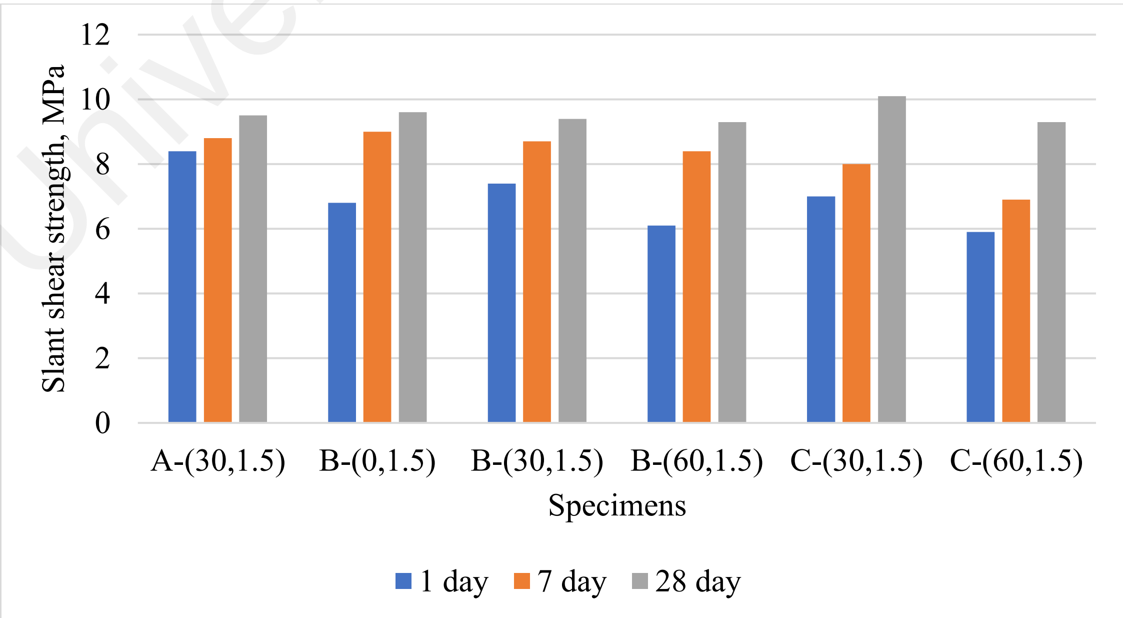

Figure 4.45 Slant shear strength of FRCC specimen at different age

At the age of 1 day, the failure mode of the composite prisms can be observed in Figure 4.46 which was mostly in between the joint of FRCC and the substrate. This happened because the bonding between FRCC with the substrate was still under development and the compressive strength of FRCC was still lower than the substrate (30 MPa). As FRCC is good in controlling cracks and does not exhibit brittle failure, cracks were not formed at relatively low load. Instead, they were formed at the weakest area which was the interface between FRCC and the substrate. Pattnaik (2015) similarly reported the failure mode occurred at the slant surface when performing slant shear strength test using repair material with lower compressive strength than the substrate. On the other hand, A-(30,1.5) had higher compressive strength (31.5 MPa) than the substrate on the 1st day and the failure mode shown in Figure 4.47 was different from the others. Hence, the substrate in A-(30,1.5)'s composite prism became the weaker part and began to fail before the FRCC. This type of failure mode is always desirable as it indicated the substrate is the weaker component of the complete repair system.

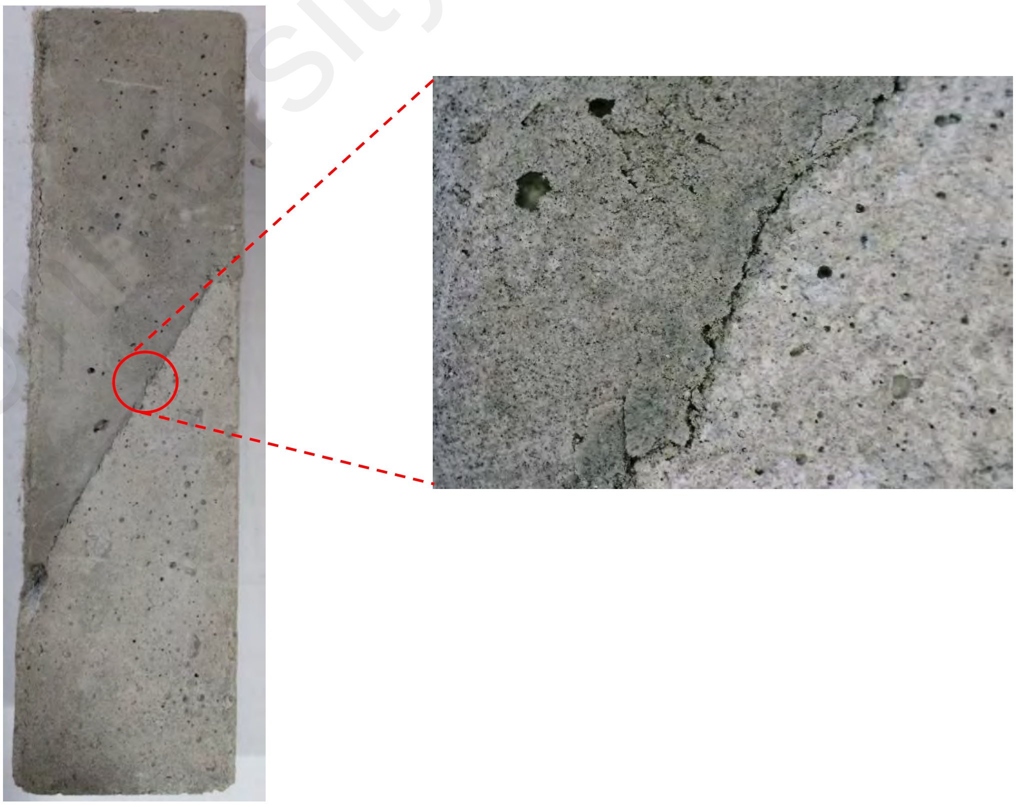

Figure 4.46 Typical failure mode of 1-day B-(0,1.5) composite prism

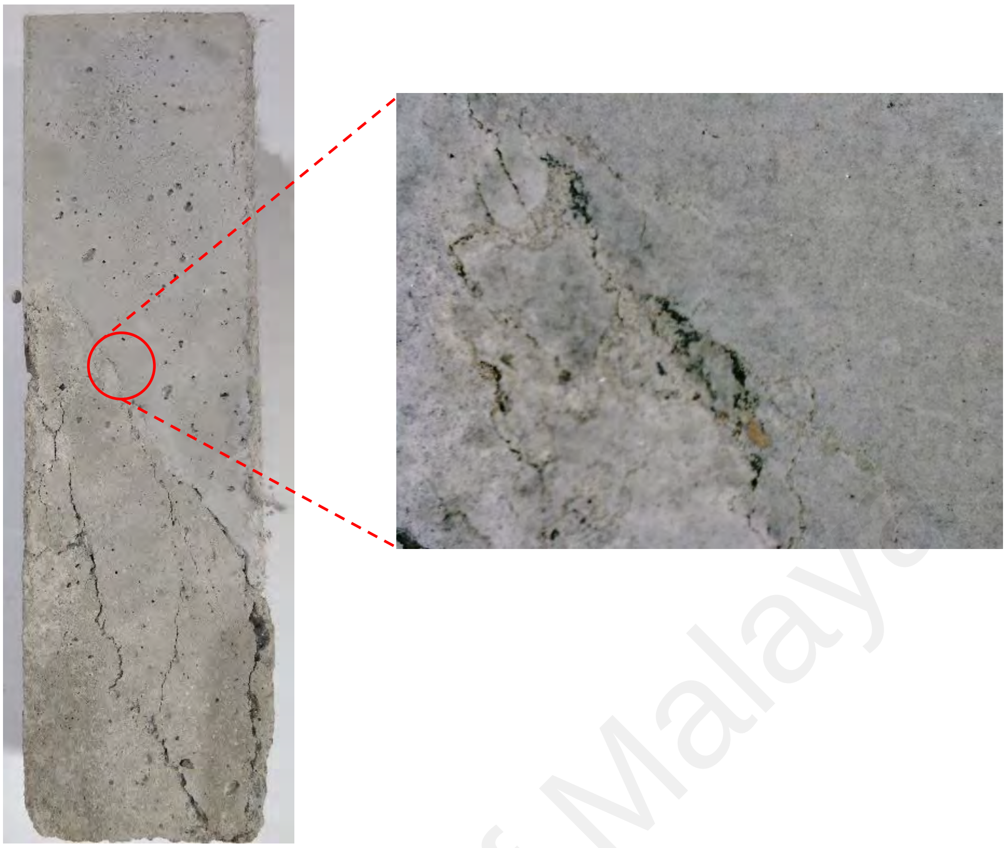

Figure 4.47 Tested 1-day A-(30,1.5) composite prism

On the other hand, as the composite prism underwent curing, the FRCC's compressive strength and bonding between FRCC and substrate were improved. As a result, the failure mode of the specimens tested on 7^{th} and 28^{th} day was different from 1-day age specimens. In Figure 4.48 and Figure 4.49, cracks were formed from the substrate, slightly passing through the joint up until FRCC; unlike in Figure 4.47, the cracks ceased to form beyond the interface between FRCC and substrate. Similarly, this type of failure can be related to substratum failure reported by Tayeh *et al.* (2013) or monolithic rupture as reported by Mustafa Sahmaran *et al.* (2013), which was considered as the most satisfactory failure mode for slant shear specimen.

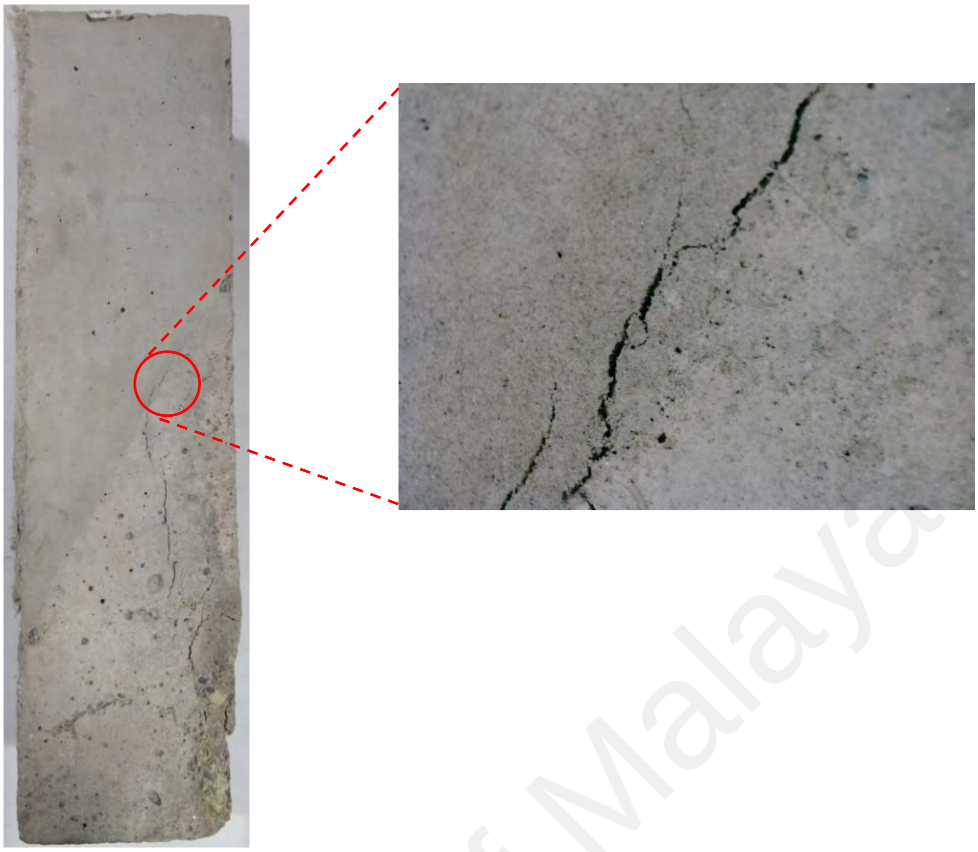

Figure 4.48 Tested 7-day C-(60,1.5) composite prism

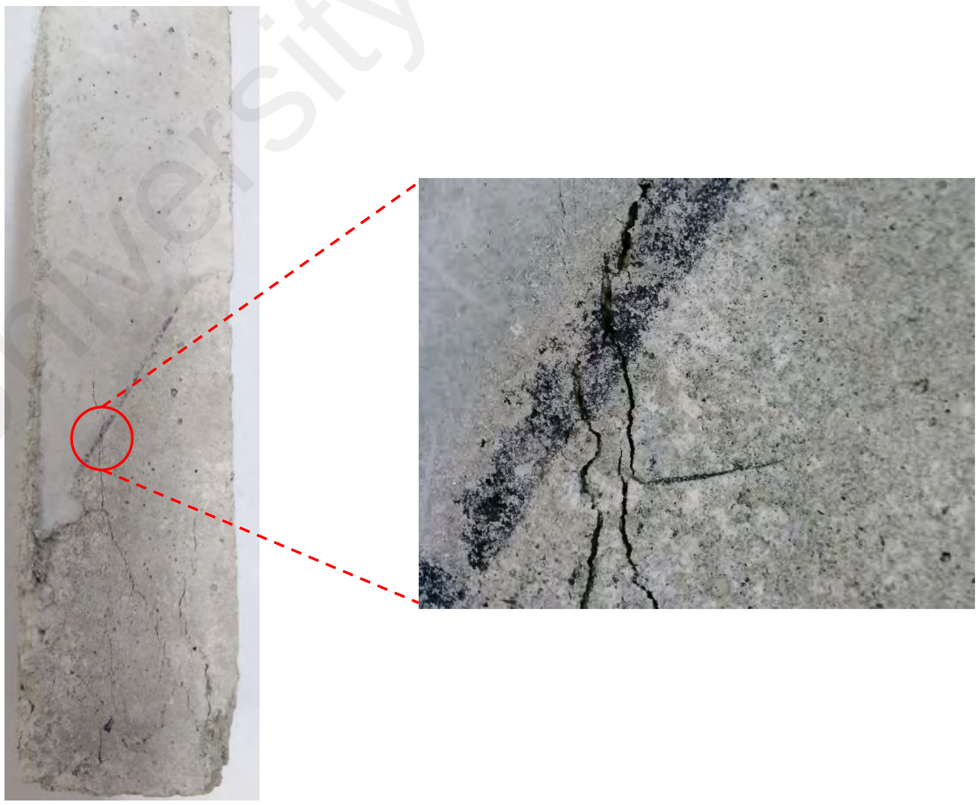

Figure 4.49 Tested 28-day B-(30,1.5) composite prism

4.3.9 Impact Strength

The chart in Figure 4.50 clearly indicates the contribution of PVA fibres on impact strength as FRCC specimens had 9 – 20 times higher impact energy compared to the specimen without fibres, namely B-(30,0). Upon impact, the fibres act as a connector to continue bridging the specimens before slipping off from the matrix. Apart from that, the impact strength shows an increasing trend with the GGBS content. Gradual increment in impact strength of about 31.12 kJ/m^2 and 79.08 kJ/m^2 was observed for the Series B mix containing 30% and 60% of GGBS replacement, respectively. Both specimens in Series C similarly shared the same trend, as highlighted by the increased impact strength of the mix.

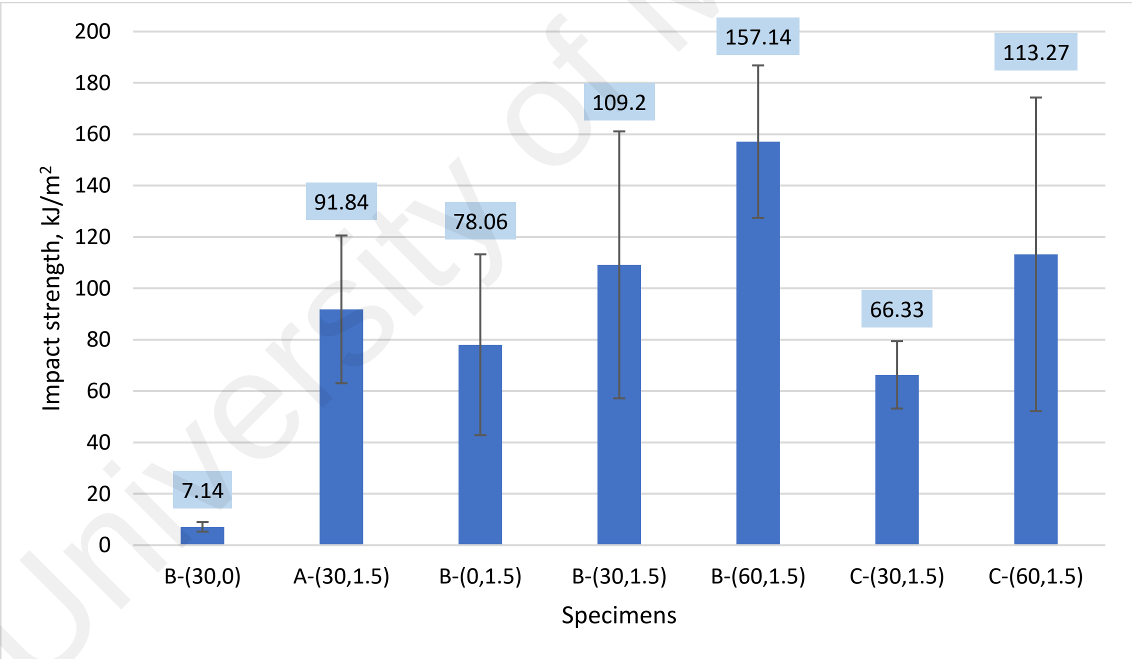

Figure 4.50 Impact strength of FRCC

However, at given percentage of GGBS, the impact strength varied for different binder content. For instance, the impact strength fluctuated from 91.84 kJ/m^2 to 109.18 kJ/m^2 and then to 66.33 kJ/m^2 respectively for A-(30,1.5), B-(30,1.5) and C-(30,1.5) specimens. This might be due to the combined factors of effectiveness in fibre dispersion and matrix toughness. When comparing A-(30,1.5) with B-(30,1.5), the latter exhibited higher impact strength than the former due to better fibre dispersion. As shown in Figure 4.51, undispersed PVA fibres were visible, whereas the fibres in Figure 4.52 shows otherwise. This shows that the better fibre distribution induced improved bridging effect which could affect the impact strength. It was expected that the PVA fibres in the higher binder content, C-(30,1.5) dispersed better than B-(30,1.5) by having better workability. However, the impact strength result showed otherwise by a reduction of 42.85 kJ/m^2 and same trend was also observed between B-(60,1.5) and C-(60,1.5) specimens. This phenomenon could be related to the greater influence of the matrix toughness.

Figure 4.51 Fracture surface of A-(30,1.5) after impact test

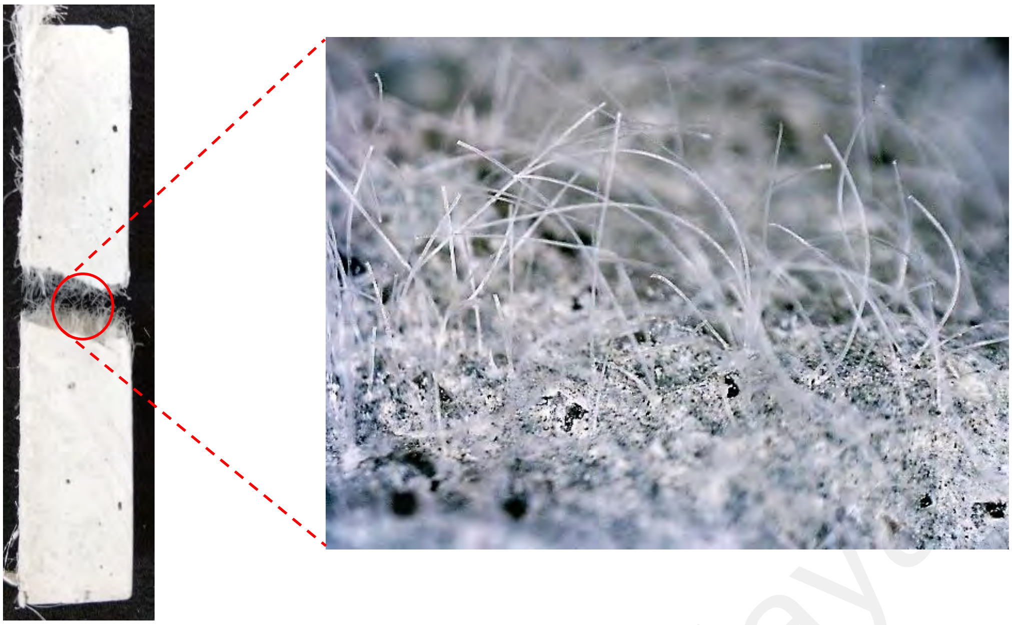

Figure 4.52 Fracture surface of B-(30,1.5) after impact test

The micrograph in Figure 4.53 and Figure 4.54 indicate the effect of binder and GGBS content respectively on the failure mode of PVA fibres after upon impact loading. In the specimen with the lowest binder content, A-(30,1.5), the PVA fibres were observed in bundled form; and the PVA fibres were increasingly well dispersed at higher binder contents. Besides that, roughening and fibrillation of PVA fibres were most severe in A-(30,1.5), followed by B-(30,1.5). This could be related to the higher matrix toughness causing greater bonding between PVA fibres and cementitious paste which was indicated by the amount of hardened matrix coated on the surface of PVA fibre. On the other hand, when looking at the effect of GGBS content, the PVA fibres shown in Figure 4.54 experienced the most deformation, including rupture in the specimen with the highest GGBS content. This was also very likely due to the better bonding between fibre and cementitious matrix which was rooted from the improved matrix toughness. Therefore, higher matrix strength from lower binder and higher GGBS content improved the matrix strength which further enhanced the bonding between fibre and matrix.

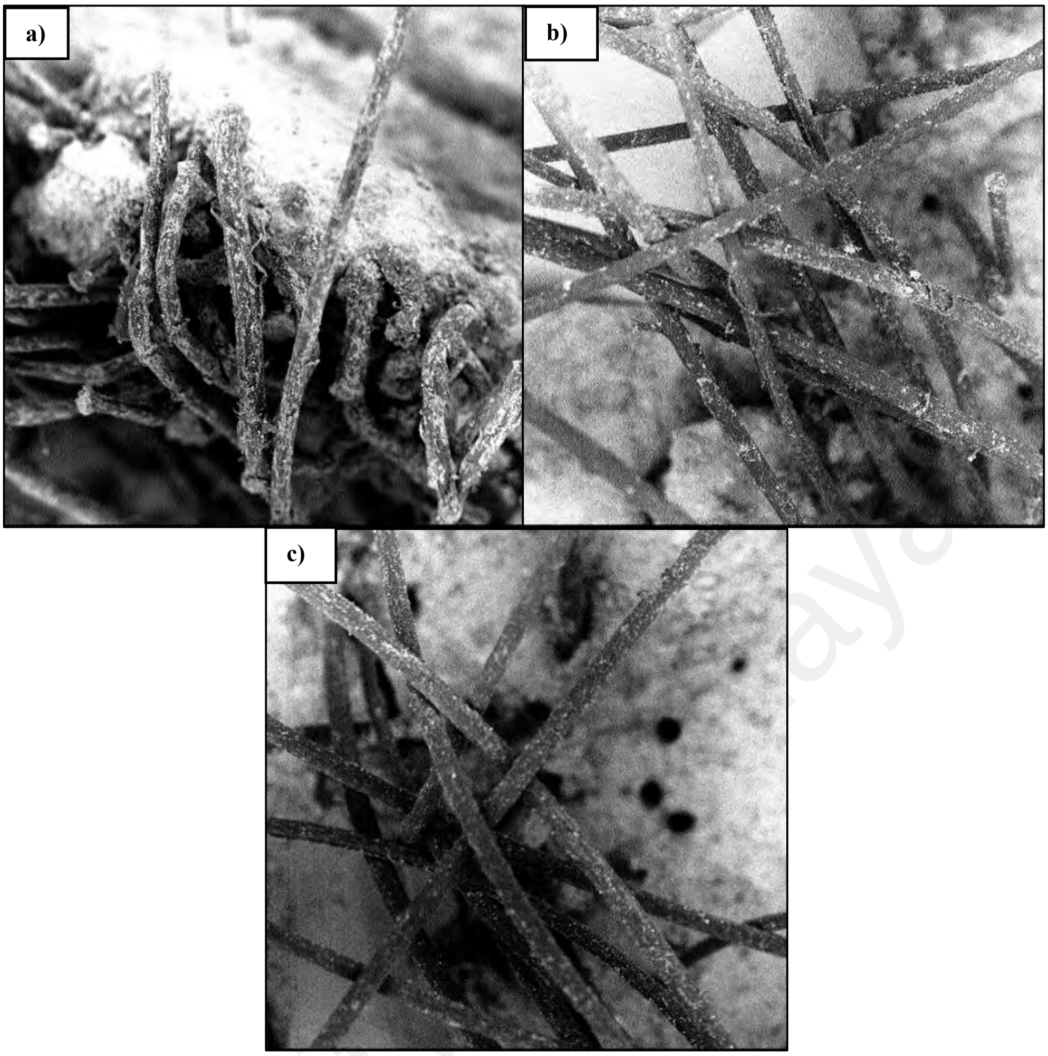

Figure 4.53 Micrograph of Charpy impact test specimen at increasing binder content: a)A-(30,1.5); b)B-(30,1.5); c)C-(30,1.5)

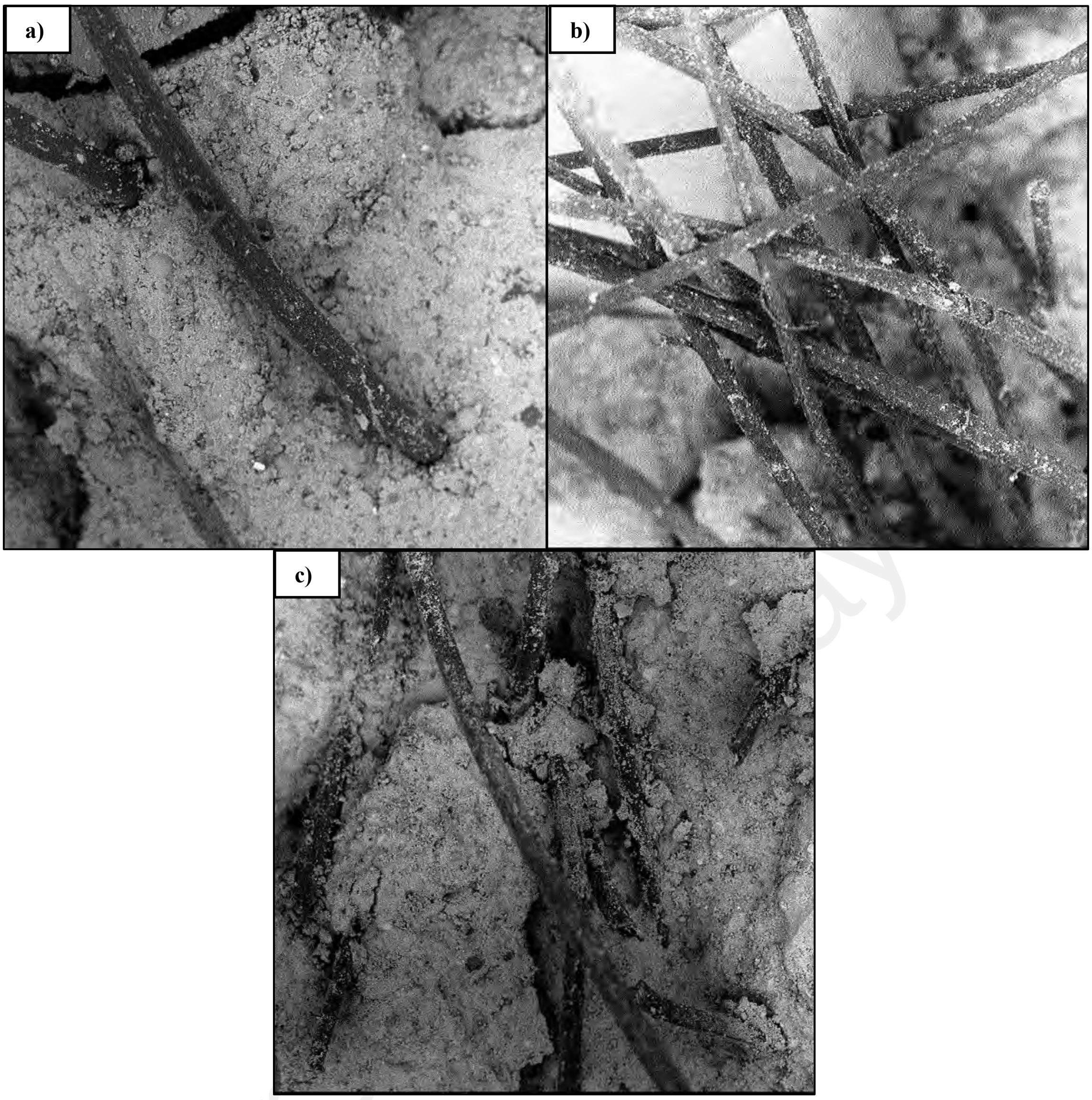

Figure 4.54 Micrograph of Charpy impact test specimen at increasing GGBS content: a)B-(0,1.5); b)B-(30,1.5); c)B-(60,1.5)

It was interesting that impact strength and flexural toughness had opposing effect due to GGBS content and binder content. At increasing GGBS content, flexural toughness was found to decrease whereas impact strength showed otherwise. Similarly, at increasing binder content, flexural toughness showed improvement whereas impact strength had varied effect. Overall, the measured impact strength was evidently much higher (approximately 17 – 122 times) than flexural toughness. Similar finding was also reported by researchers Atahan *et al.* (2012), as the impact strength recorded was higher than flexural toughness, though it was only approximately at threefold. This was due to the specimen size (350 mm x 50 mm x 15 mm) used was same in both impact and flexural strength tests. As compared to the specimen size (60 mm x 14 mm x 14 mm) used in this research, the geometry of it allowed more resistance against impact loading. In general, the higher magnitude in impact strength was due to the difference in the loading nature, where one is instantaneous dynamic loading and the other is static flexural loading. Indirectly, loading speed and duration affect the friction and interfacial stress between PVA fibre and matrix which consequently causing fibre ruptured at flexural strength test (Figure 4.38) and pulled out at impact test (Figure 4.52). As additional proof, the strands of PVA fibre shown in Figure 4.53 and Figure 4.54 mostly had smooth edge and experienced less roughening and fibrillation.

However, the COV recorded in this impact test was in the range of 18.9 % – 53.9 % which is considered to be high. This was due to the limitation in the specimen size for a standard Charpy impact test. As such, the fibre distribution might be affected and less evenly distributed. Therefore, a larger cross section of specimen can be considered in future for more consistent results.

CHAPTER 5: CONCLUSION

5.1 Introduction

This chapter summarises the findings on the investigation of ternary blended binder PVA FRCC as repair material and provides a few recommendations for future studies.

5.2 Conclusion

The workability of FRCC and the fibre dispersion were found to improve with the usage of higher binder content. However, the effect from GGBS varied at different binder content, but it was found that 30 % GGBS replacement had the most optimum result. The compressive strength of FRCC was significantly benefited from increasing GGBS, particularly in early age. However, the effect of increasing binder content on compressive strength showed otherwise. It can be summarized that lower binder and higher GGBS content contributed higher matrix strength.

The test results in second phase showed the different binder and GGBS contents imparted different effects on the mechanical properties of FRCC. In splitting tensile strength, lower binder content induced better result whereas the usage of GGBS exhibited improvement if the content did not exceed 30%. For flexural strength test, higher binder content and lower GGBS content led to higher flexural strength. When it comes to slant shear strength, the effect of binder and GGBS content was not significant. Instead, it was governed by the mechanical compatibility between substrate and the repair material. Therefore, the FRCC with the lowest difference in compressive strength to the substrate gained the highest slant shear strength. On the other hand, impact strength can be enhanced with higher matrix strength and good fibre dispersion.

For the flexural behavior, higher GGBS content yielded higher first crack strength. However, this offset the performance of PVA fibre in post-cracking stage and led to lower ultimate flexural strength, post crack to first crack strength ratio, deflection, number of crack lines and flexural toughness. On the other hand, 1100kg/m^3 binder content induced the best result in terms of the overall flexural performance, which includes post peak strength, number of crack lines and flexural toughness.

By accounting the aforementioned properties, it can be concluded that, in overall, the inclusion of GGBS in replacing 30% of fly ash potentially improved the performance of FRCC in terms of compressive strength, impact strength and flexural behaviour. Other than that, binder content should be sufficiently used, at minimum 1100kg/m^3 to attain good fibre dispersion, which also affects the performance of FRCC. With the fulfilment of minimum requirement, the developed ternary blended binder FRCC can be potentially used as repair material.

5.3 Recommendation

In this research, the experimental work was restricted mainly by the availability of facility and time constraint. There are other aspects that were not covered in the present study. The following recommendations are suggested for future investigation:

1. Direct tensile test can be done to determine the tensile-strain curve and tensile strain capacity for FRCC. This would help to verify the slip-hardening behaviour in the developed FRCC.
2. The developed ECC can be evaluated with commercially available high-performance fibre reinforced mortar.
3. Further testing on dimensional and electrochemical compatibilities such as restrained shrinkage and chloride penetration test can be performed in order to find out the durability of the developed FRCC.

4. Different water-to-binder content and higher range of GGBS content can be investigated in this research.
5. Different method of bonding test between FRCC and substrate can be performed.

REFERENCES

Aïtcin, P. C. (2016a). 1 - The importance of the water–cement and water–binder ratios *Science and Technology of Concrete Admixtures* (pp. 3-13): Woodhead Publishing.

Aïtcin, P. C. (2016b). 3 - Portland cement *Science and Technology of Concrete Admixtures* (pp. 27-51): Woodhead Publishing.

Aïtcin, P. C. (2016c). 4 - Supplementary cementitious materials and blended cements *Science and Technology of Concrete Admixtures* (pp. 53-73): Woodhead Publishing.

ASTM. (2007). *Standard Test Method for Flow of Hydraulic Cement Mortar (ASTM C 1437)* West Conshohocken, PA, ASTM International

ASTM. (2013). *Standard Test Method for Tensile Strength of Concrete Surfaces and the Bond Strength or Tensile Strength of Concrete Repair and Overlay Materials by Direct Tension (Pull-off Method) (ASTM C1583)* West Conshohocken, ASTM International

Atahan, H. N., Pekmezci, B. Y., & Tuncel, E. Y. (2012). Behavior of PVA fiber-reinforced cementitious composites under static and impact flexural effects. *Journal of Materials in Civil Engineering, 25*(10), 1438-1445.

Austin, S., Robins, P., & Pan, Y. (1995). Tensile bond testing of concrete repairs. *Materials and Structures, 28*(5), 249.

Austin, S., Robins, P., & Pan, Y. (1999). Shear bond testing of concrete repairs. *Cement and Concrete Research, 29*(7), 1067-1076.

Ayub, T., Shafiq, N., & Nuruddin, M. F. (2014a). Effect of Chopped Basalt Fibers on the Mechanical Properties and Microstructure of High Performance Fiber Reinforced Concrete. *Advances in Materials Science and Engineering, 2014*, 14.

Ayub, T., Shafiq, N., & Nuruddin, M. F. (2014b). Mechanical Properties of High-performance Concrete Reinforced with Basalt Fibers. *Procedia Engineering, 77*, 131-139.

Bamforth, P., & et al. (2008). *Properties of concrete for use in Eurocode 2. How to optimise the engineering properties of concrete in design to Eurocode 2*: The Concrete Centre.

Bentur, A., & Mindess, S. (2006). *Fibre reinforced cementitious composites*: CRC Press.

Bentz, D. P., De la Varga, I., Muñoz, J. F., Spragg, R. P., Graybeal, B. A., Hussey, D. S., . . . LaManna, J. M. (2018). Influence of substrate moisture state and roughness on interface microstructure and bond strength: Slant shear vs. pull-off testing. *Cement and Concrete Composites, 87*, 63-72.

Bilim, C. (2006). *The use of ground granulated blast furnace slag in cement based materials.* (Ph.D), Çukurova University.

Björnström, J., & Chandra, S. (2003). Effect of superplasticizers on the rheological properties of cements. *Materials and Structures, 36*(10), 685-692.

BSI. (1999a). *Products and systems for the protection and repair of concrete structures - Test methods - Determination of slant shear strength (BS EN 12615:1999)* London, British Standards Institution

BSI. (1999b). *Products and systems for the protection and repair of concrete structures. Test methods. Measurement of bond strength by pull-off. (EN 1542)* London, BSI

BSI. (2005). *Products and systems for the protection and repair of concrete structures — Definitions, requirements, quality control and evaluation of conformity — Part 3: Structural and non-structural repair (BS EN 1504-3:2005)* London, British Standards Institution

BSI. (2009a). *Testing hardened concrete. Compressive strength of test specimens (BS EN 12390-3:2009)* London, BSI

BSI. (2009b). *Testing hardened concrete. Tensile splitting strength of test specimens (BS EN 12390-6:2009)* London, BSI

Chen, Y., Yu, J., & Leung, C. K. Y. (2018). Use of high strength Strain-Hardening Cementitious Composites for flexural repair of concrete structures with significant steel corrosion. *Construction and Building Materials, 167*, 325-337.

Choi, J. I., & Lee, B. Y. (2015). Bonding Properties of Basalt Fiber and Strength Reduction According to Fiber Orientation. *Materials, 8*(10), 6719-6727.

Dave, N., Misra, A. K., Srivastava, A., & Kaushik, S. K. (2017). Setting time and standard consistency of quaternary binders: The influence of cementitious material addition and mixing. *International Journal of Sustainable Built Environment, 6*(1), 30-36.

De Koker, D., & Van Zijl, G. (2004). *Extrusion of engineered cement-based composite material.* Paper presented at the Proceedings of the 6th RILEM Symposium on Fiber-Reinforced Concretes (FRC).

Emmons, P. H., & Vaysburd, A. M. (1995). *Performance Criteria for Concrete Repair Materials. Phase 1.*

Ezziane, M., Kadri, T., Molez, L., Jauberthie, R., & Belhacen, A. (2015). High temperature behaviour of polypropylene fibres reinforced mortars. *Fire Safety Journal, 71*(Supplement C), 324-331.

Fakharifar, M., Dalvand, A., Arezoumandi, M., Sharbatdar, M. K., Chen, G., & Kheyroddin, A. (2014). Mechanical properties of high performance fiber reinforced cementitious composites. *Construction and Building Materials, 71*(Supplement C), 510-520.

FDOT. (2016). *Standard Specifications for Road and Bridge Construction* Florida Department of Transportation

Ferrara, L., Krelani, V., & Moretti, F. (2016). Autogenous healing on the recovery of mechanical performance of High Performance Fibre Reinforced Cementitious Composites (HPFRCCs): Part 2 – Correlation between healing of mechanical performance and crack sealing. *Cement and Concrete Composites, 73*(Supplement C), 299-315.

Figueiredo, A. D. d., & Ceccato, M. R. (2015). Workability Analysis of Steel Fiber Reinforced Concrete Using Slump and Ve-Be Test. *Materials Research, 18*(6), 1284-1290.

Gerges, N. N., Issa, C. A., & Fawaz, S. (2015). Effect of construction joints on the splitting tensile strength of concrete. *Case Studies in Construction Materials, 3*, 83-91.

Grantham, M., Basheer, P. A. M., Magee, B., & Soutsos, M. (2014). *Concrete Solutions 2014*: CRC Press.

Grünewald, S. (2004). Performance-based design of self-compacting fibre reinforced concrete.

Güneyisi, E., Gesoğlu, M. J. M., & Structures. (2008). A study on durability properties of high-performance concretes incorporating high replacement levels of slag. *41*(3), 479-493.

Guo, T., Xie, Y., & Weng, X. (2018). Evaluation of the bond strength of a novel concrete for rapid patch repair of pavements. *Construction and Building Materials, 186*, 790-800.

Hakamy, A., Shaikh, F., & Low, I. M. (2015). Characteristics of nanoclay and calcined nanoclay-cement nanocomposites. *Composites Part B: Engineering, 78*, 174-184.

Horikoshi, T., Ogawa, A., Saito, T., Hoshiro, H., Fischer, G., & Li, V. (2006). *Properties of Polyvinylalcohol fiber as reinforcing materials for cementitious composites.* Paper presented at the International RILEM workshop on HPFRCC in structural applications.

Hossain, K. M. A., Lachemi, M., Sammour, M., & Sonebi, M. (2013). Strength and fracture energy characteristics of self-consolidating concrete incorporating polyvinyl alcohol, steel and hybrid fibres. *Construction and Building Materials, 45*(Supplement C), 20-29.

Hou, L., Wang, J., Huang, T., Shen, C., Aslani, F., & Chen, D. (2019). Flexural behaviour of corroded reinforced concrete beams repaired with ultra-high toughness cementitious composite. *Construction and Building Materials, 211*, 1127-1137.

Ikotun, B. D., Fanourakis, G. C., & Mishra Bhardwaj, S. (2017). The effect of fly ash, β-cyclodextrin and fly ash-β-cyclodextrin composites on concrete workability and strength. *Cement and Concrete Composites, 78*(Supplement C), 1-12.

Jiang, C., Fan, K., Wu, F., & Chen, D. (2014). Experimental study on the mechanical properties and microstructure of chopped basalt fibre reinforced concrete. *Materials & Design, 58*(Supplement C), 187-193.

Johnston, C. D., & Gray, R. J. (1978). *Uniaxial tensile testing of steel fibre reinforced cementitious composites*. Paper presented at the Testing and Test Methods of Fibre Mechanics of FRC composites 169 Cement Composites, Proc. RILEM Symp., Lancaster, England.

Kanda, T., & Li, V. C. J. J. o. E. m. (1999). Effect of fiber strength and fiber-matrix interface on crack bridging in cement composites. *125*(3), 290-299.

Kapelko, A. (2006). Possibilities of cement content reduction in concretes with admixture of superplasticiser SNF. *Journal of civil engineering and management, 12*(2), 117-126.

Kim, J.-K., Kim, J.-S., Ha, G. J., & Kim, Y. Y. (2007). Tensile and fiber dispersion performance of ECC (engineered cementitious composites) produced with ground granulated blast furnace slag. *Cement and Concrete Research, 37*(7), 1096-1105.

Kim, Y. Y., Fischer, G., Lim, Y. M., & Li, V. C. (2004). Mechanical performance of sprayed engineered cementitious composite using wet-mix shotcreting process for repair applications. *Materials Journal, 101*(1), 42-49.

Kosmatka, S. H., Kerkhoff, B., & Panarese, W. C. (2011). *Design and control of concrete mixtures*: Portland Cement Assoc.

Li, G. X., Zhang, A., Song, Z. P., Liu, S. J., & Zhang, J. B. (2018). Ground granulated blast furnace slag effect on the durability of ternary cementitious system exposed to combined attack of chloride and sulfate. *Construction and Building Materials, 158*(Supplement C), 640-648.

Li, M., & Li, V. (2011). Behavior of ECC/Concrete Layered Repair System under Drying Shrinkage Conditions. *Journal of Restoration of Buildings and Monuments, 12*.

Li, M., & Li, V. C. (2011). High-Early-Strength Engineered Cementitious Composites for Fast, Durable Concrete Repair-Material Properties. *Aci Materials Journal, 108*(1), 3-12.

Li, M., & Li, V. C. (2013). Rheology, fiber dispersion, and robust properties of Engineered Cementitious Composites. *Materials and Structures, 46*(3), 405-420.

Li, P. P., Yu, Q. L., & Brouwers, H. J. H. (2017). Effect of PCE-type superplasticizer on early-age behaviour of ultra-high performance concrete (UHPC). *Construction and Building Materials, 153*, 740-750.

Li, V. C. (2004). High performance fiber reinforced cementitious composites as durable material for concrete structure repair.

Li, V. C., Horii, H., Kabele, P., Kanda, T., & Lim, Y. M. (2000). Repair and retrofit with engineered cementitious composites. *Engineering Fracture Mechanics, 65*(2–3), 317-334.

Li, X., Wang, J., Bao, Y., & Chen, G. (2017). Cyclic behavior of damaged reinforced concrete columns repaired with high-performance fiber-reinforced cementitious composite. *Engineering Structures, 136*(Supplement C), 26-35.

Lim, Y. M., & Li, V. C. (1997). Durable repair of aged infrastructures using trapping mechanism of engineered cementitious composites. *Cement and Concrete Composites, 19*(4), 373-385.

Lin, C., Kayali, O., Morozov, E. V., & Sharp, D. J. (2014). Influence of fibre type on flexural behaviour of self-compacting fibre reinforced cementitious composites. *Cement and Concrete Composites, 51*(Supplement C), 27-37.

Lin, C., Kayali, O., Morozov, E. V., & Sharp, D. J. (2017). Development of self-compacting strain-hardening cementitious composites by varying fly ash content. *Construction and Building Materials, 149*, 103-110.

Lin, Z., & Li, V. C. (1997). Crack bridging in fiber reinforced cementitious composites with slip-hardening interfaces. *Journal of the Mechanics and Physics of Solids, 45*(5), 763-787.

Magalhães, M. d. S., Toledo Filho, R. D., & Fairbairn, E. d. M. R. (2015). Thermal stability of PVA fiber strain hardening cement-based composites. *Construction and Building Materials, 94*(Supplement C), 437-447.

Marchon, D., & Flatt, R. J. (2016). 8 - Mechanisms of cement hydration *Science and Technology of Concrete Admixtures* (pp. 129-145): Woodhead Publishing.

Marlowe, I. (2003). *Emission factors programme Task 4(b): review of cement sector pollution inventory.* Retrieved from Culham Science Park:

Meng, D., Huang, T., Zhang, Y. X., & Lee, C. K. (2017). Mechanical behaviour of a polyvinyl alcohol fibre reinforced engineered cementitious composite (PVA-ECC) using local ingredients. *Construction and Building Materials, 141*(Supplement C), 259-270.

Merta, I., & Tschegg, E. K. (2013). Fracture energy of natural fibre reinforced concrete. *Construction and Building Materials, 40*(Supplement C), 991-997.

Momayez, A., Ehsani, M. R., Ramezanianpour, A. A., & Rajaie, H. (2005). Comparison of methods for evaluating bond strength between concrete substrate and repair materials. *Cement and Concrete Research, 35*(4), 748-757.

Morgan, D. R. (1996). Compatibility of concrete repair materials and systems. *Construction and Building Materials, 10*(1), 57-67.

Muzenski, S., Flores-Vivian, I., & Sobolev, K. (2015). Hydrophobic engineered cementitious composites for highway applications. *Cement and Concrete Composites, 57*, 68-74.

Nam, J., Kim, G., Lee, B., Hasegawa, R., & Hama, Y. (2016). Frost resistance of polyvinyl alcohol fiber and polypropylene fiber reinforced cementitious composites under freeze thaw cycling. *Composites Part B: Engineering, 90*(Supplement C), 241-250.

Pakravan, H. R., Jamshidi, M., & Latifi, M. (2017). The effect of hydrophilic (polyvinyl alcohol) fiber content on the flexural behavior of engineered cementitious composites (ECC). *Journal of the Textile Institute, 109*(1), 79-84.

Pakravan, H. R., Latifi, M., & Jamshidi, M. (2016). Ductility improvement of cementitious composites reinforced with polyvinyl alcohol-polypropylene hybrid fibers. *Journal of Industrial Textiles, 45*(5), 637-651.

Pan, Z., Wu, C., Liu, J., Wang, W., & Liu, J. (2015). Study on mechanical properties of cost-effective polyvinyl alcohol engineered cementitious composites (PVA-ECC). *Construction and Building Materials, 78*(Supplement C), 397-404.

Pan, Z. F., Wu, C., Liu, J. Z., Wang, W., & Liu, J. W. (2015). Study on mechanical properties of cost-effective polyvinyl alcohol engineered cementitious composites (PVA-ECC). *Construction and Building Materials, 78*, 397-404.

Pattnaik, R. R. (2015). Investigation on ASTM C882 test procedure of slant shear bond strength of concrete repair material. *International Journal of Civil, Structural, Environmental and Infrastructure Engineering Research and Development (IJCSEIERD), 5*(2), 1-6.

Ramachandran, V. S. (1996). 3 - Admixture Interactions in Concrete *Concrete Admixtures Handbook (Second Edition)* (pp. 95-136). Park Ridge, NJ: William Andrew Publishing.

Redon, C., Li, V. C., Wu, C., Hoshiro, H., Saito, T., & Ogawa, A. (2001). Measuring and modifying interface properties of PVA fibers in ECC matrix. *Journal of Materials in Civil Engineering, 13*(6), 399-406.

Reis, J. M. L. (2006). Fracture and flexural characterization of natural fiber-reinforced polymer concrete. *Construction and Building Materials, 20*(9), 673-678.

Richardson, A. (2005). Bond characteristics of structural polypropylene fibres in concrete with regard to post-crack strength and durable design. *Structural survey, 23*(3), 210-230.

Richardson, A. E. (2006). Compressive strength of concrete with polypropylene fibre additions. *Structural survey, 24*(2), 138-153.

Rossi, P. (2001). Ultra-High Performance Fiber-Reinforced Concretes. *Concrete international, 23*(12), 46-52.

Sadrmomtazi, A., Tahmouresi, B., & Saradar, A. (2018). Effects of silica fume on mechanical strength and microstructure of basalt fiber reinforced cementitious composites (BFRCC). *Construction and Building Materials, 162*, 321-333.

Sahmaran, M., Lachemi, M., Hossain, K. M. A., Ranade, R., & Li, V. C. (2009). Influence of Aggregate Type and Size on Ductility and Mechanical Properties of Engineered Cementitious Composites. *Aci Materials Journal, 106*(3), 308-316.

Sahmaran, M., Yücel, H. E., Yildirim, G., Al-Emam, M., & Lachemi, M. (2013). Investigation of the bond between concrete substrate and ECC overlays. *Journal of Materials in Civil Engineering, 26*(1), 167-174.

Said, S. H., & Razak, H. A. (2015). The effect of synthetic polyethylene fiber on the strain hardening behavior of engineered cementitious composite (ECC). *Materials & Design, 86*, 447-457.

Said, S. H., Razak, H. A., & Othman, I. (2015). Flexural behavior of engineered cementitious composite (ECC) slabs with polyvinyl alcohol fibers. *Construction and Building Materials, 75*(Supplement C), 176-188.

Shafiq, N., Ayub, T., & Khan, S. U. (2016). Investigating the performance of PVA and basalt fibre reinforced beams subjected to flexural action. *Composite Structures, 153*(Supplement C), 30-41.

Shaikh, F. U. A. (2013). Deflection hardening behaviour of short fibre reinforced fly ash based geopolymer composites. *Materials & Design, 50*, 674-682.

Sherir, M. A. A., Hossain, K. M. A., & Lachemi, M. (2015). Structural Performance of Polymer Fiber Reinforced Engineered Cementitious Composites Subjected to Static and Fatigue Flexural Loading. *Polymers, 7*(7), 1299-1330.

Silfwerbrand, J. L. (2009). 8 - Bonded concrete overlays for repairing concrete structures. In N. Delatte (Ed.), *Failure, Distress and Repair of Concrete Structures* (pp. 208-243): Woodhead Publishing.

Sivakumar, A., & Santhanam, M. (2007). Mechanical properties of high strength concrete reinforced with metallic and non-metallic fibres. *Cement and Concrete Composites, 29*(8), 603-608.

Tayeh, B. A., Bakar, B. A., Johari, M. M., & Voo, Y. L. (2013). Evaluation of bond strength between normal concrete substrate and ultra high performance fiber concrete as a repair material. *Procedia Engineering, 54*, 554-563.

Thomas, M. (2007). *Optimizing the use of fly ash in concrete* (Vol. 5420): Portland Cement Association Skokie, IL.

Topçu, İ. B. (2013). 10 - High-volume ground granulated blast furnace slag (GGBFS) concrete *Eco-Efficient Concrete* (pp. 218-240): Woodhead Publishing.

Wahyuni, A. S., Supriani, F., Elhusna, & Gunawan, A. (2014). The Performance of Concrete with Rice Husk Ash, Sea Shell Ash and Bamboo Fibre Addition. *Procedia Engineering, 95*(Supplement C), 473-478.

Wang, S. X., & Li, V. C. (2007). Engineered cementitious composites with high-volume fly ash. *Aci Materials Journal, 104*(3), 233-241.

Wang, W., & Chouw, N. (2017). The behaviour of coconut fibre reinforced concrete (CFRC) under impact loading. *Construction and Building Materials, 134*(Supplement C), 452-461.

Won, J.-P., Lee, J.-H., & Lee, S.-J. (2015). Flexural behaviour of arch-type steel fibre reinforced cementitious composites. *Composite Structures, 134*(Supplement C), 565-571.

Xu, G., & Shi, X. (2017). Exploratory Investigation into a Chemically Activated Fly Ash Binder for Mortars. *Journal of Materials in Civil Engineering, 29*(11), 06017018.

Yıldırım, G., Şahmaran, M., Al-Emam, M., Hameed, R., Al-Najjar, Y., & Lachemi, M. (2015). Effects of Compressive Strength, Autogenous Shrinkage, and Testing Methods on Bond Behavior of High-Early-Strength Engineered Cementitious Composites. *Aci Materials Journal, 112*(3).

Yıldırım, G., Şahmaran, M., & Anıl, Ö. (2018). 15 - Engineered cementitious composites-based concrete. In F. Pacheco-Torgal, R. E. Melchers, X. Shi, N. D. Belie, K. V. Tittelboom, & A. Sáez (Eds.), *Eco-Efficient Repair and Rehabilitation of Concrete Infrastructures* (pp. 387-427): Woodhead Publishing.

Yoo, D.-Y., Lee, J.-H., & Yoon, Y.-S. (2013). Effect of fiber content on mechanical and fracture properties of ultra high performance fiber reinforced cementitious composites. *Composite Structures, 106*(Supplement C), 742-753.

Yu, J., & Leung, C. K. Y. (2017). Strength Improvement of Strain-Hardening Cementitious Composites with Ultrahigh-Volume Fly Ash. *Journal of Materials in Civil Engineering, 29*(9), 8.

Yuan, F., Pan, J. L., & Leung, C. K. Y. (2013). Flexural Behaviors of ECC and Concrete/ECC Composite Beams Reinforced with Basalt Fiber-Reinforced Polymer. *Journal of Composites for Construction, 17*(5), 591-602.

Yucel, H. E., Jashami, H., Sahmaran, M., Guler, M., & Yaman, I. O. (2013). Thin ECC overlay systems for rehabilitation of rigid concrete pavements. *Magazine of Concrete Research, 65*(2), 108-120.

Yurdakul, E. (2010). *Optimizing concrete mixtures with minimum cement content for performance and sustainability*: Iowa State University.

Yusof, M. A., Nor, N. M., Zain, M. F. M., Peng, N. C., Ismail, A., Sohaimi, R. M., & Zaidi, A. M. A. (2011). Mechanical properties of hybrid steel fibre reinforced concrete with different aspect ratio. *Australian Journal of Basic and Applied Sciences, 5*(7), 159-166.

Zanotti, C., & Randl, N. (2019). Are concrete-concrete bond tests comparable? *Cement and Concrete Composites, 99*, 80-88.

Zhang, Z., & Zhang, Q. (2017). Self-healing ability of Engineered Cementitious Composites (ECC) under different exposure environments. *Construction and Building Materials, 156*(Supplement C), 142-151.

Zhou, X., R. Slater, J., E. Wavell, S., & Oladiran, O. (2012). *Effects of PFA and GGBS on Early-Ages Engineering Properties of Portland Cement Systems* (Vol. 10).

LIST OF PUBLICATIONS AND PAPERS PRESENTED

Loh, Z. P., Mo, K. H., Tan, C. G., & Yeo, S. H. (2019). Mechanical characteristics and flexural behaviour of fibre-reinforced cementitious composite containing PVA and basalt fibres. *Sādhanā, 44*(4), 98. doi:10.1007/s12046-019-1072-6

Mo, K. H., **Loh, Z. P.**, Tan, C. G., Alengaram, U. J., & Yap, S. P. (2018). Behaviour of Fibre-reinforced Cementitious Composite containing High-Volume Fly Ash at Elevated Temperatures. *Sādhanā*. doi:10.1007/s12046-018-0937-4